Aus der

Medizinischen Klinik und Poliklinik III

Klinikum der Ludwig-Maximilians-Universität München

The role of T-cell exhaustion for cancer immunotherapy

Dissertation
zum Erwerb des Doctor of Philosophy (Ph.D.)
an der Medizinischen Fakultät der

Ludwig-Maximilians-Universität zu München

vorgelegt von:
Nora Philipp, geb. Zieger

aus
Heilbronn/Deutschland

Jahr
2024

Mit Genehmigung der Medizinischen Fakultät der

Ludwig-Maximilians-Universität zu München

Erstes Gutachten:	Prof. Dr. Marion Subklewe
Zweites Gutachten:	PD Dr. Andreas Moosmann
Drittes Gutachten:	Prof. Dr. Sebastian Kobold
Viertes Gutachten:	PD Dr. Dr. Angelika Riemer
Dekan:	Prof. Dr. med. Thomas Gudermann
Tag der mündlichen Prüfung:	11.01.2024

Affidavit

Affidavit

Philipp, Nora
_____
Surname, first name

_____
Street

_____
Zip code, town, country

I hereby declare, that the submitted thesis entitled:

The role of T-cell exhaustion for cancer immunotherapy
……

is my own work. I have only used the sources indicated and have not made unauthorised use of services of a third party. Where the work of others has been quoted or reproduced, the source is always given.

I further declare that the dissertation presented here has not been submitted in the same or similar form to any other institution for the purpose of obtaining an academic degree.

Munich,15.01.2024
place, date

Nora Philipp
Signature doctoral candidate

Confirmation of congruency

Confirmation of congruency between printed and electronic version of the doctoral thesis

Philipp, Nora

Surname, first name

Street

Zip code, town, country

I hereby declare, that the submitted thesis entitled:

The role of T-cell exhaustion for cancer immunotherapy

is congruent with the printed version both in content and format.

Munich, 15.01.2024 — place, date

Nora Philipp — Signature doctoral candidate

Table of content

List of abbreviations

AML	Acute myeloid leukemia
AP-1	Activator protein 1
Axi-cel	Axicabtagene Ciloleucel
BCR-ABL	breakpoint cluster region-Ableson tyrosine kinase
BiTE	Bispecific T-cell engager
BsAb	Bispecific antibody
CAR	Chimeric antigen receptor
CD3ε	CD3 epsilon
cGAMP	cyclic GMP-AMP
cGAS	cyclic GMP-AMP synthase
DC	Dendritic cell
DLBCL	Diffuse large B-cell lymphoma
Eomes	Eomesodermine
ER	Endoplasmic reticulum
IDO	Indoleamine 2,3-Dioxygenase
IFN	interferon
IFNAR	interferon α/β receptor
IL	Interleukin
IRF3	interferon regulatory factor 3
ISG	interferon-stimulated genes
KO	Knockout
LAG-3	lymphocyte activation gene 3
LCK	lymphocyte-specific protein tyrosine kinase
MRD	Minimal residual disease
NFAT	Nuclear factor of activated T-cells
NR4A	nuclear receptor subfamily 4A
PD-1	programmed cell death protein 1
PD-L1	Programmed cell death protein-ligand 1
Ph	Philadelphia chromosome
r/r BCP-ALL	relapsed/refractory B-cell precursor acute lymphoblastic leukemia
scFv	single-chain variable fragment
STAT	signal transducer and activator of transcription
STING	stimulator of interferon genes

T-bet	T-box transcription factor
TBK1	TANK-binding kinase 1
TCF-1	T cell factor-1
TCR	T-cell receptor
TF	Transcription factor
TFI	Treatment-free interval
Tim-3	T-cell immunoglobulin and mucin domain 3
TME	Tumor microenvironment
TNF	Tumor necrosis factor
TOX	thymocyte selection-associated high mobility group box protein
T_{PEX}	precursor exhausted T cell
T_{TEX}	Terminally exhausted T cell

1. List of publications

This thesis includes two publications that have been accepted for publication in peer-reviewed journals:

"T-cell exhaustion induced by continuous bispecific molecule exposure is ameliorated by treatment-free intervals"

Nora Philipp, Maryam Kazerani, Alyssa Nicholls, Binje Vick, Jan Wulf, Tobias Straub, Michaela Scheurer, Amelie Muth, Gerulf Hänel, Daniel Nixdorf, Monika Sponheimer, Malte Ohlmeyer, Sonja M. Lacher, Bettina Brauchle, Anetta Marcinek, Lisa Rohrbacher, Alexandra Leutbecher, Kai Rejeski, Oliver Weigert, Michael von Bergwelt-Baildon, Sebastian Theurich, Roman Kischel, Irmela Jeremias, Veit Bücklein, Marion Subklewe

Blood. 2022 Sep 8;140(10):1104-1118. doi: 10.1182/blood.2022015956. PMID: 35878001

"STING agonism turns human T cells into interferon-producing cells but impedes their functionality"

Niklas Kuhl, Andreas Linder, **Nora Philipp**, Daniel Nixdorf, Hannah Fischer, Simon Veth, Gunnar Kuut, Teng Teng Xu, Sebastian Theurich, Thomas Carell, Marion Subklewe, Veit Hornung

EMBO Rep. 2023 Mar 6;24(3):e55536. doi: 10.15252/embr.202255536. Epub 2023 Jan 27. PMID: 36705069; PMCID: PMC9986811.

1.1 Contribution to publication I

"T-cell exhaustion induced by continuous bispecific molecule exposure is ameliorated by treatment-free intervals"

I contributed to this publication by conceptualizing, conducting, analyzing and interpreting all *in vitro* experiments. Moreover, I wrote the manuscript and conveyed the review process until final publication.

1.2 Contribution to publication II

"STING agonism turns human T cells into interferon-producing cells but impedes their functionality"

I contributed to this publication by conducting, analyzing and interpreting all metabolic experiments (shown in Figure 5E+F).

2. Introductory summary

2.1 T cell-based immunotherapy in hematologic malignancies

T cell-based immunotherapy is a novel platform for the treatment of malignancies based on redirecting T-cells to target antigen-expressing tumor cells. Proof-of-concept was originally demonstrated in the context of allogeneic hematopoietic stem cell transplantation in which adoptively transferred T cells have been shown to successfully eradicate leukemic cells [1]. Since then, the following T cell-based immunotherapeutic platforms have evolved: 1) Checkpoint inhibitors that boost endogenous, pre-existing T-cell responses, 2) T cell-recruiting bispecific antibodies (BsAbs) which activate and redirect T cells to tumor cells, and 3) tumor antigen-specific T-cell receptor (TCR)- or chimeric antigen receptor (CAR)-engineered T cells that are engineered ex vivo and re-infused to elicit anti-tumor responses (Figure 1).

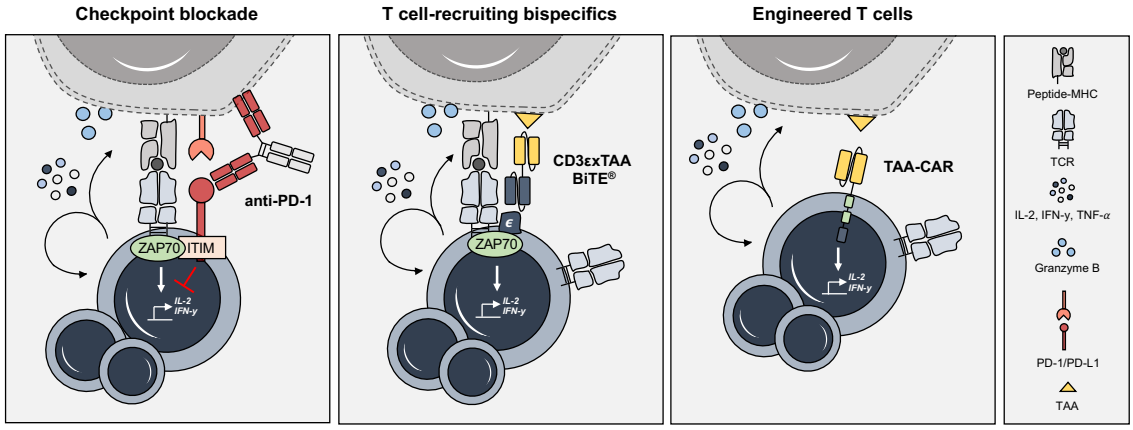

Figure 1: T cell-based immunotherapies. Adapted from [2-4]. Grey=tumor cell, blue=T cell, BiTE=Bispecific T-cell engager, CAR=chimeric antigen receptor, CD3ε=CD3 epsilon, ITIM= Immunoreceptor tyrosine-based inhibitory motif, MHC=major histocompatibility complex, PD-1=programmed cell death protein-1, PD-L1= programmed cell death protein ligand-1, TAA=tumor-associated antigen, TCR=T-cell receptor, ZAP70= Zeta-chain-associated protein kinase 70.

A prerequisite for efficient and safe redirection of T cells against tumor cells is the identification of a tumor-associated target antigen. Targeting the B-cell lineage antigen CD19 using T cell-recruiting bispecific antibodies or CAR T cells confines cytotoxicity to the B-cell compartment and has shown high efficacy in the treatment of patients with relapsed/refractory (r/r) or minimal residual disease-positive (MRD^+) acute lymphoblastic leukemia (ALL) [5, 6] and diffuse large B-cell lymphoma (DLBCL) [7]. Recently, two other BsAb constructs have been approved that target CD20 (Mosunetuzumab, [8]) and B-cell maturation antigen (BCMA) (Teclistamab, [9]) in the context of follicular lymphoma and multiple myeloma, respectively.

In contrast, the heterogeneous landscape of antigens expressed in myeloid malignancies like acute myeloid leukemia (AML) has so far hampered the identification of an AML-specific antigen with low or no expression on healthy tissue. The lack of a suitable target antigen still limits the efficacy of T cell-based immunotherapies in AML with no approved AML-targeting BsAbs or CAR T cells to date.

2.2 T cell-recruiting bispecific antibodies

Numerous T cell-recruiting bispecific antibody formats have been developed in the past years, ranging from small constructs of two single-chain variable fragments (scFv) with different specificity fused by a linker (e.g. BiTEs) to larger constructs with silenced F_c parts and multiple antigen binding domains (e.g. CrossMAbs) (Figure 2A-D). Although different in their pharmacokinetic properties, all formats follow the same mode of action: upon simultaneous binding to a tumor-associated antigen (TAA) and to human CD3 (part of the TCR complex) T cells are activated at the tumor site. This induces T-cell proliferation and secretion of cytolytic molecules which leads to the killing of the tumor cell [10, 11] (Figure 2E).

Blinatumomab was the first in class CD19xCD3 BsAb and has revolutionized the therapeutic landscape of B-cell precursor ALL (BCP-ALL). In 2014 it received first approval by the FDA followed by the EMA in 2015 for the treatment of Philadelphia chromosome-negative (Ph-) r/r BCP-ALL [12].

Blinatumomab is a BsAb in BiTE (**Bi**specific **T**-cell **E**ngager) format that consists of a human anti-CD3 scFv fused to a human anti-CD19 scFv. Due to its small size (~55 kDa), it has a short serum half-life of approximately 2 hours in patients and is therefore administered as a continuous intravenous infusion over 28 days [6, 13]. In clinical trials blinatumomab significantly increased the median overall survival of Ph^- BCP-ALL patients compared to standard-of-care chemotherapy [5] and yielded response rates of >80 % in MRD^+ and 43 % in r/r patients [6, 14]. In 2018 and 2019, respectively, blinatumomab also received FDA and EMA approval for MRD^+ BCP-ALL [14].

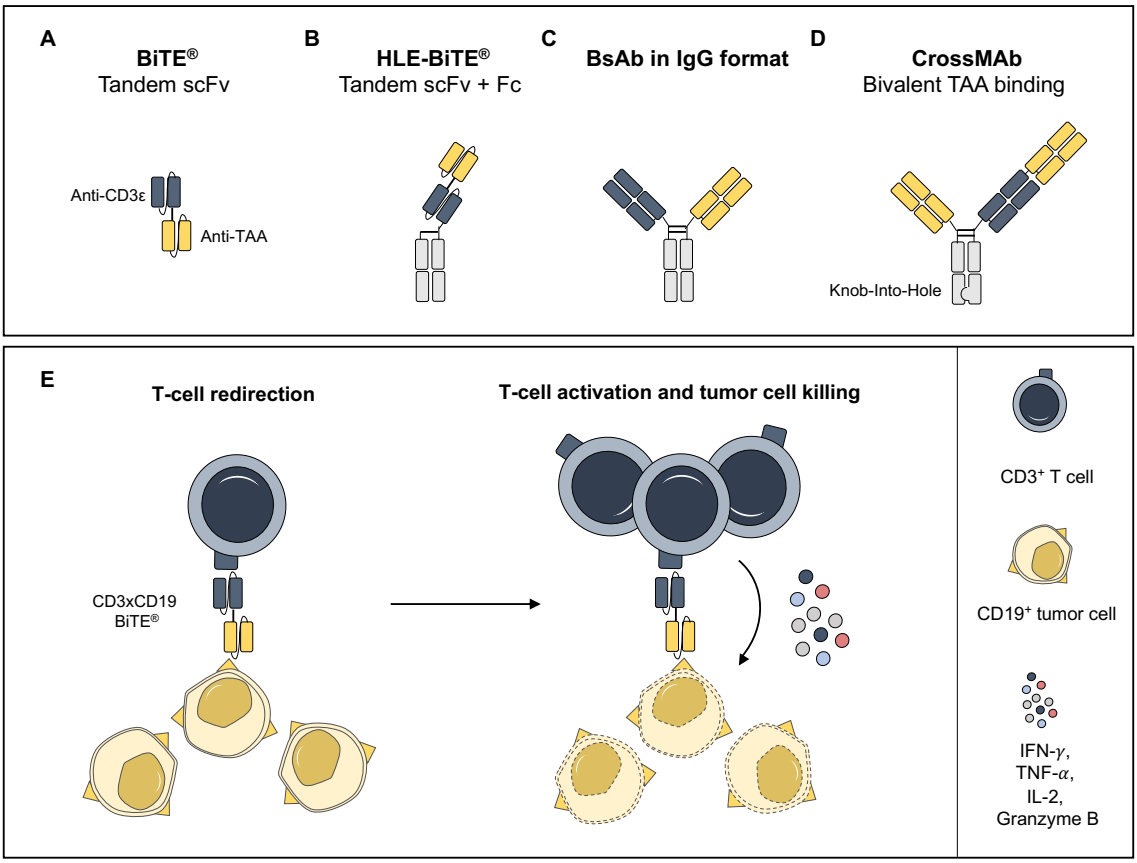

Figure 2: Bispecific antibody formats and mode of action. Adapted from [2, 15-18]. BsAb=bispecific antibody, HLE=half-life extended, scFv=single-chain variable fragment.

The clinical success of blinatumomab has fueled the development of other BsAb constructs in the past years and led to an increasing number of clinical trials [18]. In hematologic malignancies, two new constructs received approval in 2022 for the treatment of r/r follicular lymphoma (Mosunetuzumab, [8]) and r/r multiple myeloma (Teclistamab, [9]). Despite encouraging response rates, a considerable fraction of patients treated with the approved BsAbs relapses or remains refractory to therapy (blinatumomab 18 months relapse-free survival = 54 % in the MRD^+ BCP-ALL patient cohort, [14]). Similar findings have been made in patients receiving CD19-targeted CAR T-cell therapy. Although up to 65 % of r/r DLBCL patients show complete response to CAR T-cell therapy, the majority of patients remain primary refractory or relapse early (Event-free survival 8.5 months, [7]). Thus, unraveling and understanding resistance mechanisms that limit the efficacy of T cell-based immunotherapy is of high relevance to improving the clinical outcome of patients suffering from various types of cancers.

2.3 Mechanisms of resistance to T cell-based immunotherapy

The anti-tumor T-cell response elicited by T cell-based immunotherapy depends on tumor-intrinsic and extrinsic parameters. Tumors have evolved to escape immune surveillance by providing a hostile and immunosuppressive tumor microenvironment (TME) that negatively impacts T-cell activity and persistence. Intrinsically, tumors can modulate the expression of tumor-associated target antigens, HLA molecules, or inhibitory checkpoint molecules to avoid recognition or suppress T-cell function [19]. Furthermore, tumors can downregulate intracellular DNA-damage sensors including the cGAS/STING pathway to circumvent cell death and immune recognition [20, 21]. Extrinsically, persistent antigen stimulation of T cells combined with immunosuppressive signals in the TME drive T-cell exhaustion and limit T cell-based immunotherapy [22-26] (**Publication I: Philipp et al. 2022**). In the following chapters, the role of the cGAS/STING pathway as well as T-cell exhaustion in cancer immunotherapy will be further elaborated.

2.3.1 The cGAS/STING axis

The cyclic GMP-AMP synthase (cGAS) and its receptor stimulator of interferon genes (STING) known as the cGAS/STING axis is an ancient anti-viral defense pathway that is known to be active in innate immune cells. cGAS senses double-stranded DNA that is present in the cytosol, e.g. viral DNA in an infected cell [27] leading to the production of the second messenger cyclic GMP-AMP (cGAMP) [28]. cGAMP activates STING at the endoplasmic reticulum's (ER) membrane [29] and leads to STING translocation from the ER to the Golgi. This results in the activation of TANK-binding kinase 1 (TBK1) and interferon regulatory factor 3 (IRF3) [30]. The latter induces the production of pro-inflammatory type I interferons (IFNs) like IFN-α and IFN-β [31]. Subsequently, type I IFNs engage the interferon α/β receptor (IFNAR) which is also expressed in T cells. Of note, type I IFNs can bind IFNAR in an autocrine or paracrine manner [32, 33] (**Publication II: Kuhl et al. 2023**). IFNAR engagement leads to signal transducer and activator of transcription (STAT1/2)-dependent induction of interferon-stimulated genes (ISGs) and elicits an anti-viral response. Additionally, STING activation can induce cell death [34, 35] and NF-kB signaling through IKK activation and a yet unknown mechanism [36] (Figure 3).

Besides cGAS role in viral defense, it has been discovered that cGAS does not only sense non-self but also self-DNA derived from mitochondria or the nucleus that enters the cytosol upon mitochondrial or mitotic stress [37-39]. Hence, cGAS is also considered a sensor for DNA damage and plays a role in the development of cancer and cellular senescence [40, 41]. dsDNA derived from tumors is present at high levels in the TME

and induces cGAS/STING activation and secretion of type I IFNs in antigen-presenting cells like dendritic cells (DCs). This in turn leads to DC maturation, presentation of peptides on MHC molecules, and priming of tumor-specific T cells. Furthermore, dsDNA in the TME can induce STING activation in the tumor stroma which has been linked to improved endothelial adhesion and higher infiltration of lymphocytes into the tumor [32, 42, 43]. Indeed, suppression of the cGAS/STING pathway has been observed in several cancers to circumvent immune recognition and apoptosis [20]. It is well appreciated that the success of radiation and chemotherapy can at least in part be attributed to STING activation in innate immune cells through increased DNA damage and thus increased immunogenicity of tumor cells [40, 44-46]. These observations have fueled the development of STING agonists for combination treatment with immunotherapy in cancer patients [47, 48].

2.3.2 The cGAS/STING axis in T cells

Interestingly, it has been discovered that STING is also expressed in T cells [49]. Although its role in T cells remains poorly understood, impaired T-cell proliferation [50, 51], reduced memory formation [50, 52, 53], and increased cell death [54, 55] have been related to STING activation. These findings potentially explain the limitations of STING agonists in clinical trials so far [48]. In line with these observations, we have shown that simultaneous CD3/CD28 T-cell activation and STING engagement with the second messenger cGAMP leads to decreased proliferation, impaired metabolic activity, and increased cell death in primary human T cells, while potently inducing the expression of ISGs and IFN-β secretion [33] (**Publication II: Kuhl et al. 2023).** Knockout (KO) studies to unravel STING-mediated impairment of T-cell function have reported conflicting results: STING-deficient tumor-infiltrating T cells in mice were more resistant to cell death [56]. However, functional impairment of STING KO T cells was reported in an antigen-specific mouse model [57]. Clearly, further studies are needed to unravel the role of the cGAS/STING pathway in T cells and its implications for immunotherapy.

Pro-inflammatory type I IFNs secreted by innate immune cells in the TME have also been linked to T-cell dysfunction. While IFN-α/β signaling is required for an efficient acute antiviral response [58] and optimal priming and differentiation of T cells [32], persistently high levels of IFN-α/β in chronic viral infection skew T cells towards terminal differentiation [59] and induce T-cell death [60, 61]. Furthermore, T cell-inhibitory molecules like programmed cell death protein-ligand 1 (PD-L1) and Indoleamine 2,3-Dioxygenase (IDO) are induced upon high and persistent IFN-α/β levels [62]. Accordingly, IFNAR blockade in T cells prior to and during chronic, but not acute viral infection resulted in enhanced

viral control [63, 64], highlighting the context-dependent role of IFN-α/β in modulating T-cell function.

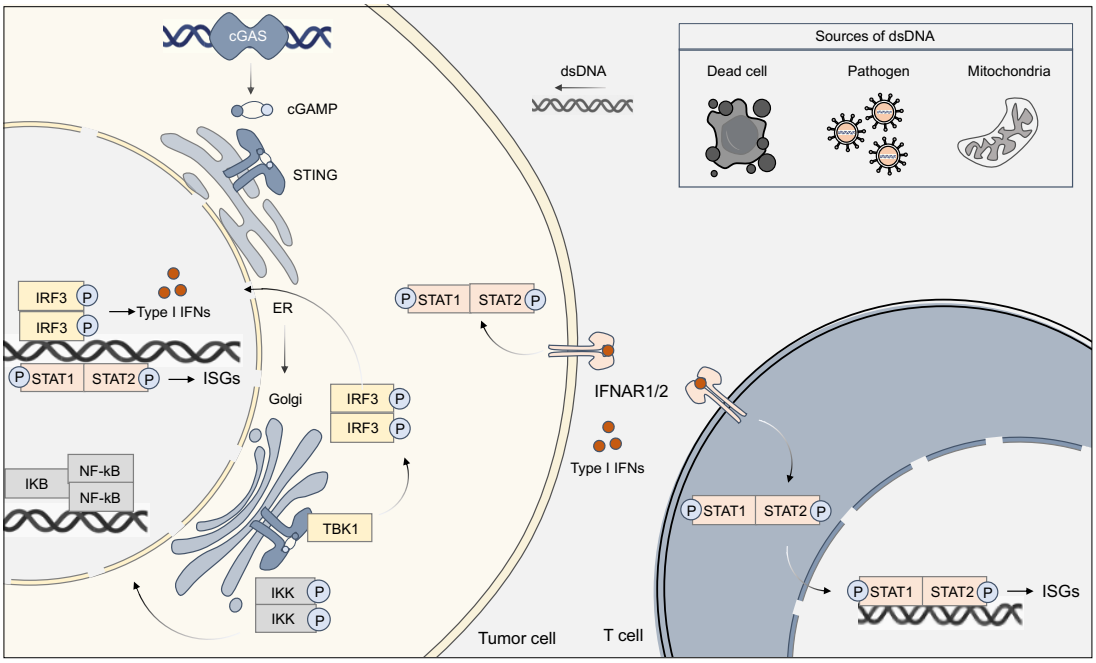

Figure 3: Overview of the cGAS-STING pathway. Adapted from [65-67].

2.3.3 The concept of T-cell exhaustion

T-cell exhaustion has been first discovered in T cells in a murine chronic viral infection model [22, 68]. Since then, it has also been identified in human chronic viral infection [23, 24], as well as in cancer [19, 69-71]. T-cell exhaustion is induced by persistent antigen stimulation, although the contribution of multiple other factors including a proinflammatory cytokine milieu (see chapter cGAS/STING pathway) has been reported. Exhaustion is defined as progressive and hierarchical loss of effector function. Upon continued antigen exposure, T cells first lose their ability to secrete IL-2, followed by decreased cytotoxic activity and proliferative potential. Finally, T cells lose the ability to secrete the effector cytokines tumor necrosis factor-α (TNF-α) and IFN-y and ultimately undergo apoptosis [23]. The loss of effector function is accompanied by an impaired metabolic program [72] and sustained upregulation of coinhibitory checkpoint molecules like lymphocyte activation gene 3 (LAG-3), T-cell immunoglobulin and mucin domain 3 (Tim-3), and programmed cell death protein 1 (PD-1). Together, these traits are termed hallmark features of T-cell exhaustion [23, 24] (Figure 4).

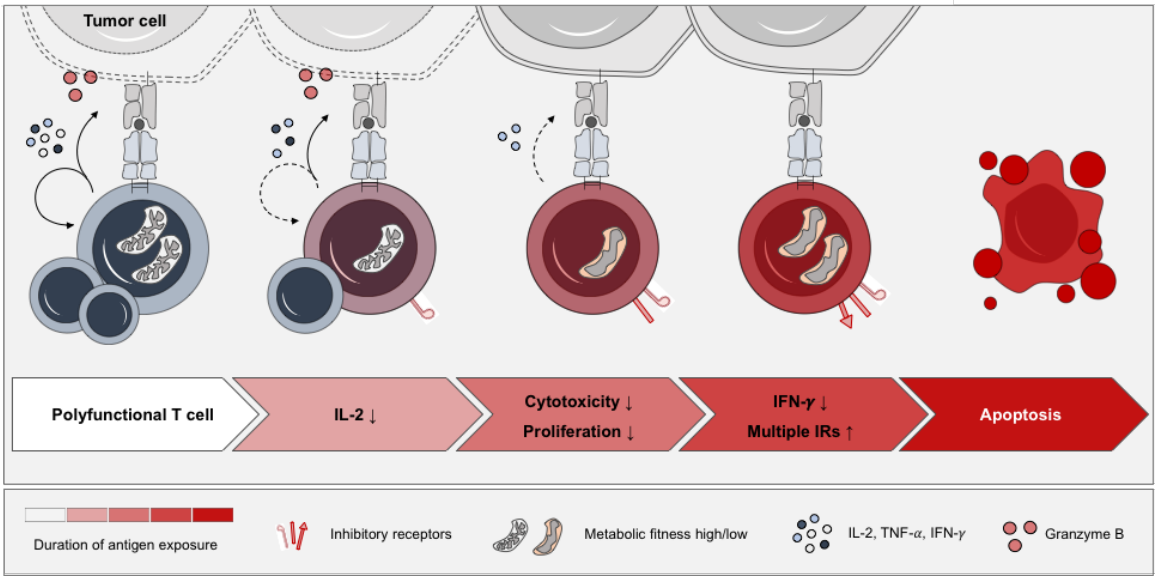

Figure 4: Hallmarks of T-cell exhaustion. Adapted from [23, 25, 73].

Exhausted T cells exert a distinct transcriptional and epigenetic program that differs considerably from effector or memory T cells [74-76]. Although the transcriptional network in exhausted T cells is not yet fully understood, it has been discovered that exhausted T cells reuse transcription factors (TFs) that are also expressed in effector and memory T cells, but participate in different transcriptional circuits [75, 77]. T-box transcription factor (T-bet) and Eomesodermin (Eomes) both have roles in T-cell differentiation. In acute infection, T-bet drives effector function while Eomes promotes memory formation, quiescence, and stemness. Yet, in chronic infection T-bet and Eomes are both indispensable for the formation and persistence of exhausted T-cell subsets [78, 79] and Eomes is highly expressed in terminally exhausted T cells [73]. Another major transcriptional regulator with distinct functions in T-cell exhaustion is the TF thymocyte selection-associated high mobility group box protein (TOX) [80-82]. While TOX is also expressed in $CD8^+$ effector cells [83], it can cooperate with the nuclear receptor subfamily 4A (NR4A) to drive the induction of coinhibitory checkpoint molecules and an exhaustion-associated transcriptional program. Both TOX and NR4A are regulated by the calcineurin-dependent TF Nuclear factor of activated T-cells (NFAT) [81, 84]. NFAT in turn is a known mediator of T-cell effector programs and forms heterodimers with activator protein 1 (AP-1) family transcription factors (Fos-Jun) in activated and highly functional T cells [85-87]. However, in exhausted T cells, the balance between NFAT and AP-1 family members is skewed towards NFAT, which leads to an increase of partnerless NFAT in the nucleus [23, 88]. Partnerless NFAT induces TOX and NR4A and the transcription of exhaustion-

associated genes (e.g. PDCD1) [81, 89, 90]. Despite major advances identifying transcriptional and epigenetic players involved in T-cell exhaustion, further studies are needed to better understand the transcriptional networks in exhausted T cells.

T cell factor-1 (TCF-1) is another key TF for T-cell differentiation and is highly expressed in memory and precursor-exhausted T cells (T_{PEX}) and is crucial for the self-renewal capacity of T_{PEX} cells. It has been suggested that the presence of TCF-1 in T cells under chronic antigen stimulation distinguishes TCF-1^{+} functional precursors from TCF-1^{-} terminally exhausted T cells [91-93].

2.3.4 Progenitor and terminally exhausted T-cell subsets

Based on the differential expression of TFs and surface molecules as well as functional characteristics, different stages of T-cell exhaustion have been defined (Figure 5, [73, 76, 94, 95]: Early after antigen encounter, T cells differentiate into killer cell lectin-like receptor subfamily G, member 1 (KLRG-1) positive terminal effector cells and, in case of antigen clearance, a small fraction differentiates into CD127^{+} memory progenitor T cells [96]. If the antigen persists, progenitor exhausted T cells (T_{PEX}) form, characterized by the expression of TCF-1, accompanied by PD-1, TOX, and T-bet^{lo} expression. Importantly, the T_{PEX} subset can exert effector function, self-renew, and is responsive to checkpoint blockade [59, 95, 97, 98]. T_{PEX} cells can then give rise to terminally exhausted (T_{TEX}) T cells characterized by the absence of TCF-1 and the presence of PD-1, Tim-3, TOX, NR4A, T-bet^{lo}, and Eomes^{hi} expression [73, 78, 99]. Intriguingly, recent evidence suggests that transcriptional and epigenetic T-cell exhaustion programs are reversible [25]. In this light, identifying strategies to reprogram terminally exhausted T_{TEX} into functional T_{PEX} cells will be crucial to for achieving durable T-cell responses in patients.

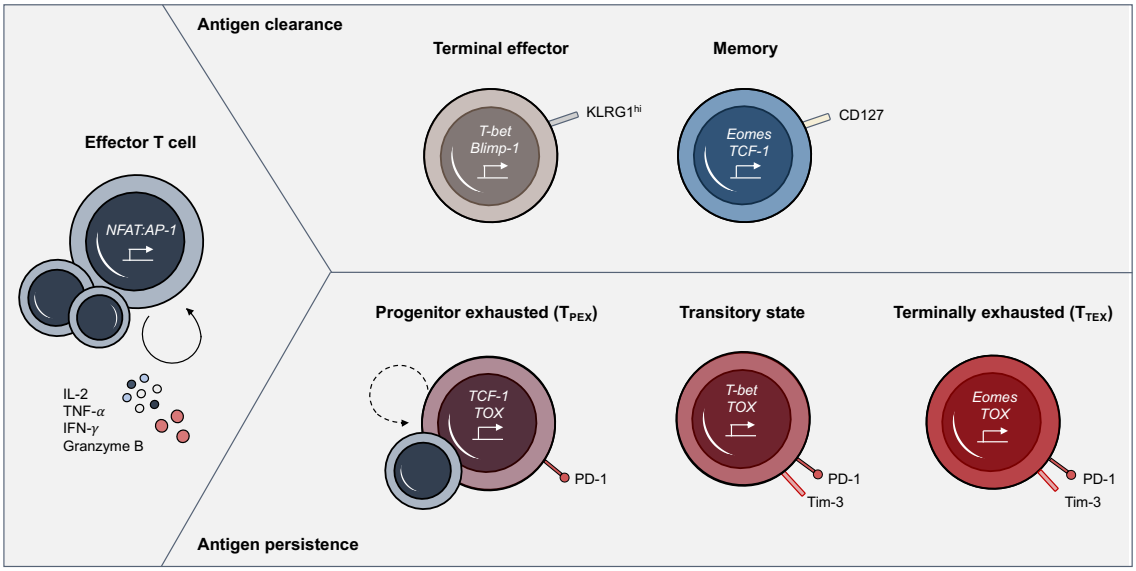

Figure 5: Exhausted T-cell subsets. Adapted from [72, 73, 76]. 2020

2.4 T-cell exhaustion in T cell-based immunotherapy

T-cell exhaustion has also been observed in cancer patients [70] with solid tumors [19, 69] or leukemias [71, 100, 101]. It is therefore unsurprising that durable anti-tumor responses achieved by T cell-based immunotherapy in these patients are still rare [102, 103]. In CAR T cells, exhaustion has been extensively studied in the past years. Induced by tonic CAR signaling or persistent antigen stimulation, CAR T-cell exhaustion has been identified in several preclinical [25, 104, 105] as well as clinical studies [106]. In the context of BsAb therapy, the role of exhaustion is less clear; however, clinical evidence suggests that T-cell function is a major contributor to a patient's response. In an early clinical study, T-cell function in patients was correlated to response to blinatumomab [107]. Furthermore, it was shown that the frequency of T regulatory cells in the peripheral blood of patients negatively correlated to response [108] and enrichment of exhausted T cells was identified in a small cohort of blinatumomab non-responders [109]. In a longitudinal study, we could demonstrate that T-cell function significantly declines in r/r BCP-ALL patients under continuous blinatumomab therapy. These clinical observations led us to develop a stable *in vitro* model system to comprehensively study BsAb-induced T-cell exhaustion [26] (**Publication I: Philipp et al. 2022**). Therein, we mimic continuous T-cell stimulation with a CD3xCD19 blinatumomab-like BsAb for 28 days *in vitro*. We could show that continuous exposure to the BsAb induced hallmark features of T-cell exhaustion *in vitro* and *in vivo*. Our data indicate that indeed, continuous exposure of T cells to BsAbs induces exhaustion and suggests that clinical application schedules of BsAbs need to be reconsidered.

2.5 Strategies to increase the efficacy of T cell-based immunotherapy

In light of the mounting evidence pointing towards T-cell exhaustion as a major limitation of T cell-based immunotherapy, numerous approaches are currently being studied to prevent T-cell exhaustion and increase T-cell responses in patients. Strategies range from the engagement of costimulatory molecules or blockade of inhibitory checkpoints over metabolic reinforcement, small molecule inhibitors to genetic engineering. In the following, selected approaches are highlighted.

A straightforward strategy to reinvigorate exhausted T cells is blockage of inhibitory checkpoint molecules expressed on exhausted T cells. Indeed, the combination of a

CD3xCD33 BsAb with the anti-PD-1 checkpoint inhibitor nivolumab led to increased efficacy of the BsAb in a preclinical acute myeloid leukemia model [110]. Based on similar observations in CAR T cells, several clinical trials have been initiated combining CAR T cells and immune checkpoint blockage [111-114]. However, recent preclinical studies including our own have shown that blockade of PD-1 alone is not sufficient to revert T-cell exhaustion under BsAb [26] (**Publication I: Philipp et al. 2022**) or CAR T-cell therapy [25].

Instead, we and others have identified treatment-free intervals (TFIs) or resting periods for T cells as a powerful strategy to prevent exhaustion. In an inducible CAR T cell model, resting of CAR T cells led to the reversal of transcriptomic, epigenetic, and functional hallmark features of exhaustion [25]. In concordance, by disrupting the detrimental continuous stimulation of T cells with BsAb via a TFI (Schedule: 1 week BsAb continuously - 1 week TFI; 2 cycles) we could significantly reinvigorate T-cell function *in vitro* and *in vivo*. Also, intermittent stimulation induced transcriptional remodeling of exhausted T cells towards a functional TCF-1$^+$ phenotype [26] (**Publication I: Philipp et al. 2022**). These observations emphasize that T-cell exhaustion is not a transcriptionally and epigenetically fixed program but a - to some extent - reversible state. Hence, the identification of strategies to reprogram terminally exhausted T cells could greatly improve T-cell responses in patients.

The Src kinase family inhibitor dasatinib inhibits TCR or CAR downstream-signaling by the blockage of lymphocyte-specific protein tyrosine kinase (LCK) phosphorylation in a dose-dependent manner [115, 116]. Dasatinib is also an inhibitor of the constitutively active BCR-ABL tyrosine kinase present in Ph$^+$ cancers and is currently tested in combination with the BsAb blinatumomab [117]. Intriguingly, continuous application of combined dasatinib and blinatumomab led to an increased frequency of peripheral lymphocytes and a 95 % overall survival rate of patients with Ph$^+$ ALL [117, 118]. Despite the fact that in this study the direct anti-tumor effect of dasatinib on the Ph$^+$ ALL cells cannot be distinguished from its effect on T cells, these data suggest that inhibition of TCR signaling might prevent T-cell exhaustion and maintain durable T-cell responses in patients. Due to the fact that dasatinib potently modulates T-cell function, we envision that combination of blinatumomab and intermittent Src kinase family inhibitors (e.g. dasatinib or ponatinib) as a surrogate for TFIs could be a powerful strategy to increase T-cell responses also in Ph$^-$ ALL patients.

3. Summary of publications

3.1 Publication I

T-cell exhaustion induced by continuous bispecific molecule exposure is ameliorated by treatment-free intervals

The role of T-cell exhaustion for T cell-recruiting BsAb therapy remains poorly understood. Given the fact that blinatumomab is administered as a continuous infusion over 28 days, we hypothesized that similar to the situation in chronic viral infections, T cells continuously exposed to a BsAb are rendered dysfunctional and exhausted. Having confirmed that T cells of r/r BCP-ALL patients become dysfunctional during blinatumomab therapy, we next set out to mimic continuous BsAb exposure of T cells for up to 28 days in an *in vitro* model system. Intriguingly, we could show that continuous BsAb stimulation led to upregulation and co-expression of coinhibitory checkpoint molecules, induction of the exhaustion-related TF TOX, decreasing secretion of effector cytokines, decreasing proliferative and cytotoxic capacity as well as glycolytic and mitochondrial impairment. Furthermore, we observed transcriptional induction of exhaustion-associated genes and transcriptional down-regulation of memory- and stemness-associated genes in continuously BsAb-stimulated T cells. Together, we could show that continuous BsAb stimulation induced hallmark features of T-cell exhaustion.

In a second step, we aimed to reinvigorate exhausted T cells by intermittent rather than continuous BsAb stimulation. Indeed, upon intermittent BsAb stimulation, we observed downregulation of inhibitory checkpoint molecules and found that secretion of effector cytokines, proliferative and cytotoxic potential as well as glycolytic and mitochondrial capacity was increased compared to continuously BsAb-stimulated T cells. Also, intermittently stimulated T cells transcriptionally induced memory-associated genes and downregulated exhaustion-associated genes. Lastly, intermittently but not continuously BsAb-stimulated T cells showed robust expansion and efficient killing of leukemic cells in an *in vivo* ALL patient-derived xenograft model.

In summary, we provide evidence that T-cell exhaustion induced by continuous antigen exposure limits the efficacy of BsAb-mediated immunotherapy and that adaptation of application schedules have the potential to strongly improve T-cell responses in patients.

3.2 Publication II

STING agonism turns human T cells into interferon-producing cells but impedes their functionality

STING is classically expressed by innate immune cells as a mechanism of anti-viral defense. Its role in human T cells and possible implications in T cell-based immunotherapy remain to be elucidated. We, therefore, set out to study the impact of the STING agonist cGAMP on the function of primary human T cells and unravel the underlying molecular mechanisms via CRISPR/Cas9 KO studies. We confirmed that both, cGAS and STING are expressed and functional in primary human T cells. Simultaneous TCR (CD3/CD28) and STING engagement (cGAMP) led to strong phosphorylation of STING, IRF3, and STAT1 and was required for the secretion of type I IFNs. KO studies confirmed that cGAMP-mediated effects in $CD4^+$ T cells were entirely STING-dependent and could be enhanced by concomitant TCR signaling. Moreover, release of IFN-β was dependent on STING, downstream IRF3 activation and in parts on IFNAR1 expression, pointing towards a positive feedback loop of type I IFNs in T cells. Mechanistically, using several small molecule inhibitors of TCR downstream signaling, we demonstrated that NF-kB signaling as well as Ca^{2+} flux was required for cGAMP-mediated STING activation and IFN-β release.

Interestingly, besides the type I IFN response, cGAMP treatment induced STING- and IRF3-dependent apoptosis in T cells. On the other hand, cGAMP treatment led to IRF3-independent impairment of T-cell proliferation. Also, substantial metabolic impairment, as evidenced by reduced basal and maximal mitochondrial respiration and glycolytic capacity, was observed in T cells upon simultaneous TCR and STING engagement.

Together, we provide valuable mechanistic insights into the cGAS/STING pathway in activated human T cells. Our findings may contribute to optimize current treatment strategies for cancer patients using STING agonists in combination with T cell-based immunotherapy.

4. Publication I

blood® Regular Article

IMMUNOBIOLOGY AND IMMUNOTHERAPY

T-cell exhaustion induced by continuous bispecific molecule exposure is ameliorated by treatment-free intervals

Nora Philipp,[1,2] Maryam Kazerani,[1,2] Alyssa Nicholls,[1,2] Binje Vick,[3,4] Jan Wulf,[1,2] Tobias Straub,[5] Michaela Scheurer,[1,2] Amelie Muth,[2] Gerulf Hänel,[1,2] Daniel Nixdorf,[1,2] Monika Sponheimer,[1,2] Malte Ohlmeyer,[1,2] Sonja M. Lacher,[1,2] Bettina Brauchle,[1,2] Anetta Marcinek,[1,2] Lisa Rohrbacher,[1,2] Alexandra Leutbecher,[1,2] Kai Rejeski,[1,2] Oliver Weigert,[1,3,6] Michael von Bergwelt-Baildon,[1] Sebastian Theurich,[1] Roman Kischel,[7,8] Irmela Jeremias,[3,4,9] Veit Bücklein,[1,2] and Marion Subklewe[1-3]

[1]Department of Medicine III, University Hospital, Ludwig Maximilian University (LMU) Munich, Munich, Germany; [2]Laboratory for Translational Cancer Immunology, LMU Gene Center, Munich, Germany; [3]German Cancer Consortium (DKTK) and German Cancer Research Center (DKFZ), Heidelberg, Germany; [4]Helmholtz Zentrum München, German Research Center for Environmental Health (HMGU), Munich, Germany; [5]Bioinformatics Unit, Biomedical Center, LMU Munich, Martinsried, Germany; [6]Experimental Leukemia and Lymphoma Research, Department of Medicine III, University Hospital, LMU Munich, Munich, Germany; [7]AMGEN Research Munich GmbH, Munich, Germany; [8]AMGEN Inc., Thousand Oaks, CA; and [9]Department of Pediatrics, Dr. von Hauner Children's Hospital, University Hospital, LMU, Munich, Germany

KEY POINTS

- **Continuous exposure to a CD19xCD3 bispecific molecule induces T-cell exhaustion.**
- **Treatment-free intervals transcriptionally reprogram and functionally reinvigorate T cells.**

T-cell–recruiting bispecific molecule therapy has yielded promising results in patients with hematologic malignancies; however, resistance and subsequent relapse remains a major challenge. T-cell exhaustion induced by persistent antigen stimulation or tonic receptor signaling has been reported to compromise outcomes of T-cell–based immunotherapies. The impact of continuous exposure to bispecifics on T-cell function, however, remains poorly understood. In relapsed/refractory B-cell precursor acute lymphoblastic leukemia patients, 28-day continuous infusion with the CD19xCD3 bispecific molecule blinatumomab led to declining T-cell function. In an in vitro model system, mimicking 28-day continuous infusion with the half-life–extended CD19xCD3 bispecific AMG 562, we identified hallmark features of exhaustion arising over time. Continuous AMG 562 exposure induced progressive loss of T-cell function (day 7 vs day 28 mean specific lysis: 88.4% vs 8.6%; n = 6; *P* = .0003). Treatment-free intervals (TFIs), achieved by AMG 562 withdrawal, were identified as a powerful strategy for counteracting exhaustion. TFIs induced strong functional reinvigoration of T cells (continuous vs TFI-specific lysis on day 14: 34.9% vs 93.4%; n = 6; *P* < .0001) and transcriptional reprogramming. Furthermore, use of a TFI led to improved T-cell expansion and tumor control in vivo. Our data demonstrate the relevance of T-cell exhaustion in bispecific antibody therapy and highlight that T cells can be functionally and transcriptionally rejuvenated with TFIs. In view of the growing number of bispecific molecules being evaluated in clinical trials, our findings emphasize the need to consider and evaluate TFIs in application schedules to improve clinical outcomes.

Introduction

T-cell–recruiting bispecific antibodies comprise a novel immunotherapeutic platform for the treatment of hematological malignancies and are currently being investigated in clinical trials.[1] The CD20xCD3 bispecifics glofitamab[2,3] and mosunetuzumab[4] have shown encouraging results in phase-I trials in patients with indolent or aggressive lymphomas. In patients with acute myeloid leukemia (AML), the CD123xCD3 molecule flotetuzumab demonstrated promising response rates.[5] To date, the only FDA-approved bispecific molecule is the CD19xCD3 molecule blinatumomab for treatment of relapsed/refractory (r/r) and minimal residual disease-positive (MRD^+) B-cell precursor acute lymphoblastic leukemia (BCP-ALL).[6-9]

Bispecific antibodies are administered using varying application schedules (continuous to weekly infusions) to achieve serum levels that support efficient T-cell recruitment. Owing to their short circulation half-lives, both flotetuzumab and blinatumomab are administered to eligible patients by 28-day continuous intravenous infusion (c.i.v.) during the first cycle.[5,9] Rates of response to blinatumomab in clinical trials were significantly higher compared with standard-of-care chemotherapy, with 43% in r/r and 81% in MRD^+ patients.[9,10] These results are encouraging; however, they also highlight that a considerable portion of patients remain refractory to therapy. To improve the response to bispecific antibodies, a better understanding of resistance mechanisms is urgently needed.

First clinical evidence that highly functional T cells are required for successful bispecific molecule therapy was provided by a phase-II follow-up analysis of r/r BCP-ALL patients treated with blinatumomab. Response to blinatumomab positively correlated with $CD3^+$ T-cell expansion,[11] whereas the frequency of regulatory T cells prior to therapy negatively correlated to response.[12] Furthermore, enrichment of exhausted T cells was reported in r/r BCP-ALL patients unresponsive to blinatumomab.[13]

T-cell exhaustion has been described in chronic viral infection in mice,[14,15] humans,[16,17] and, more recently, in cancer.[18-20] Upon continuous antigen exposure, T cells coexpress inhibitory checkpoint molecules including programmed cell death protein 1 (PD-1), T-cell immunoglobulin and mucin domain 3 (Tim-3), and lymphocyte activation gene 3 (LAG-3). Concomitantly, T cells enter a state of hypo-responsiveness, characterized by gradual loss of functions such as cytokine secretion, proliferation, and cytotoxicity.[16,21-23] Translating this concept into the clinical setting of bispecific therapies, we hypothesized that T-cell exhaustion occurs during continuous exposure to bispecific antibodies and contributes to resistance to therapy.

We therefore investigated the relevance of continuous long-term bispecific molecule stimulation on T-cell function and exhaustion in an in vitro model system using a CD19xCD3 half-life–extended bispecific molecule (AMG 562) for proof of concept. We demonstrate that continuous stimulation with bispecifics over 28 days induces T-cell exhaustion and we provide evidence that disruption of this stimulation using treatment-free intervals (TFIs) maintains high T-cell functionality and induces transcriptional reprogramming. Finally, we report improved antileukemic efficacy of TFI-stimulated vs continuously stimulated T cells in a patient-derived xenograft (PDX) ALL mouse model.

Methods

Assessment of ex vivo T-cell function of r/r BCP-ALL patients

T cells were isolated from peripheral blood mononuclear cells using the Pan T Cell Isolation Kit (Miltenyi Biotec, Bergisch Gladbach, Germany) and cocultured with the $CD19^+$ ALL cell line REH in culture medium (supplemental Table 1 and supplemental Materials and Methods, available on the *Blood* Web site) at an effector/target ratio (E:T) of 1:3 and 0.5 ng/mL blinatumomab or control construct. After 72 hours, cells were stained with AquaLiveDead and with antibodies against CD2, CD4, CD8, and CD19. Blinatumomab-mediated lysis of REH cells was determined using flow cytometry as described in Equation 1. On day 6, IFN-γ secretion was analyzed in supernatants via cytometric bead array (CBA):

$$\%\ \text{specific lysis} = \left(1 - \frac{CD19^+\ \text{target cell count blinatumomab}}{CD19^+\ \text{target cell count control construct}}\right) \times 100. \quad (1)$$

28-day stimulation of healthy donor T cells with AMG 562

Healthy donor (HD) T cells were isolated from peripheral blood mononuclear cells using the Human T Cell Isolation Kit (STEMCELL Technologies, Vancouver, Canada) and cocultured with irradiated OCI-Ly1 cells in culture medium (E:T = 1:4) containing 5 ng/mL AMG 562. On day 3, culture medium, target cells, and AMG 562 were replenished. On day 7, T cells were isolated from cultures (stimulation cycle 1) and functionally tested, as detailed below. Remaining T cells were recultured with OCI-Ly1 cells and AMG 562, as described above (stimulation cycle 2). The T cells underwent 4 stimulation cycles. For experiments implementing TFIs, T cells were cocultured with OCI-Ly1 cells in absence of AMG 562 during stimulation cycles 2 (days 7-14) and 4 (days 21-28).

Immunophenotyping of T cells

On days 3 and 7 of each stimulation cycle, cultures were stained with AquaLiveDead and antibodies against CD2, CD4, CD8, T-cell receptor αβ (TCRαβ), PD-1, Tim-3, and LAG-3. Additionally, cells were intranuclearly stained for the transcription factor TOX. Corresponding isotype controls were used. Median fluorescence intensity (MFI) ratios were calculated with Equation 2:

$$\text{MFI ratio} = \frac{\text{MFI stained sample}}{\text{MFI isotype control}}. \quad (2)$$

Quantification of cytokine secretion

Cytokine levels in supernatants were measured using CBA. In some experiments, isolated T cells were restimulated with phorbol myristate acetate (PMA; 20 ng/mL) and ionomycin (750 ng/mL) in the presence of GolgiStop/GolgiPlug solution containing monensin (25 nM) and brefeldin A (10 ng/mL; all Sigma-Aldrich, St. Louis, MO) for 4 hours at 37°C with 5% CO_2. Subsequently, cells were stained with AquaLiveDead and antibodies against CD2, CD4, and CD8, then permeabilized and stained intracellularly with antibodies against IFN-γ and TNF-α or corresponding isotype controls.

Proliferation and cytotoxicity assays

T cells were cocultured with hCD19-Ba/F3 or OCI-Ly1 cells (E:T = 1:1) and 5 ng/mL AMG 562 or control construct. After 72 hours, cells were stained with AquaLiveDead and antibodies against CD2, CD4, CD8, and CD19. AMG 562-mediated lysis of $CD19^+$ target cells and T-cell proliferation was calculated as described in Equations 1 and 3:

$$\text{Fold change} = \frac{CD2^+\ \text{cell count day3}}{CD2^+\ \text{cell count day0}}. \quad (3)$$

Cytotoxicity assays against OCI-Ly1 cells were incubated for 4 hours with GolgiStop/GolgiPlug solution followed by staining with AquaLiveDead and antibodies against CD2, CD4, CD8, and CD19. Then, cells were permeabilized and stained intracellularly for granzyme B or isotype control.

Metabolic stress tests

T cells were stimulated for 48 hours with CD3/CD28 Dynabeads (Thermo Fisher Scientific, Waltham, MA). After bead depletion, 2.5×10^5 T cells/well were plated on a poly-D-lysine-coated 96-well plate. Mitochondrial and glycolysis stress tests were performed on a Seahorse XFe96 Analyzer using corresponding kits (Agilent, Santa Clara, CA). Metabolic rate was normalized to cell count using a Cytation 1 reader (BioTek Instruments, Inc., Winooski, VT).

Bulk RNA sequencing

5×10^5 viable $CD3^+$ T cells were sorted and lysed in Trizol (Sigma-Aldrich). RNA was isolated using the RNA Clean and Concentrator-25 Kit (Zymo Research, Freiburg, Germany). Libraries were prepared using the NEBNext Ultra II Directional RNA Library Prep Kit for Illumina (New England BioLabs, Frankfurt, Germany).

In vivo studies

NOD.Cg-Prkdc^{scid} IL2rg^{tm1Wjl}/SzJ (NSG) mice were engrafted with PDX-ALL-265 cells expressing enhanced firefly luciferase and GFP. On day 28, mice received human T cells stimulated in vitro with AMG 562 for 14 days either continuously or with a TFI from day 7 to 14. Subsequently, mice were treated weekly with AMG 562 or control construct (cBiTE). Leukemia burden was monitored twice weekly by bioluminescence imaging.[24,25] The study protocol was reviewed and approved by local government authorities.

Statistical analysis

Prism 8 v.8.4.3. (471) (GraphPad Software, LLC) was used for data visualization and statistical analysis. The Mann-Whitney test, the Kruskal-Wallis and Dunn's multiple comparisons test, or two-way ANOVA and Sidak's multiple comparisons test was used for statistical testing, as specified in the respective figure legends. Not significant (ns) $P > .05$; *$P < .05$; **$P < .01$; ***$P < .001$; ****$P \leq 0.0001$.

Results

T cells of r/r ALL patients receiving blinatumomab show signs of dysfunction

We hypothesized that continuous exposure to bispecific molecules leads to T-cell exhaustion in patients. Hence, we tested ex vivo T-cell function of r/r BCP-ALL patients that received blinatumomab c.i.v. over 28 days (Table 1). Patient T cells showed high cytotoxicity and IFN-γ secretion prior to blinatumomab treatment. However, both significantly decreased ex vivo during blinatumomab c.i.v. (Figure 1A, mean specific lysis: prior = 73.1% vs during = 31.5%; $P = .0052$). Longitudinal analysis of T-cell function during the first blinatumomab cycle revealed a significant decline in ex vivo cytotoxicity and IFN-γ secretion within the first 2 weeks of blinatumomab c.i.v. Interestingly, T-cell function increased upon cessation of blinatumomab therapy (Figure 1B, mean specific lysis: day 0 = 73.1% vs day 14 = 17.4%; $P = .0176$; day 0 vs post = 48.5%; ns). These observations support the hypothesis that continuous exposure with bispecifics may lead to impaired T-cell function in patients.

Establishment of a continuous T-cell stimulation system in vitro with the CD19xCD3 bispecific AMG 562

Next, we aimed to translate the clinical setting into a stable, reproducible in vitro model system. We therefore established long-term T-cell stimulation with the CD19xCD3 bispecific molecule AMG 562 over 28 days. The diffuse large B-cell lymphoma cell line OCI-Ly1 was identified as suitable $CD19^+$ target cell line with slow AMG 562-mediated lysis kinetics to ensure the continued presence of the target antigen for at least 3 days (Figure 1C; mean specific lysis: SEM cells = 91.0% vs OCI-Ly1 cells = 20.8%; $P = .0073$). OCI-Ly1 cells express high levels of CD19, and HD T cells in coculture with OCI-Ly1 showed robust AMG 562-mediated activation and proliferation after 72 hours (Figure 1D-F; supplemental Figure 1B-C). Furthermore, costimulatory and coinhibitory molecule expression in OCI-Ly1 was comparable to primary ALL samples (n = 20, Figure 1G). The following data are based on 28-day cocultures with HD T cells and OCI-Ly1 cells in the presence of AMG 562, unless otherwise indicated (Figure 2A).

Continuous T-cell stimulation with AMG 562 over 28 days induces T-cell exhaustion in vitro

Immunophenotyping during AMG 562 stimulation showed that only a minor fraction of T cells coexpressed the inhibitory receptors (IRs) PD-1, Tim-3, and LAG-3 at baseline. However, after 7 days of AMG 562 stimulation, more than 60% of $CD4^+$ and $CD8^+$ T cells coexpressed 3 IRs. Coexpression was maintained until day 28 of continuous stimulation (Figure 2B; supplemental Figure 2A-B; mean % $CD8^+$ T cells: day 0 = 0.05% vs day 7 = 64.0%; $P = .004$; day 0 vs day 28 = 42.7%). Coexpression of IRs was accompanied by gradual upregulation of the transcription factor TOX (Figure 2B; supplemental Figure 2A-B; mean MFI ratio of $CD8^+$ T cells: day 0 = 4.2 vs day 28 = 12; $P = .0001$). Importantly, TOX upregulation was accompanied by progressive T-cell dysfunction. Comprehensive functional analysis revealed T-cell dysfunction starting approximately 2 weeks after AMG 562 stimulation commenced. Cytokine secretion into culture supernatants decreased significantly over the course of AMG 562 stimulation (Figure 2C; supplemental Figure 2E, mean IL-2 secretion: day 3 = 16 000 pg/mL vs day 24 = 75 pg/mL; $P < .0001$). We also observed that coexpression of IFN-γ and TNF-α by $CD4^+$ and $CD8^+$ T cells upon restimulation with PMA/ionomycin declined over time (Figure 2D, IFN-γ^+TNF-α^+ mean of $CD8^+$: day 0 = 19.6%, day 7 = 23.1%, day 21 = 9.9%). Furthermore, AMG 562-mediated T-cell proliferation and cytotoxicity against hCD19-Ba/F3 cells were highest with T cells extracted from the coculture on day 7, but significantly decreased with further AMG 562 stimulation (Figure 2E; $CD2^+$ fold change after 3 days of assay: day 7 = 2.1 vs day 28 = 0.05; $P < .0001$; mean specific lysis: day 7 = 88.4% vs day 28 = 8.6%; $P = .0003$). Similar results were observed in cytotoxicity assays against OCI-Ly1 cells (Figure 2F; supplemental Figure S2C). Importantly, T-cell exhaustion occurred upon continuous BsAb stimulation using different target cell lines and BsAbs (supplemental Figure 2F-G). Together, we found that continuous stimulation with AMG 562 for up to 28 days induced T-cell exhaustion.

TFIs reinvigorate T-cell function in vitro

We then hypothesized that disruption of continuous antigen exposure might allow the functional recovery of T cells and to ameliorate exhaustion. We therefore implemented resting periods (the aforementioned TFIs) between days 7-14 and days 21-28 by removing AMG 562 from cocultures and compared the function of T cells that had undergone TFIs with cells continuously (CONT) stimulated with AMG 562 (Figure 3A). During TFIs, a significantly smaller fraction of $CD4^+$ and $CD8^+$ T cells coexpressed PD-1, Tim-3, and LAG-3 (Figure 3B; supplemental Figure 3A, mean % of $CD8^+$ T cells at day 14: CONT = 57% vs TFI = 21.8%; $P = .013$). This effect was transient and coexpression was reestablished upon restimulation with AMG 562 (Figure 3B; supplemental Figure 3A, mean % of $CD8^+$ T

Table 1. Characteristics of r/r BCP-ALL patients prior to blinatumomab therapy

Patient	Age	Sex	Ph	Interval ID - blinatumomab (mo)	Prior therapies	Cytoreductive therapy prior to blinatumomab	Start of cytoreductive therapy prior to blinatumomab	Prior allo-SCT	Blast % (BM) prior to blinatumomab	Days sampled under blinatumomab
R1	37	m	−	21	GMALL induction I, II and consolidation I conditioning therapy for allo-SCT: TBI (3 × 6 Gy), cyclophosphamide	Vin/Dex	day −12	+	54	48
R2	35	m	−	9	GMALL induction I, II; HAM, FLAG	Vin	day −17	−	30 (PB)	14/21
R3	51	m	−	32	GMALL protocol (<55a, complete)	Cy	day −4	−	40	0/7/28
R4	32	m	−	5	GMALL induction I, II	−	−	−	52	1/8/28
R5	30	f	−	32	GMALL protocol (<55a, complete); repeated GMALL induction I	−	−	−	5	1/7/22
R6	70	f	+	18	EWALL elderly (complete, including dasatinib)	Cy/Dex	day −9	−	88	−2/12/28
R7	68	f	−	4	GMALL elderly (induction I, II)	−	−	−	24	0/7/42
R8	32	f	−	11	GMALL induction I, II and consolidation I conditioning therapy for allo-SCT: TBI (3 × 4 Gy), etoposide	−	−	+	70	0/21
R9	58	m	−	14	GMALL protocol (<55a, until consolidation IV)	FLAG-Ida	day −10	−	60	−1/7/44
R10	34	m	−	22	GMALL induction I, II and consolidation I conditioning therapy for allo-SCT: FLAMSA - TBI (2 × 4 Gy)	−	−	+	8	−1/7
R11	22	m	−	7	GMALL induction I, II and consolidation I FLAG-Ida	Cy/Dox/Vin	day −8	−	2	8/28/44
R12	20	m	−	46	CoALL protocol (complete); GMALL induction I, II and consolidation I, imatinib	−	−	−	70	0/16/22
R13	72	m	−	5	GMALL elderly (induction I, II, and consolidation I, II)	Cy	day −4	−	39	0/8/15

allo-SCT, allogeneic stem cell transplantation; BCP-ALL, B-cell precursor acute lymphoblastic leukemia; BM, bone marrow; Cy, cyclophosphamide; Dex, dexamethasone; Dox, doxorubicin; EWALL, European Working Group on Adult ALL; f, female; FLAG-Ida, fludarabine, Ara-C, G-CSF–idarubicin; FLAMSA, Fludarabin, Ara-C, Amsacrine; GMALL, German Multicenter Study Group For Adult ALL; ID, initial diagnosis; m, male; mo, month; PB, peripheral blood; Ph, Philadelphia chromosome; r/r, relapsed/refractory; TBI, total body irradiation; Vin, vincristine.

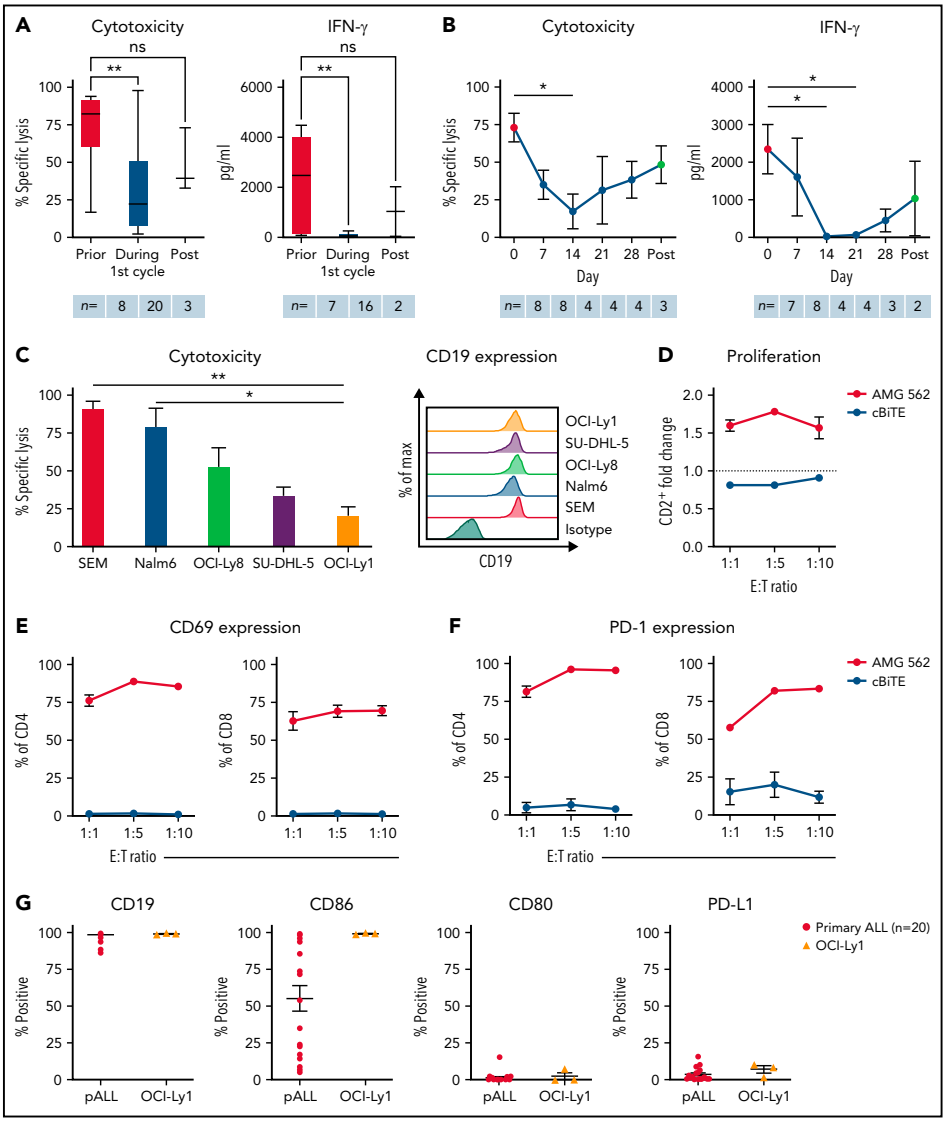

Figure 1. T cells of blinatumomab-treated ALL patients show signs of exhaustion ex vivo. (A) Blinatumomab-mediated cytotoxicity (n = 8–20) on day 3 and IFN-γ secretion (n = 7–16) on day 6 of T cells against REH cells (blinatumomab/control BiTE = 0.5 ng/mL, E:T = 1:3). The T cells were isolated from ALL patients prior to ("pre"), during and after the first cycle of blinatumomab therapy. (B) Blinatumomab-mediated cytotoxicity (n = 3–8) on day 3 and IFN-γ secretion (n = 2–8) on day 6 of T cells against REH cells (blinatumomab/control BiTE = 0.5 ng/mL, E:T = 1:3). The T cells were isolated from ALL patients at different timepoints during the first cycle of blinatumomab therapy. (C) AMG 562-mediated cytotoxicity (n = 3–6) and of HD T cells against ALL (SEM, Nalm6) and diffuse large B cell lymphoma (OCI-Ly8, SU-DHL-5, OCI-Ly1) cell lines (supplemental Table 1) after 4 days (AMG 562/control BiTE = 5 ng/mL, E:T = 1:3). Representative histograms of CD19 expression on ALL and diffuse large B cell lymphoma cell lines are shown. (D) $CD2^+$ fold change (n = 3) of HD T cells and (E-F) percentage of $CD69^+$ and PD-1^+ among $CD4^+$ and $CD8^+$ T cells after 3 days of cytotoxicity assay (AMG 562/control BiTE = 5 ng/mL) against OCI-Ly1 cells; n = 3. (G) Percentage of $CD19^+$, $CD86^+$, $CD80^+$, and PD-$L1^+$ primary ALL (n = 20) and OCI-Ly1 cells (n = 3). Boxplot whiskers indicate minima and maxima, and boxes represent the lower quartile, the median, and the upper quartile. All other graphs present mean ± SEM values. Statistical analysis: Kruskal–Wallis and Dunn's multiple comparison test (A–C); $^{ns}P > .05$; $^{*}P < .05$; $^{**}P < .01$. ALL, acute lymphoblastic leukemia; cBiTE, control BiTE, bispecific control construct; E:T, effector/target ratio; HD, healthy donor; ns, not significant; pALL, primary ALL; ± SEM, standard error of the mean.

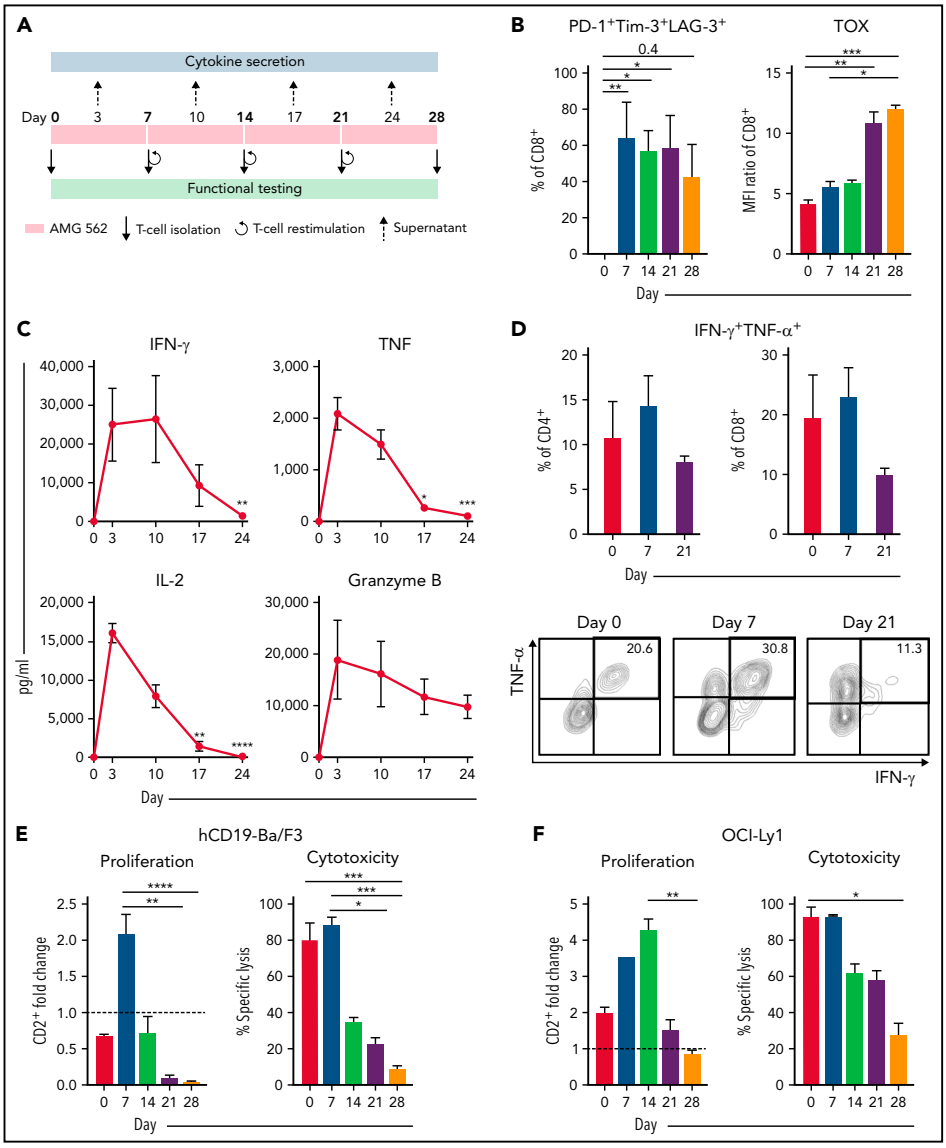

Figure 2. Continuous stimulation with AMG 562 induces T-cell exhaustion. (A) Timeline of continuous T-cell stimulation with AMG 562 and functional testing over 28 days. (B) Percentage of $CD8^+$ T cells coexpressing PD-1, Tim-3, and LAG-3 and the MFI ratio of TOX during continuous AMG 562 stimulation; n = 6. (C) Cytokine and granzyme B levels in coculture supernatants determined by CBA; n = 3–9. Significant differences compared with day 3 are indicated. (D) Percentage of IFN-γ and TNF-α double-positive $CD4^+$ and $CD8^+$ T cells after PMA/ionomycin restimulation. Representative examples of $CD8^+$ T cells from 1 donor are shown; n = 3. (E-F) AMG 562-mediated $CD2^+$ fold change (n = 3) and cytotoxicity against hCD19-Ba/F3 cells (E) or OCI-Ly1 cells (F) after 3 days (AMG 562/cBiTE = 5 ng/mL, E:T = 1:1); n = 6. Data are mean ± SEM values. Statistical analysis: Kruskal–Wallis and Dunn's multiple comparison test (B,C,E,F); *$P < .05$; **$P < .01$; *** $P < .001$; ****$P < .0001$. CBA, cytometric bead array; E:T, effector/target ratio; LAG-3, lymphocyte activation gene 3; MFI, median fluorescence intensity; PD-1, programmed cell death protein 1; PMA, phorbol myristate acetate;± SEM, standard error of the mean.

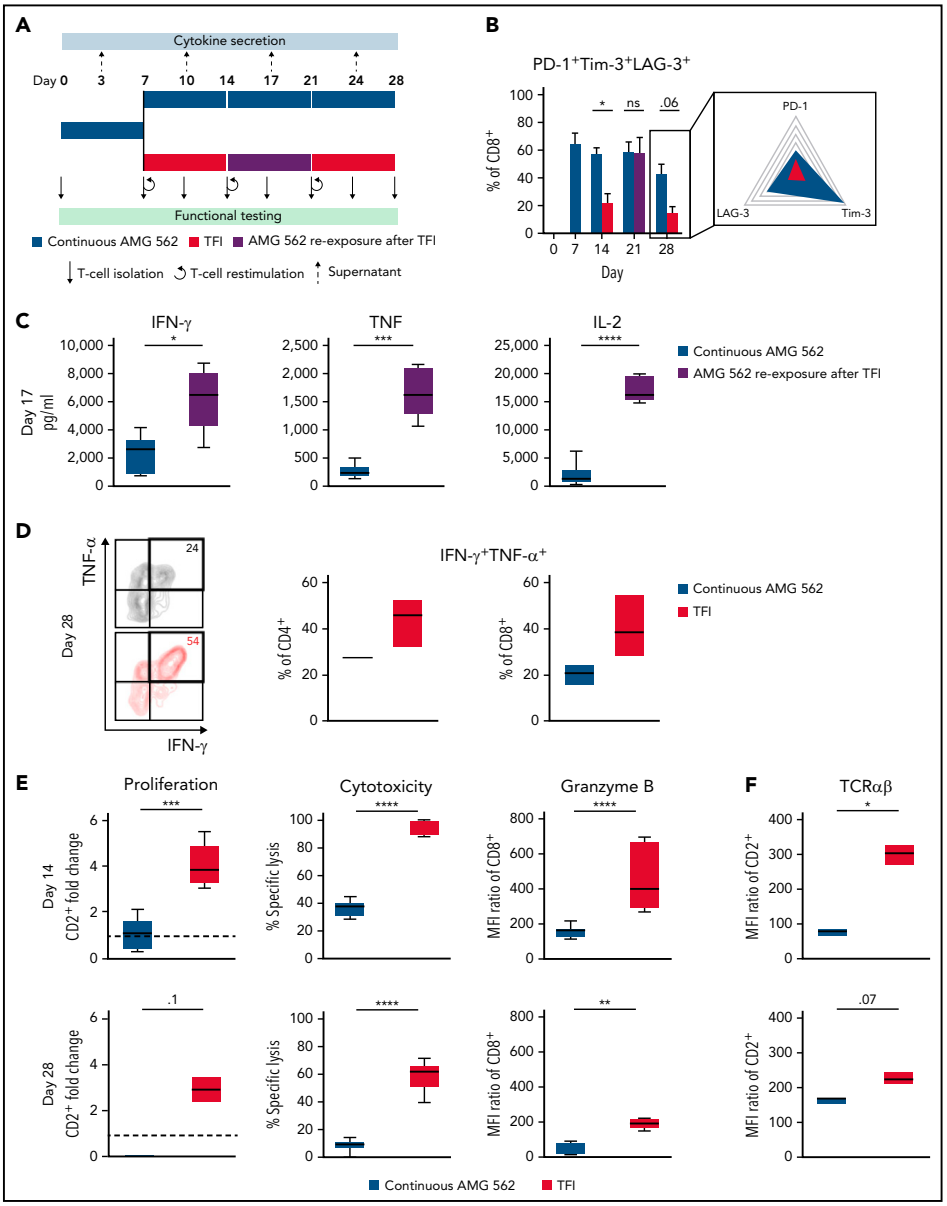

Figure 3. TFIs reinvigorate T-cell function. (A) Timeline of continuous vs TFI T-cell stimulation with AMG 562 over 28 days. (B) Percentage of $CD8^+$ T cells coexpressing PD-1, Tim-3, and LAG-3; n = 6. The spider plot (right) indicates coexpression on day 28 in continuously stimulated vs rested T cells from 1 representative donor. (C) Cytokine levels determined by CBA in coculture supernatants on day 17; n = 6. (D) Percentage of IFN-γ and TNF-α double-positive $CD4^+$ and $CD8^+$ T cells after PMA/ionomycin restimulation on day 28 of coculture; n = 3. Representative plots of $CD8^+$ T cells from 1 donor are shown. (E) AMG 562-mediated $CD2^+$ fold change (n = 3), cytotoxic capacity against hCD19-Ba/F3 cells (n = 6) and granzyme B expression (n = 6) of isolated T cells after 14 or 28 days of coculture. (F) TCR

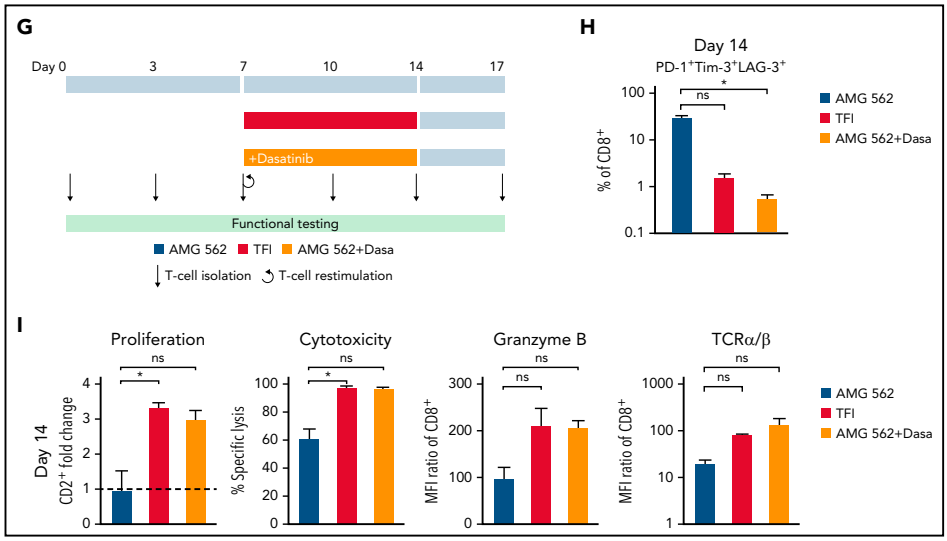

Figure 3 (continued) expression of T cells (n = 3) quantified by immunophenotyping during coculture. (G) Timeline of AMG 562+dasatinib-mediated T-cell stimulation in comparison with continuous or TFI stimulation over 17 days. Dasatinib = 100 nM. (H) Percentage of $CD8^+$ T cells coexpressing PD-1, Tim-3, and LAG-3; n = 3. (I) T-cell proliferation, cytotoxicity, Granzyme B, and TCR expression; n = 3. Boxplot whiskers indicate minima and maxima, and boxes represent the lower quartile, the median, and the upper quartile. Bar graphs present mean ± SEM values. Statistical analysis: 2-way ANOVA and Sidak's multiple comparison test (B,C,E-F,H–I); $^{ns}P > .05$; $^*P < .05$; $^{**}P < .01$; $^{***}P < .001$; $^{****}P < .0001$. CBA, cytometric bead array; LAG-3, lymphocyte activation gene 3; ns, not significant; PD-1, programmed cell death protein 1; PMA, phorbol myristate acetate; ± SEM, standard error of the mean; TCR, T-cell receptor; TFI(s), treatment-free interval(s).

cells at day 21: CONT = 58.7% vs TFI = 57.8%; $P > .99$). Despite the reexpression of IRs, secretion of cytokines on day 17 of the long-term culture was significantly higher in TFI-stimulated T cells (Figure 3C, mean IL-2 secretion: CONT = 1889 pg/mL vs TFI = 17 724 pg/mL; $P < .0001$). In concordance, TFIs increased the percentage of IFN-γ^+TNF-α^+ T cells upon PMA/ionomycin restimulation as compared with continuously stimulated T cells on day 28 of culture (Figure 3D, mean % of $CD8^+$ T cells: CONT = 20.6% vs TFI = 38.2%). Also, TFIs markedly reinvigorated AMG 562-mediated T-cell proliferation on days 14 and 28 of long-term culture (Figure 3E, mean $CD2^+$ fold change after 3 days of assay; day 14: CONT = 1.1 vs TFI = 4.1; $P = .002$; day 28: CONT = 0.06 vs TFI = 2.8; $P = .09$). This was accompanied by significantly increased cytotoxicity (mean specific lysis; day 14: CONT = 34.9% vs TFI = 93.4%; $P < .0001$; day 28: CONT = 8.6% vs TFI = 58.7%; $P < .0001$) and granzyme B production (mean MFI ratio of $CD8^+$ T cells; day 14: CONT = 144.5 vs TFI = 451.8; $P < .0001$; day 28: CONT = 45.5 vs TFI = 196.1; $P = .0038$). Importantly, T-cell exhaustion and reinvigoration by a TFI could be reproduced by using the AML cell line Molm-13 and a CD33xCD3 half-life extended bispecific molecule for continuous or TFI-stimulation (supplemental Figure 3G). We also observed that T cells upregulated TCRαβ during TFIs (Figure 3F, mean MFI ratio of $CD2^+$; day 14: CONT = 74.3 vs TFI = 299.6; $P = .016$), pointing toward a possible mechanism behind the enhanced function in TFI-stimulated T cells. Notably, inhibition of TCR signaling by intermittent addition of the Src kinase inhibitor dasatinib[26,27] during continuous AMG 562 stimulation led to similar results (Figure 3G-I; supplemental Figure 4).

TFIs maintain high metabolic fitness of T cells

Highly functional T cells have significant energy demands, and T-cell exhaustion confers changes in the T cell's metabolic program.[28] We therefore hypothesized that exhausted and TFI-stimulated T cells possess distinct metabolic phenotypes and compared the metabolic profiles of continuously AMG 562-stimulated with TFI-stimulated T cells. Indeed, loss of effector function in continuously stimulated T cells (Figure 2) was accompanied by mitochondrial impairment (Figure 4A, oxygen consumption rate [OCR], in pmol/min/1000 cells; mean maximal OCR: day 0 = 3.3 vs day 14 = 1.0; $P = .0169$). Strikingly, on day 14, TFI-stimulated T cells showed significantly higher basal and maximal mitochondrial respiration and spare respiratory capacity (SRC; Figure 4B, OCR in pmol/min/1000 cells; mean maximal OCR: CONT = 3.9 vs TFI = 13.5; $P = .0079$; SRC: CONT = 2.2 vs TFI = 8.5; $P = .0317$). Furthermore, TFI-stimulated T cells maintained higher glycolytic capacity and glycolytic reserve (Figure 4C, mean glycolytic reserve in mpH/min/1000 cells: CONT = 0.2 vs TFI = 0.6; $P = .0397$). Similar effects were observed even after 28 days of continuous vs TFI AMG 562 stimulation (supplemental Figure 3E-F). Overall, these data indicate that continuously AMG 562-stimulated T cells are metabolically impaired, whereas a TFI maintains high metabolic fitness.

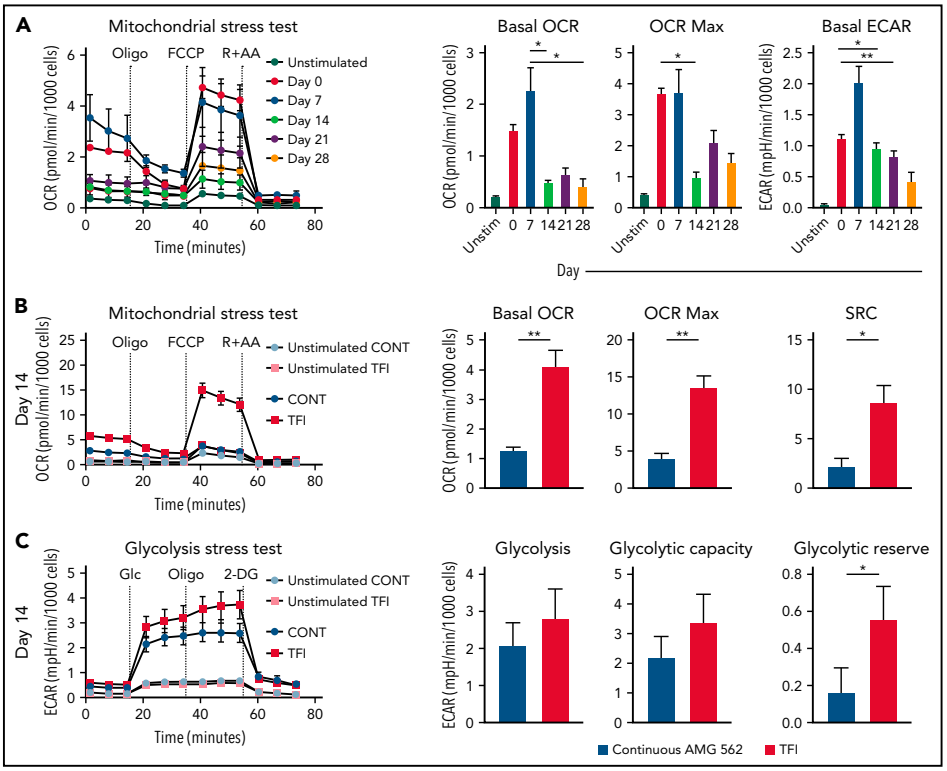

Figure 4. TFIs maintain high T-cell metabolic fitness. (A) Kinetic plot and corresponding bar graphs of normalized OCR obtained during mitochondrial stress test of T cells continuously stimulated with AMG 562; n = 3. (B) Kinetic plot and corresponding bar graphs of normalized OCR obtained during mitochondrial stress test of T cells after 14 days of continuous vs TFI AMG 562 stimulation; n = 5. (C) Kinetic plot and corresponding bar graphs of normalized ECAR obtained during glycolysis stress test of T cells after 14 days of continuous vs TFI AMG 562 stimulation; n = 5. All graphs present mean ± SEM values. Statistical analysis: Kruskal–Wallis and Dunn's multiple comparison test (A); 2-way ANOVA and Sidak's multiple comparison test (B-C); $*P < .05$; $**P < .01$. ECAR, extracellular acidification rate; OCR, oxygen consumption rate; ±SEM, standard error of the mean; TFI(s), treatment-free interval(s).

TFIs induce transcriptional reprogramming of T cells

Next, we performed bulk RNA sequencing of T cells after continuous AMG 562 stimulation or with TFIs to identify transcriptional profiles that drive the profound functional and metabolic differences observed. Samples were processed in 3 batches as shown in supplemental Figure 6I. Unbiased principal component analysis revealed separate clustering of samples according to timepoint and/or treatment (Figure 5A). Differentially expressed gene analysis of day-14 TFI vs CONT T cells identified 1902 significantly upregulated and 2603 downregulated genes ($P_{adj} < .05$). Unsupervised clustering of the top 100 differentially expressed genes showed striking similarity in gene expression patterns in unstimulated (day 0) and day-14 TFI T cells (Figure 5C), suggesting transcriptional reprogramming. Intriguingly, memory-related genes were highly enriched on day 14 of the TFI stimulation (*TCF7*, *IL7R*, and *SELL*; Figure 5B-D). Genes related to cell cycle (*CCNB1* and *CDK1*) and activation (*IL2RA*) were downregulated in day-14 TFI vs CONT T cells (Figure 5B-C). In line with functional reinvigoration (Figure 3), genes involved in T-cell exhaustion (*NR4A3*, *IRF4*, *PDCD1*, *LAG3*) were downregulated in day-14 TFI compared with continuously stimulated T cells (Figure 5B). Pathway analysis of day-14 TFI vs CONT T cells confirmed downregulation of the cell cycle (G2M checkpoint, normalized enrichment score [NES] = −2.47, $P_{adj} = 6.3E^{-10}$) and metabolism (MTORC1 signaling, NES = −2.27, OXPHOS, NES = −2.03; $P_{adj} = 6.3E^{-10}$) in line with T-cell quiescence during a TFI (Figure 5E). Gene set enrichment analysis also showed enrichment of memory- compared with effector-related genes identified in a chronic lymphocytic choriomeningitis virus infection model[29] in day-14 TFI-stimulated T cells (Figure 5F; GSE9650, NES = −1.95, false-discovery rate $q = 0.0$). Together, these data suggest that day-14 TFI-stimulated T cells were functionally and transcriptionally rejuvenated during the TFI.

Interestingly, after 7 days of restimulation with AMG 562 (day-21 TFI) T cells reexpressed genes involved in activation, growth

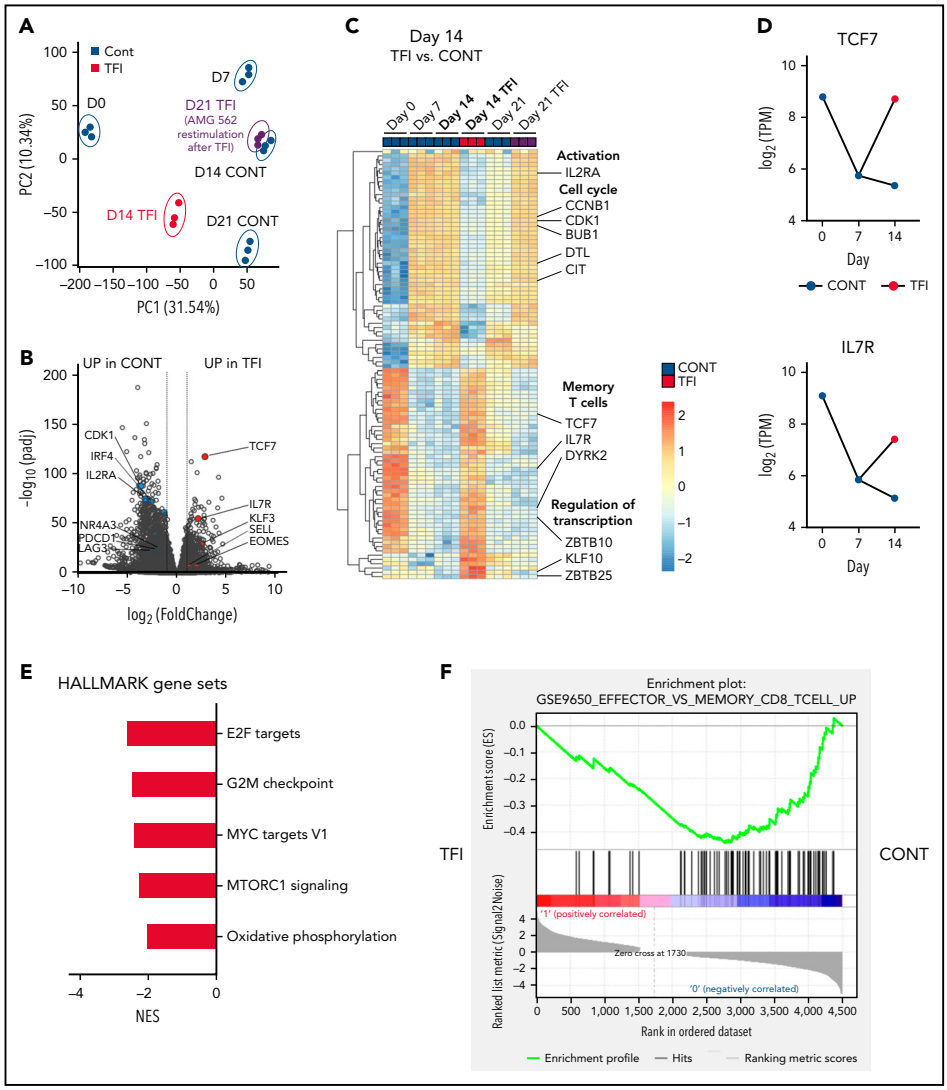

Figure 5. T cells are transcriptionally reprogrammed during TFIs. (A) Principal component analysis. (B) Volcano plot of day 14 TFI vs CONT T cells; $P_{adj} < .05$. Selected genes are highlighted as significantly downregulated (blue) or significantly upregulated (red) in TFI vs CONT cells. (C) Heatmap with hierarchical clustering of the top 100 differentially expressed genes in day-14 TFI vs CONT T cells; $P_{adj} < .05$. Selected genes are highlighted. (D) Log_2(TPM) expression level of *TCF7* and *IL7R* across timepoints 0, 7, and 14 days in TFI vs CONT T cells. (E) Pathways enriched in day-14 TFI vs CONT T cells; $P_{adj} < .05$. (F) Gene set enrichment analysis of day-14 TFI vs CONT T cells using MSigDB and the gene set GSE9650_EFFECTOR_VS_MEMORY_CD8_TCELL_UP.[29] Line plots present mean ± SEM values. CONT, continuously; NES, normalized enrichment score; ±SEM, standard error of the mean; TFI(s), treatment-free interval(s).

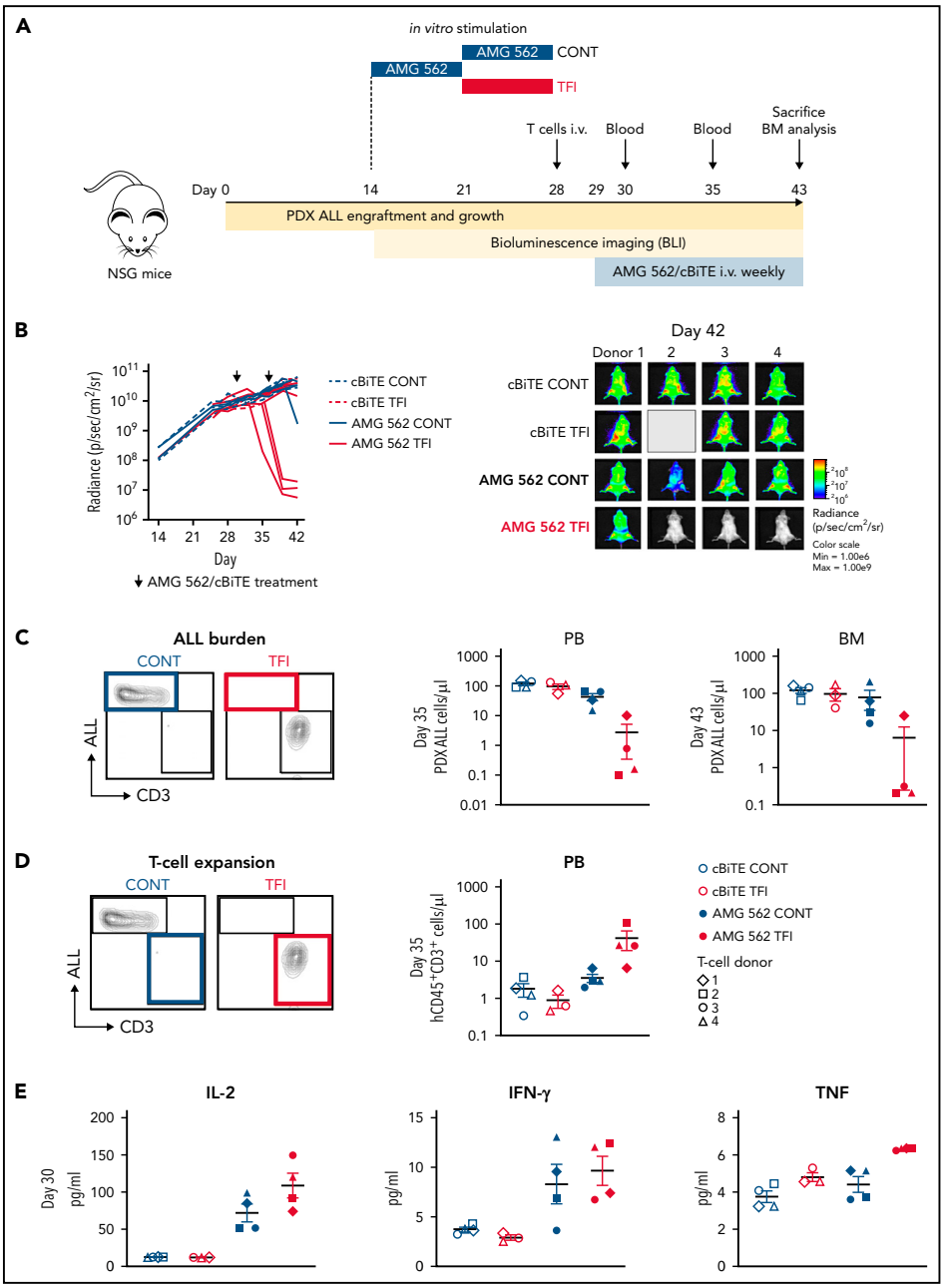

Figure 6.

(*DPP4* and *SLC3A2*) and cell cycle (*CDK1* and *PLK1*) whereas exhaustion-related genes (*LAG-3*, *BTLA*, and *NFATC1*) were downregulated compared with continuously stimulated cells (supplemental Figure 6A-C). This confirmed the enhanced effector function in day-21 TFI vs continuously stimulated T cells, although the effect was less pronounced compared with day 14 (supplemental Figure 3B-D). Furthermore, we found upregulation of natural killer receptor genes in day-21 CONT vs TFI T cells, which has recently been linked to dysfunctional chimeric antigen receptor (CAR) T-cell states[30] (supplemental Figure 6H). Pathway analysis revealed that identical pathways downregulated on day-14 TFI-receiving T cells were enriched by day 21 and effector- rather than memory-related genes were enriched in a gene set enrichment analysis (supplemental Figure 6D-E). These data suggest that day-21 TFI T cells are reactivated upon AMG 562 reexposure and less exhausted than continuously stimulated T cells. However, we observed downregulation of effector-associated genes (*GZMK* and *IL-2*) and enrichment of exhaustion-associated genes (*TOX* and *CD244*) in day-21 TFI vs day-7 T cells (supplemental Figure 6F-G). These observations underline that upon restimulation with AMG 562 after a TFI T-cell function tends to decrease again (supplemental Figure 3B-F) and support the notion that TFIs have the potential to delay but not to fully prevent exhaustion.

TFIs improve AMG 562-mediated leukemia control in vivo

Lastly, we aimed to confirm the in vivo relevance of a TFI for enhanced T-cell function. Thus, HD T cells were stimulated in vitro for 14 days continuously with AMG 562 or with a TFI, and subsequently transplanted into NSG mice bearing PDX-ALL cells (Figure 6A). Strikingly, T cells receiving a TFI, but not those continuously stimulated, were able to clear the leukemia in mice receiving AMG 562 treatment, as quantified by bioluminescence imaging and peripheral blood) and bone marrow analysis (Figure 6B-C; supplemental Figure 7; mean PDX-ALL cells/μL in bone marrow on day 43 post-ALL engraftment: CONT = 75.0 vs TFI = 6.2). We also observed greater expansion of TFI T cells in peripheral blood 6 days after initial AMG 562 injection in vivo (Figure 6D; mean $CD3^+$ cells/μL: CONT = 3.5 vs TFI = 41.5) and higher levels of human cytokines in murine plasma 1 day after first AMG 562 injection in vivo (Figure 6E; mean concentration of IL-2: CONT = 71.9 pg/mL vs TFI = 108.6 pg/mL). Together, these data confirm that a TFI preserved the high antileukemic activity of T cells in vivo, whereas continuously stimulated T cells failed to control the tumors.

Discussion

T-cell-recruiting bispecific antibodies have shown promising response rates in patients. However, a considerable portion of patients remain refractory to therapy.[9] One contributor to resistance to therapy is preexisting T-cell dysfunction in patients.[11,13] Independent of initial T-cell compartment composition, however, continuous antigen stimulation via the TCR,[29,31] or tonic CAR signaling,[26,32] have been postulated as major causes of T-cell exhaustion. Therefore, to improve patient outcomes, a deeper understanding of the development of T-cell function during therapy with bispecifics is needed. We demonstrate here that ex vivo T-cell function of r/r BCP-ALL patients deteriorated during blinatumomab c.i.v., particularly within the first 14 days of therapy. In a study in pediatric ALL patients, those that showed no response to blinatumomab on day 15 also failed to reach MRD negativity on day 29.[33] This hints that response occurs early during treatment and leads to the hypothesis that continuous exposure to bispecifics induces T-cell exhaustion. We are the first to comprehensively analyze T-cell exhaustion in the context of bispecifics using a stable 28-day in vitro model system. We could thereby mimic chronic exposure to a bispecific antibody over a clinically relevant time period and monitor T-cell function in a standardized manner. Using this system, we observed gradual upregulation of TOX and multiple IRs over the course of AMG 562 stimulation, accompanied by progressive decline in cytokine secretion, T-cell proliferation, and cytotoxicity. These findings recapitulate well-known hallmark features of exhaustion identified in chronic viral infection and cancer,[16,23,34] underlining the suitability of our model system to study T-cell exhaustion.

Strategies to preserve T-cell function and achieve durable antitumor responses are urgently needed. Using our model system, we show that a powerful strategy to maintain T-cell function is disruption of continuous bispecific stimulation with TFIs. Using this strategy, we report a sustained high level of secretion of effector cytokines, T-cell proliferation, and cytotoxicity over 28 days, with metabolic reinvigoration and transcriptional reprogramming of T cells. In concordance, recent studies demonstrated the functional reinvigoration of a tonically signaling GD2-CAR by invoking resting periods.[26] Furthermore, a phase I/II study reported an improved safety profile for r/r AML patients receiving intermittent flotetuzumab treatment in combination with stepwise dosing during week 1, dexamethasone pretreatment, and tocilizumab.[5] Another phase I/II study, treating Ph^+ ALL patients with dasatinib[26,27] in combination with blinatumomab c.i.v., reported an overall survival rate of 95%[35] and an increase in peripheral lymphocytes,[36] consistent with our observation that T-cell function can be reinvigorated to a similar extent using TFIs or pharmacological inhibition of TCR signaling with dasatinib (Figure 3; supplemental Figure 4). Together, these studies underline the potential of TFIs for reinvigorating T cells and for fine-tuning T-cell responses in patients.

We show improved expansion and tumor control of in vitro TFI-stimulated T cells using an ALL-PDX mouse model. While this model system underlines the relevance of the rested T-cell phenotype in vivo, suitable mouse models need to be developed in

Figure 6. TFIs improve AMG 562-mediated control of ALL in vivo. (A) Timeline of in vivo experiment: PDX-ALL cells were transplanted into NSG mice. T cells (4 donors) were stimulated in vitro for 14 days continuously or with TFI cells (days 7-14) and subsequently injected into NSG mice 28 days post engraftment. Mice were treated with AMG 562/control BiTE = 5 ng/mL on days 1 and 8 post T-cell injection. T-cell function and ALL burden was analyzed via bioluminescence imaging and flow cytometry. (B) Quantification of bioluminescence imaging signals (left panel) and images of mice on day 42 after engraftment (right panel). See supplemental Figure 7B for images of all timepoints. (C) Flow cytometry analysis of PDX-ALL cells detected in PB on day 35 and in BM on day 43. Representative plots from 1 T-cell donor are shown. (D) $CD3^+$ T-cell expansion in PB on day 35. Representative plots from 1 T-cell donor are shown. (E) Human cytokine levels detected in murine plasma on day 30. All graphs present mean ± SEM values. BM, bone marrow; cBiTE, control BiTE, bispecific control construct; CONT, continuously; PB, peripheral blood; PDX-ALL, patient-derived xenograft acute lymphoblastic leukemia; NSG, NOD.Cg-Prkdc^{scid} IL2rg^{tm1Wjl}/SzJ; ±SEM, standard error of the mean; TFI(s), treatment-free interval(s).

future studies to mimic continuous vs intermittent BsAb administration in vivo.

Targeting PD-1/PD-L1 to overcome T-cell exhaustion has shown efficacy in cancer. The combination of a CD33xCD3 BiTE® construct with disruption of PD-1/PD-L1 signaling increased antitumor responses in preclinical AML models.[37] Similar findings in CAR T cells[38-40] led to the initiation of clinical trials.[41] Intriguingly, T-cell reinvigoration through TFIs was much more efficient than continuous AMG 562 + nivolumab (a PD-1 inhibitor) treatment, the latter showing no to modest T-cell reinvigoration (supplemental Figure 5). In concordance, PD-1 blockade alone failed to reverse phenotypic and transcriptomic hallmarks of exhaustion in CAR T cells.[26] This highlights the need to deepen our understanding of the molecular networks involved in T-cell exhaustion.

T-cell metabolism is closely associated with effector function.[28,42,43]. In metabolic stress tests TFIs significantly enhanced T-cell metabolic fitness, along with increased effector function. In line with these observations, enhanced expansion, persistence, and survival of BBζ vs 28ζ CAR T cells have been linked to higher mitochondrial capacity.[44] In chronic lymphocytic leukemia patients, high metabolic fitness of CAR T cells prior to infusion correlated with response to therapy,[45] underlining the importance of metabolic fitness for successful immunotherapy.

High SRC, observed in TFI-stimulated T cells, is a hallmark feature of memory T cells,[28] and is consistent with upregulation of memory-associated genes in day-14 TFI-stimulated T cells. Transcriptional reprogramming of T cells during a TFI recapitulates findings made in transiently rested CAR T cells[26] and preclinical models of resolved chronic infection,[46] and confirmed the superior function of TFI- compared with continuously AMG 562-stimulated T cells. Intriguingly, we found that reinvigorated function in day-14 TFI-stimulated T cells coincided with sustained expression of *TCF7* (encoding TCF-1). TCF-1 is expressed in precursor-exhausted T cells (T_{PEX}) with the potential to self-renew and to give rise to terminally exhausted TCF-1-negative T cells (T_{EX}). Furthermore, T_{PEX} cells retain the ability to be functionally reinvigorated by checkpoint blockade.[47-52] Our findings support the notion that *TCF7* expression correlates with T-cell function and distinguishes T_{EX} from functional T_{PEX} cells.

In summary, we identified T-cell exhaustion as a potential mechanism contributing to resistance to bispecifics therapy in a preclinical model. The reinvigorating effect of TFIs on T cells suggests the relevance of resting periods between bispecific antibody treatment cycles. Hence, the implementation of TFIs should be considered for the design of administration schedules in the future. In light of the similarities between the exhausted T-cell phenotypes in chronic viral infections and CAR T-cell and bispecific antibody therapy, TFIs might be applicable to other T-cell–based immunotherapies.

Acknowledgments

The authors thank Sabine Sandner-Thiede, Simone Pentz, Elke Habben, Ewelina Zientara, and Bianca Kirschbaum (University Hospital, Ludwig Maximilian University Munich) and Maike Fritschle (Helmholtz Zentrum Munich) for their excellent technical support. The authors also thank O.W. and Andreas Moosmann for their expert advice. Thanks also go to Karsten Spiekermann, who kindly provided the Ba/F3 cell lines. The authors furthermore thank Eslam Katab for preliminary work on this project. They acknowledge the iFlow Core Facility of the University Hospital Munich (INST 409/225-1 FUGG) for assistance with generating the flow cytometry data.

The work was supported by the Bavarian Elite Graduate School "i-target" (to N.P.), the Else-Kröner-Fresenius Forschungskolleg CSP Cancer Immunotherapy (to V.B.), the Wilhelm-Sander Stiftung (to G.H.), the Sonderforschungsbereich SFB 338 (to M. Subklewe), and research funding from Amgen (to M. Subklewe). O.W. is supported by an Else-Kröner Excellence Fellowship from the Else-Kröner-Fresenius Stiftung (Project-ID 2021_EKES.13).

Authorship

Contribution: M. Subklewe, V.B., R.K., and N.P. designed the study and supervised the project; N.P., M.K., V.B., B.V., T.S., and M. Subklewe wrote the manuscript; N.P., A.N., J.W., M. Scheurer, A. Muth, G.H., and M.O. performed experiments and analyzed and/or interpreted the data; M. Subklewe, V.B., R.K., N.P., M.K., D.N., S.M.L., B.B., S.T., I.J., G.H., M. Sponheimer, A. Marcinek, L.R., A.L., and K.R. were involved in research design and data interpretation; O.W. and M.v.B.-B. critically reviewed and discussed the data. M.K. performed the library preparation for bulk RNA-seq and, in collaboration with T.S., conducted the bioinformatic analysis; B.V. and I.J. designed and performed the in vivo experiments.

Conflict-of-interest disclosure: M. Subklewe has received industry research support from Amgen, Gilead, Miltenyi Biotec, Morphosys, Roche, and Seattle Genetics, and has served as a consultant/advisor to Amgen, BMS, Celgene, Gilead, Pfizer, Novartis, and Roche. She sits on the advisory boards of Amgen, Celgene, Gilead, Janssen, Novartis, Pfizer, and Seattle Genetics, and serves on the speakers' bureau at Amgen, Celgene, Gilead, Janssen, and Pfizer. V.B. has received research funding from Miltenyi Biotec, Novartis, and Pfizer, and has served as a consultant/advisor to Novartis, Amgen, and Gilead. He serves on the speakers' bureau at Novartis and Pfizer. R.K. is employed at Amgen Research Munich, Germany. S.M.L. receives research funding from Roche. M.v.B.-B. has received research support from and serves on the speakers' bureau at Gilead, Miltenyi Biotec, MSD Sharpe & Dohme, Roche, Mologen, Novartis, Astellas, and BMS. K.R. received research funding from Gilead and honoraria from Gilead and Novartis. O.W. has received research funding from Roche. He serves on the speakers' bureau at Janssen and sits on the advisory board of Epizyme. S.T. has served as a consultant/advisor to Amgen, BMS, GSK, Janssen, Pfizer, Sanofi, and Takeda. The remaining authors declare no competing financial interests.

The current affiliation for B.B. is Adivo GmbH, Martinsried, Germany.

ORCID profiles: N.P., 0000-0002-3918-7795; M. Kazerani, 0000-0002-5803-4807; B.V., 0000-0003-1956-2778; G.H., 0000-0003-4685-6499; D.N., 0000-0003-1612-9952; L.R., 0000-0001-7012-2896; O.W., 0000-0002-0987-7373; S.T., 0000-0001-5706-8258; I.J., 0000-0003-1773-7677; V.B., 0000-0001-7391-7280; M.S., 0000-0003-3905-0251.

Correspondence: Marion Subklewe, Department of Medicine III, University Hospital, Ludwig Maximilian University, Munich, Germany; e-mail: Marion.Subklewe@med.uni-muenchen.de

Footnotes

Submitted 21 March 2022; accepted 7 July 2022; prepublished online on *Blood* First Edition 25 July 2022. DOI 10.1182/blood.2022015956.

RNA-seq data discussed in this publication have been deposited in the Gene Expression Omnibus database (accession number GSE196463).

The online version of this article contains a data supplement.

There is a *Blood* Commentary on this article in this issue.

The publication costs of this article were defrayed in part by page charge payment. Therefore, and solely to indicate this fact, this article is hereby marked "advertisement" in accordance with 18 USC section 1734.

REFERENCES

1. Labrijn AF, Janmaat ML, Reichert JM, Parren PWHI. Bispecific antibodies: a mechanistic review of the pipeline. *Nat Rev Drug Discov*. 2019;18(8):585-608.
2. Hutchings M, Morschhauser F, Iacoboni G, et al. Glofitamab, a novel, bivalent CD20-targeting T-cell-engaging bispecific antibody, induces durable complete remissions in relapsed or refractory B-cell lymphoma: a phase I trial. *J Clin Oncol*. 2021;39(18):1959-1970.
3. Bröske AE, Korfi K, Belousov A, et al. Pharmacodynamics and molecular correlates of response to glofitamab in relapsed/refractory non-Hodgkin lymphoma. *Blood Adv*. 2022:6(3):1025-1037.
4. Assouline SE, Kim WS, Sehn LH, et al. Mosunetuzumab shows promising efficacy in patients with multiply relapsed follicular lymphoma: updated clinical experience from a phase I dose-escalation trial. *Blood*. 2020;136(suppl 1):42-44.
5. Uy GL, Aldoss I, Foster MC, et al. Flotetuzumab as salvage immunotherapy for refractory acute myeloid leukemia. *Blood*. 2021;137(6):751-762.
6. Haas C, Krinner E, Brischwein K, et al. Mode of cytotoxic action of T cell-engaging BiTE antibody MT110. *Immunobiology*. 2009;214(6):441-453.
7. Wu J, Fu J, Zhang M, Liu D. Blinatumomab: a bispecific T cell engager (BiTE) antibody against CD19/CD3 for refractory acute lymphoid leukemia. *J Hematol Oncol*. 2015;8(1):104.
8. Zugmaier G, Klinger M, Schmidt M, Subklewe M. Clinical overview of anti-CD19 BiTE(®) and ex vivo data from anti-CD33 BiTE(®) as examples for retargeting T cells in hematologic malignancies. *Mol Immunol*. 2015;67(2 Pt A):58-66.
9. Topp MS, Gökbuget N, Stein AS, et al. Safety and activity of blinatumomab for adult patients with relapsed or refractory B-precursor acute lymphoblastic leukaemia: a multicentre, single-arm, phase 2 study. *Lancet Oncol*. 2015;16(1):57-66.
10. Kantarjian H, Stein A, Gökbuget N, et al. Blinatumomab versus chemotherapy for advanced acute lymphoblastic leukemia. *N Engl J Med*. 2017;376(9):836-847.
11. Zugmaier G, Gökbuget N, Klinger M, et al. Long-term survival and T-cell kinetics in relapsed/refractory ALL patients who achieved MRD response after blinatumomab treatment. *Blood*. 2015;126(24):2578-2584.
12. Duell J, Dittrich M, Bedke T, et al. Frequency of regulatory T cells determines the outcome of the T-cell-engaging antibody blinatumomab in patients with B-precursor ALL. *Leukemia*. 2017;31(10):2181-2190.
13. Zhao Y, Aldoss I, Qu C, et al. Tumor-intrinsic and -extrinsic determinants of response to blinatumomab in adults with B-ALL. *Blood*. 2021;137(4):471-484.
14. Zajac AJ, Blattman JN, Murali-Krishna K, et al. Viral immune evasion due to persistence of activated T cells without effector function. *J Exp Med*. 1998;188(12):2205-2213.
15. Gallimore A, Glithero A, Godkin A, et al. Induction and exhaustion of lymphocytic choriomeningitis virus-specific cytotoxic T lymphocytes visualized using soluble tetrameric major histocompatibility complex class I-peptide complexes. *J Exp Med*. 1998;187(9):1383-1393.
16. Wherry EJ. T cell exhaustion. *Nat Immunol*. 2011;12(6):492-499.
17. Schietinger A, Greenberg PD. Tolerance and exhaustion: defining mechanisms of T cell dysfunction. *Trends Immunol*. 2014;35(2):51-60.
18. Zippelius A, Batard P, Rubio-Godoy V, et al. Effector function of human tumor-specific CD8 T cells in melanoma lesions: a state of local functional tolerance. *Cancer Res*. 2004;64(8):2865-2873.
19. Kim PS, Ahmed R. Features of responding T cells in cancer and chronic infection. *Curr Opin Immunol*. 2010;22(2):223-230.
20. Fourcade J, Sun Z, Pagliano O, et al. CD8$^+$ T cells specific for tumor antigens can be rendered dysfunctional by the tumor microenvironment through upregulation of the inhibitory receptors BTLA and PD-1. *Cancer Res*. 2012;72(4):887-896.
21. Wherry EJ, Blattman JN, Murali-Krishna K, van der Most R, Ahmed R. Viral persistence alters CD8 T-cell immunodominance and tissue distribution and results in distinct stages of functional impairment. *J Virol*. 2003;77(8):4911-4927.
22. Fuller MJ, Zajac AJ. Ablation of CD8 and CD4 T cell responses by high viral loads. *J Immunol*. 2003;170(1):477-486.
23. Wherry EJ, Kurachi M. Molecular and cellular insights into T cell exhaustion. *Nat Rev Immunol*. 2015;15(8):486-499.
24. Vick B, Rothenberg M, Sandhöfer N, et al. An advanced preclinical mouse model for acute myeloid leukemia using patients' cells of various genetic subgroups and in vivo bioluminescence imaging. *PLoS One*. 2015;10(3):e0120925.
25. Ebinger S, Özdemir EZ, Ziegenhain C, et al. Characterization of rare, dormant, and therapy-resistant cells in acute lymphoblastic leukemia. *Cancer Cell*. 2016;30(6):849-862.
26. Weber EW, Parker KR, Sotillo E, et al. Transient rest restores functionality in exhausted CAR-T cells through epigenetic remodeling. *Science*. 2021;372(6537):eaba1786.
27. Mestermann K, Giavridis T, Weber J, et al. The tyrosine kinase inhibitor dasatinib acts as a pharmacologic on/off switch for CAR T cells. *Sci Transl Med*. 2019;11(499):eaau5907.
28. Zhang L, Romero P. Metabolic control of CD8$^+$ T cell fate decisions and antitumor immunity. *Trends Mol Med*. 2018;24(1):30-48.
29. Wherry EJ, Ha SJ, Kaech SM, et al. Molecular signature of CD8$^+$ T cell exhaustion during chronic viral infection. *Immunity*. 2007;27(4):670-684.
30. Good CR, Aznar MA, Kuramitsu S, et al. An NK-like CAR T cell transition in CAR T cell dysfunction. *Cell*. 2021;184(25):6081-6100.e26.
31. Schietinger A, Philip M, Krisnawan VE, et al. Tumor-specific T cell dysfunction is a dynamic antigen-driven differentiation program initiated early during tumorigenesis. *Immunity*. 2016;45(2):389-401.
32. Lynn RC, Weber EW, Sotillo E, et al. c-Jun overexpression in CAR T cells induces exhaustion resistance. *Nature*. 2019;576(7786):293-300.
33. Van Der Sluis IM, De Lorenzo P, Kotecha RS, et al. A phase 2 study to test the feasibility, safety and efficacy of the addition of blinatumomab to the interfant06 backbone in infants with newly diagnosed KMT2A-rearranged acute lymphoblastic leukemia. a collaborative study of the interfant network. *Blood*. 2021;138(suppl 1):361.
34. Pauken KE, Wherry EJ. Overcoming T cell exhaustion in infection and cancer. *Trends Immunol*. 2015;36(4):265-276.
35. Foà R, Bassan R, Vitale A, et al; GIMEMA Investigators. Dasatinib-blinatumomab for Ph-positive acute lymphoblastic leukemia in adults. *N Engl J Med*. 2020;383(17):1613-1623.
36. Puzzolo MC, Radice G, Peragine N, et al. Host immune system modulation in Ph$^+$ acute lymphoblastic leukemia patients treated with dasatinib and blinatumomab. *Blood*. 2021;138(22):2290-2293.
37. Krupka C, Kufer P, Kischel R, et al. Blockade of the PD-1/PD-L1 axis augments lysis of AML cells by the CD33/CD3 BiTE antibody construct AMG 330: reversing a T-cell-induced immune escape mechanism. *Leukemia*. 2015;30(2):484-491.
38. John LB, Devaud C, Duong CP, et al. Anti-PD-1 antibody therapy potently enhances the eradication of established tumors by gene-modified T cells. *Clin Cancer Res*. 2013;19(20):5636-5646.
39. Adusumilli PS, Zauderer MG, Rivière I, et al. A phase I trial of regional mesothelin-targeted CAR T-cell therapy in patients with malignant pleural disease, in combination with the anti-PD-1 agent pembrolizumab. *Cancer Discov*. 2021;11(11):2748-2763.
40. Poorebrahim M, Melief J, Pico de Coaña Y, L Wickström S, Cid-Arregui A, Kiessling R. Counteracting CAR T cell dysfunction. *Oncogene*. 2021;40(2):421-435.
41. Song W, Zhang M. Use of CAR-T cell therapy, PD-1 blockade, and their combination for the treatment of hematological malignancies. *Clin Immunol*. 2020;214:108382.
42. Buck MD, O'Sullivan D, Pearce EL. T cell metabolism drives immunity. *J Exp Med*. 2015;212(9):1345-1360.
43. Delgoffe GM, Powell JD. Feeding an army: the metabolism of T cells in activation,

anergy, and exhaustion. *Mol Immunol*. 2015; 68(2 Pt C):492-496.

44. Kawalekar OU, O'Connor RS, Fraietta JA, et al. Distinct signaling of coreceptors regulates specific metabolism pathways and impacts memory development in CAR T cells. *Immunity*. 2016;44(2):380-390.

45. van Bruggen JAC, Martens AWJ, Fraietta JA, et al. Chronic lymphocytic leukemia cells impair mitochondrial fitness in $CD8^+$ T cells and impede CAR T-cell efficacy. *Blood*. 2019;134(1):44-58.

46. Abdel-Hakeem MS, Manne S, Beltra JC, et al. Epigenetic scarring of exhausted T cells hinders memory differentiation upon eliminating chronic antigenic stimulation. *Nat Immunol*. 2021;22(8):1008-1019.

47. Wu T, Ji Y, Moseman EA, et al. The TCF1-Bcl6 axis counteracts type I interferon to repress exhaustion and maintain T cell stemness. *Sci Immunol*. 2016;1(6):eaai8593.

48. Utzschneider DT, Charmoy M, Chennupati V, et al. T cell factor 1-expressing memory-like $CD8^+$ T cells sustain the immune response to chronic viral infections. *Immunity*. 2016; 45(2):415-427.

49. Chen Z, Ji Z, Ngiow SF, et al. TCF-1-centered transcriptional network drives an effector versus exhausted CD8 T cell-fate decision. *Immunity*. 2019;51(5):840-855.e5.

50. Siddiqui I, Schaeuble K, Chennupati V, et al. Intratumoral $Tcf1^+PD\text{-}1^+CD8^+$ T cells with stem-like properties promote tumor control in response to vaccination and checkpoint blockade immunotherapy. *Immunity*. 2019; 50(1):195-211.e10.

51. Beltra JC, Manne S, Abdel-Hakeem MS, et al. Developmental relationships of four exhausted $CD8^+$ T cell subsets reveals underlying transcriptional and epigenetic landscape control mechanisms. *Immunity*. 2020;52(5):825-841.e8.

52. Johnson JL, Georgakilas G, Petrovic J, et al. Lineage-determining transcription factor TCF-1 initiates the epigenetic identity of T cells. *Immunity*. 2018;48(2):243-257.e10.

5. Publication II

Article

SOURCE DATA | TRANSPARENT PROCESS | OPEN ACCESS

EMBO reports

STING agonism turns human T cells into interferon-producing cells but impedes their functionality

Niklas Kuhl[1,2,†], Andreas Linder[1,2,*,†], Nora Philipp[1,3], Daniel Nixdorf[1,3], Hannah Fischer[1], Simon Veth[4], Gunnar Kuut[1], Teng Teng Xu[1,3], Sebastian Theurich[1,3,5,6], Thomas Carell[4], Marion Subklewe[1,3] & Veit Hornung[1]

Abstract

The cGAS-STING (cyclic GMP-AMP synthase-stimulator of interferon genes) axis is the predominant DNA sensing system in cells of the innate immune system. However, human T cells also express high levels of STING, while its role and physiological trigger remain largely unknown. Here, we show that the cGAS-STING pathway is indeed functional in human primary T cells. In the presence of a TCR-engaging signal, both cGAS and STING activation switches T cells into type I interferon-producing cells. However, T cell function is severely compromised following STING activation, as evidenced by increased cell death, decreased proliferation, and impaired metabolism. Interestingly, these different phenotypes bifurcate at the level of STING. While antiviral immunity and cell death require the transcription factor interferon regulatory factor 3 (IRF3), decreased proliferation is mediated by STING independently of IRF3. In summary, we demonstrate that human T cells possess a functional cGAS-STING signaling pathway that can contribute to antiviral immunity. However, regardless of its potential antiviral role, the activation of the cGAS-STING pathway negatively affects T cell function at multiple levels. Taken together, these results could help inform the future development of cGAS-STING-targeted immunotherapies.

Keywords antiviral immune response; cGAS; STING; T cell; T cell dysfunction
Subject Categories Immunology; Microbiology, Virology & Host Pathogen Interaction; Signal Transduction
DOI 10.15252/embr.202255536 | Received 3 June 2022 | Revised 5 January 2023 | Accepted 9 January 2023
EMBO Reports (2023) e55536

Introduction

Pattern recognition receptors (PRRs) of the innate immune system recognize pathogen-associated molecular patterns (PAMPs) for antimicrobial defense. Activation of a PRR instills inflammation and elicits adaptive immune responses. Among these PRRs, cyclic GMP-AMP synthase (cGAS) specifically recognizes double-stranded DNA (dsDNA) inside the cell (Sun *et al*, 2013). Upon binding to dsDNA, cGAS produces cyclic GMP-AMP (cGAMP) (Ablasser *et al*, 2013; Diner *et al*, 2013; Gao *et al*, 2013; Zhang *et al*, 2013) that serves as a second messenger that binds to and thereby activates stimulator of interferon genes (STING) (Burdette *et al*, 2011). Activation of STING allows for the phosphorylation of interferon regulatory factor 3 (IRF3) by tank-binding kinase 1 (TBK1) (Ishikawa & Barber, 2008). Phosphorylated IRF3 relocates to the nucleus and drives the expression of antiviral genes, most notably type I interferons (type I IFN), such as IFNβ (Au *et al*, 1995; Lin *et al*, 1998). Type I IFNs stimulate the expression of antiviral interferon-stimulated genes (ISGs) in an autocrine and paracrine fashion by signaling through the interferon-α/β receptor (IFNAR). To a lesser extent, activation of STING also drives NF-κB pathway activation through an unresolved, noncanonical mechanism (Abe & Barber, 2014; Fang *et al*, 2017; de Oliveira Mann *et al*, 2019).

Apart from recognizing dsDNA introduced into the cytosol during infection with DNA viruses (Sun *et al*, 2013), recent studies additionally identified nuclear DNA during genotoxic stress (Dou *et al*, 2017; Glück *et al*, 2017; Harding *et al*, 2017; Mackenzie *et al*, 2017; Yang *et al*, 2017) and mitochondrial DNA (Rongvaux *et al*, 2014; White *et al*, 2014; West *et al*, 2015) during mitochondrial stress to activate cGAS-STING signaling. In light of these findings, cGAS has been linked to DNA damage sensing and might play a role

1 Gene Center and Department of Biochemistry, Ludwig-Maximilians-Universität München, Munich, Germany
2 Department of Medicine II, University Hospital, Ludwig-Maximilians-Universität München, Munich, Germany
3 Department of Medicine III, University Hospital, Ludwig-Maximilians-Universität München, Munich, Germany
4 Department of Chemistry and Center for NanoScience (CeNS), Ludwig-Maximilians-Universität München, Munich, Germany
5 German Cancer Consortium (DKTK), Partner site Munich, Heidelberg, Germany
6 German Cancer Research Center (DKFZ), Heidelberg, Germany
*Corresponding author. Tel: +49 (0)89 2180 71110; E-mail: hornung@genzentrum.lmu.de
†These authors contributed equally to this work

in the pathogenesis of autoimmune diseases, cellular senescence, and cancer (Li & Chen, 2018).

Although cGAS-STING signaling is commonly attributed to innate immune cells, there is increasing evidence that STING is also functional in adaptive immune cells, namely T cells. While STING activation can induce a type I IFN response from murine T cells (Larkin *et al*, 2017), it has also been reported that STING engagement impacts on T cell function beyond its antiviral role. *In vivo* studies employing the expression of a gain-of-function STING mutant observed severe T cell cytopenia and a greatly reduced memory T cell compartment (Cerboni *et al*, 2017; Warner *et al*, 2017; Bouis *et al*, 2019). However, there are conflicting views regarding the mechanism: Negative effects on T cell function were reported to occur independent of IRF3 or autocrine type I IFN signaling but rather attributed to a cell-intrinsic antiproliferative effect mediated by NF-kB (Cerboni *et al*, 2017) and cell death through ER stress (Wu *et al*, 2019a). Other studies suggest an IRF3-dependent upregulation of pro-apoptotic BH3-only proteins leading to cell death (Gulen *et al*, 2017) or IRF3/IRF7-dependent impairment of mTORC1, which was associated with reduced proliferation upon T cell receptor (TCR) stimulation, respectively (Imanishi *et al*, 2019).

In line with impaired T cell function observed in these studies, preclinical models suggest that STING-agonistic antitumor regimens are limited by the concomitant activation of the pathway within T cells (Sivick *et al*, 2018). Congruently, clinical phase I/II trials combining immunotherapy with STING agonists have seen mixed results in terms of efficacy (Le Naour *et al*, 2020). However, adoptive transfer of cGAS- or STING-deficient T cells has recently provided conflicting results in the murine system. T cell-intrinsic loss of the pathway impaired T cell functions when tumor antigen-specific T cells were transferred (Li *et al*, 2020) and STING activation enhanced antitumor responses through increased differentiation into effector cells (Benoit-Lizon *et al*, 2022). However, STING deficiency seemed to protect tumor-infiltrating T cells from cell death, when transferred T cells were allowed to endogenously mount an antitumor response (Wu *et al*, 2020). The reason for these discrepancies is unclear, but it is conceivable that the STING activation threshold plays a role in these different outcomes.

Since most of these observations stem from studying murine T cells and retrieved conflicting results, we here set out to better characterize outcomes of cell-intrinsic cGAS-STING signaling in primary human T cells by employing functional assays in combination with CRISPR/Cas9 gene editing. Doing so, we aimed to dissect IRF3-dependent from IRF3-independent functions mediated by STING and assess the role of auto- and paracrine type I IFNs.

Results

cGAMP induces antiviral cytokine release from T cell receptor-activated human T cells

To investigate whether the cGAS-STING pathway is operational in human T cells, primary CD4, and CD8 T cells isolated by magnetic bead separation (purity > 90%) were treated with the physiological STING agonist 2′-3′-cGAMP (cGAMP) (Fig 1A). In both cell types, cGAMP treatment alone induced the phosphorylation of STING (pSTING) and IRF3 (pIRF3). However, cGAMP-induced phosphorylation of STING and IRF3 was strongly enhanced if the cells were additionally activated through the engagement of their TCR and the provision of a co-stimulatory signal (αCD3/CD28 antibody-coated beads). Of note, αCD3/CD28 stimulation on its own failed to engage the STING-IRF3 axis in these cells. In line with the activation of IRF3, cGAMP also led to elevated levels of phosphorylated STAT1 (pSTAT1), which acts downstream of type I IFNs binding to the interferon-α/β receptor (IFNAR), indicating release and auto- or paracrine action of type I IFNs following cGAMP treatment. To assess whether T cell-intrinsic STING signaling could trigger the production of antiviral factors, IFNβ and the interferon-induced chemokine IP10 were measured in the supernatant of cGAMP stimulated T cells (Fig 1B and C). Of note, while cGAMP by itself was insufficient to elicit the production of measurable amounts of IFNβ and IP10, these antiviral factors became readily detectable in the supernatant of T cells co-treated with cGAMP and αCD3/CD28. Concentrations of IFNβ in the supernatant peaked at 16 h and remained detectable until 48 h, while the release of IP10 followed delayed kinetics, consistent with it being an interferon-stimulated gene (ISG). The release of IFNα, however, was quite heterogenous between donors with only one donor responding to αCD3/CD28/cGAMP co-treatment (Fig EV1A). To address whether the strong enhancement of STING and IRF3 phosphorylation observed in cGAMP- and αCD3/CD28-treated cells was due to auto- or paracrine effects, e.g., by TCR-dependent cytokines, we treated the cells with the translation inhibitor cycloheximide (CHX). These experiments, however, revealed that *de novo* protein synthesis was not required for this effect. CHX-treated cells showed the same enhancement of STING and IRF3 phosphorylation as untreated cells (Fig 1D), and the mRNA expression of IFNB and OASL remained unperturbed under these conditions (Fig 1E). Of note, CHX completely blunted the secretion of IFNγ that was seen in TCR-stimulated T cells (Fig EV1B). In line with these findings, using supernatant from αCD3/CD28-treated cells in conjunction with cGAMP stimulation was not able to substitute for the direct stimulation of T cells to trigger IFNβ expression (Fig EV1C). Further, to explore if STING activation in T cells is restricted to certain subsets (naïve, effector, memory), MACS-isolated naïve CD4 T cells were stimulated with cGAMP side by side with pan CD4 T cells from the same donor. Like the unsorted CD4 T cell population, naïve CD4 T cells also showed potent STING and IRF3 phosphorylation and IFNβ production when cGAMP and αCD3/CD28 beads were provided together (Fig EV1D and E). Taken together, these data show that primary human T cells display functional STING signaling upon exposure to cGAMP and that concomitant activation of the TCR greatly enhances signaling and is required for the release of antiviral cytokines. In addition, the synergy between STING and TCR stimulation is induced at a cell-intrinsic level.

Innate sensors cGAS and STING are operational in primary human T cells

Stimulator of interferon genes activation and subsequent type I IFN release induces the upregulation of interferon-stimulated genes (ISGs). Intrigued by the marked increase in STING signaling in human T cells through concomitant TCR activation, we set out to

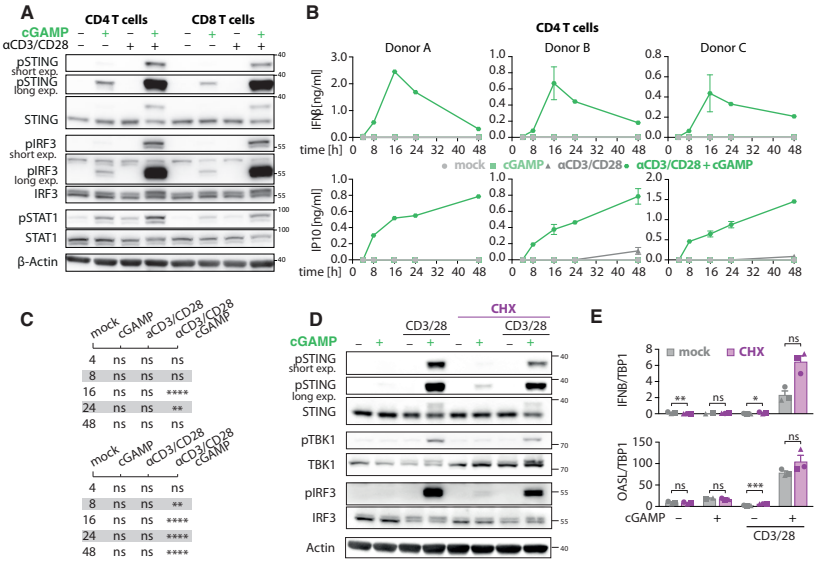

Figure 1. cGAMP treatment in addition to TCR stimulation leads to antiviral cytokine release in primary human T cells.

A CD4 and CD8 T cells were stimulated with cGAMP (20 μg/ml) and αCD3/CD28 beads as indicated. Cell lysates after 4 h of stimulation were analyzed by immunoblotting. Blots depict one representative donor out of three.

B CD4 T cells were stimulated with cGAMP (20 μg/ml) and αCD3/CD28; and human IFNβ (top) and IP10 levels (bottom) in the supernatant were analyzed by ELISA at the indicated time points. Data panels depict mean ± SD of biological duplicates from three independent donors.

C Statistics from (B) across all three donors indicate significance by a repeated-measures two-way ANOVA with Dunnett correction for multiple testing: ****$P < 0.0001$; **$P < 0.01$; ns, not significant.

D CD4 T cells were left untreated or pretreated with cycloheximide (2 μg/ml) for 2 h, then treated with cGAMP (20 μg/ml) and αCD3/CD28 (3/28) for 4 h. Lysates were analyzed by immunoblotting. One representative donor out of two is shown.

E CD4 T cells were left untreated or pretreated with cycloheximide (2 μg/ml) for 2 h, then treated with cGAMP (20 μg/ml) and αCD3/CD28 (3/28) for 4 h, then analyzed by quantitative PCR for *IFNB1* and *OASL* expression. Data are depicted as mean + SEM of three independent donors (for cGAMP treated cells without CHX only two data points were obtained). Statistics were determined by a two-way ANOVA on log-transformed data using Šidák correction for multiple testing: ***$P < 0.001$; **$P < 0.01$; *$P < 0.05$; ns, not significant.

Source data are available online for this figure.

characterize this phenotype more thoroughly by employing an unbiased approach. To this end, the same conditions as in the previous experiment were employed: T cells were either left untreated or stimulated with cGAMP and additionally stimulated using αCD3/CD28 beads or not (Fig EV2A). To account for potential impurities in our T cell preparations and STING-independent effects of cGAMP, these experiments were conducted in CD4 T cell clones that were either wildtype (WT) or in which the STING locus was disrupted by CRISPR/Cas9 gene editing (*STING1*$^{-/-}$). Pooled clones were stimulated for 4 h in triplicates and then subjected to RNA-Seq analysis. Principal component analysis (PCA) retrieved four distinct groups representing the four experimental conditions of the WT clones (Fig 2A): unstimulated cells (gray), cGAMP treatment (green), αCD3/CD28 treatment (purple), and αCD3/CD28 + cGAMP co-treatment (blue). Clustering of these groups was confirmed by *k*-means clustering (Fig EV2B). Of note, cGAMP-treated *STING1*$^{-/-}$ clones clustered with unstimulated WT cells, while *STING1*$^{-/-}$ cells co-treated with αCD3/CD28 and cGAMP clustered with WT cells stimulated with αCD3/CD28 only. These observations support the notion that there are no STING-independent effects of cGAMP in human T cells. Apart from that, WT and *STING1*$^{-/-}$ T cells showed minor differences in gene expression under steady-state conditions (Fig EV2C) or following αCD3/CD28 treatment (Fig EV2D). To this end, a few ISGs were expressed in WT, but not in *STING1*$^{-/-}$ cells, suggesting a steady-state activity of the STING pathway in the absence of exogenous triggers. Focusing on transcripts associated with a type I IFN response among the most variable genes (Fig EV2E) showed a strong ISG induction following STING activation in T cells: cGAMP treatment led to a STING-dependent upregulation of classical ISGs, whose expression was enhanced when co-treating with αCD3/CD28 (Fig 2B). This was corroborated by comparing the main clusters retrieved in the PCA to identify

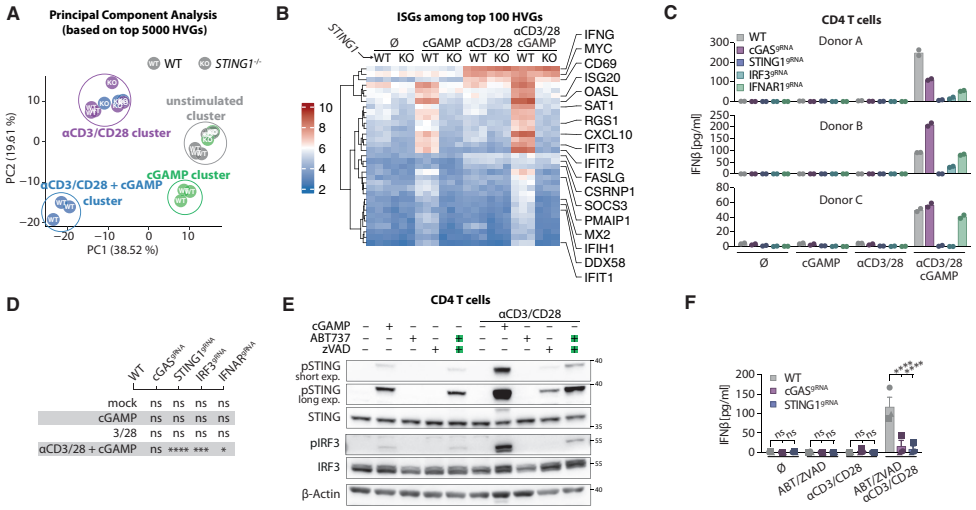

Figure 2. Primary human T cells display canonical STING signaling.

A Pooled CD4 T cell WT and *STING1*$^{-/-}$ clones were stimulated in triplicates with cGAMP (20 μg/ml) and αCD3/CD28 for 4 h and analyzed by RNA sequencing. Principal component analysis based on the top 5,000 highly variable genes (HVGs).

B Heatmap showing interferon-stimulated genes (ISGs) among the top 100 HVGs according to (Samarajiwa *et al*, 2009) clustered hierarchically across all conditions and replicates. Color coding corresponds to normalized and log2-transformed read counts. Genes differentially expressed between cGAMP-treated and cGAMP + αCD3/CD28-treated conditions are annotated.

C CRISPR/Cas9 targeted CD4 T cells for indicated genes were treated with cGAMP (20 μg/ml) and αCD3/CD28 beads for 48 h. Human IFNβ levels were analyzed by ELISA. Data panels depict the mean of biological duplicates from three independent donors.

D Statistics from (C) across all three donors indicate significance by a repeated-measures two-way ANOVA with Dunnett correction for multiple testing: ****$P < 0.0001$; ***$P < 0.001$; *$P < 0.05$; ns, not significant.

E CD4 T cells were stimulated with the indicated stimuli for 4 h. Lysates were analyzed by immunoblotting. One representative donor out of three is shown.

F CRISPR/Cas9 targeted CD4 T cells for the indicated genes were treated with the indicated stimuli for 48 h. Human IFNβ levels were analyzed by ELISA. Data are depicted as mean + SEM of three independent donors. Statistics indicate significance by two-way ANOVA with Dunnett correction for multiple testing: ****$P < 0.0001$; ns, not significant.

Source data are available online for this figure.

differentially expressed genes: While cGAMP treatment alone could already induce expression of several ISGs (e.g., *IFIT2*, *IFIT3*, *OASL*, *IFIT1*) (Fig EV2F), treatment with αCD3/CD28 mostly induced genes associated with TCR stimulation and NF-κB signaling (e.g., *TNF*, *CD69*, *NFKBID*, *IFNG*) (Fig EV2G). Of note, many ISGs were among those genes differentially expressed between cGAMP-treated cells and cGAMP + αCD3/CD28-treated cells; verifying that co-treatment with αCD3/CD28 enhances ISG expression (Fig EV2H). Altogether, these data implicated that STING activation in human T cells leads to an antiviral transcriptional program that is enhanced and diversified by concomitant TCR stimulation.

To validate if cGAS-STING signaling in human T cells employs canonical components of signal transduction, we generated polyclonally CRISPR/Cas9-edited CD4 T cells targeting *CGAS*, *STING1*, *IRF3*, and *IFNAR1*. Analyzing levels of the respective proteins by immunoblotting revealed a substantial loss of expression from the targeted locus (Fig EV3A). Successful disruption of IFNAR-signaling in *IFNAR1* targeted cells was confirmed by exposing T cells to IFNα2a, which revealed decreased STAT1 phosphorylation in cells nucleofected with gRNAs directed against *IFNAR1* but not other targets. T cells obtained by this approach were then treated with cGAMP with or without αCD3/CD28 co-treatment and analyzed for IFNβ levels in the supernatant (Fig 2C and D). As expected, co-treatment with cGAMP and αCD3/CD28 resulted in IFNβ release from WT and cGAS-deficient cells. Yet, IFNβ release was entirely dependent on STING and IRF3, suggesting canonical signaling downstream of STING activation in T cells. IFNβ release was also partially dependent on IFNAR1, suggesting an enhancement of IFNβ production through a positive feedback loop. To evaluate the contribution of autocrine type I IFNs, *IFNAR1* deficient cells were analyzed for IFNβ and IP10 secretion in a time course experiment. As polyclonal gene targeting of *IFNAR1* still led to residual STAT1 phosphorylation upon exposure to IFNα (Fig EV3A), clonal *IFNAR1*-deficient T cells were employed for this experiment. STING activation by cGAMP and αCD3/CD28 treatment led to initial IFNAR1-independent IFNβ release after 8 h. Consecutive IFNβ secretion,

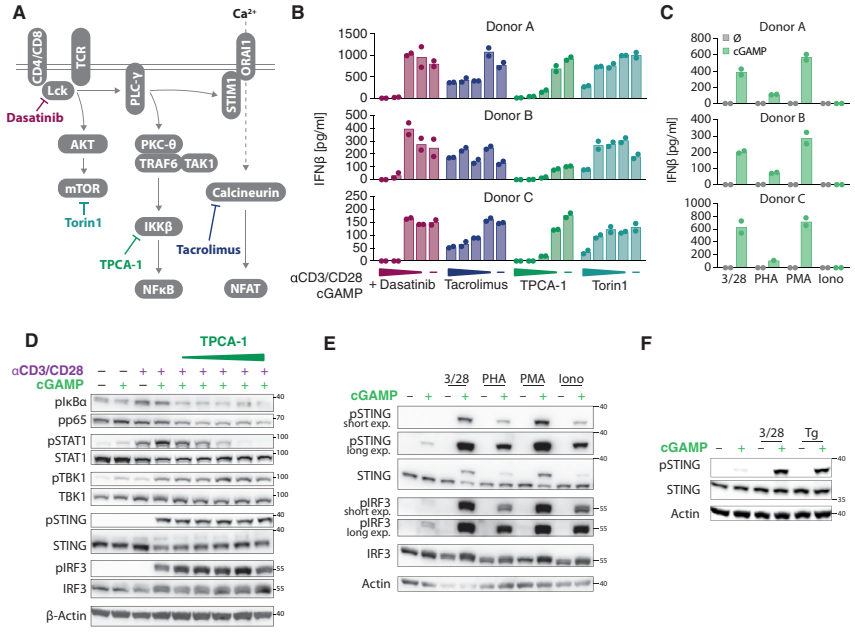

Figure 3. Critical role for NF-kB signaling in STING-driven antiviral immunity.

A Simplified model of signaling downstream of TCR engagement.

B CD4 T cells were pretreated with Dasatinib (100, 10, 1 and 0.1 nM), Tacrolimus (1,000, 100, 10 and 1 nM), TPCA-1 (4, 2, 1 and 0.5 μM), and Torin1 (50, 5, 0.5 and 0.05 nM) for 30 min, then treated with cGAMP (20 μg/ml) and αCD3/CD28 for 16 h. Human IFNβ levels in the supernatant were analyzed by ELISA. Data panels depict the mean of biological duplicates from three independent donors.

C CD4 T cells were treated with cGAMP (20 μg/ml) and indicated additional stimuli for 16 h. Human IFNβ levels were analyzed by ELISA. Data panels depict the mean of biological duplicates from three independent donors (for cGAMP and PHA-treated cells of Donor C only one data point was obtained).

D CD4 T cells were treated with cGAMP and indicated stimuli together with increasing concentrations of TPCA-1 for 4 h. Cell lysates were analyzed by immunoblotting. One representative donor out of two is shown.

E, F CD4 T cells were stimulated with cGAMP (20 μg/ml) and additional stimuli as indicated. Cell lysates after 4 h of stimulation were analyzed by immunoblotting. One representative donor out of two is shown.

Source data are available online for this figure.

however, was mostly dependent on IFNAR1 (Fig EV3B), again suggesting that a positive feedback loop was operable. IP10 release was completely dependent on IFNAR1 throughout the whole time course (Fig EV3C), indicating that autocrine type I IFN signaling is critical to reinforce antiviral cytokine production upon STING activation in human T cells. In summary, IFNβ release from human T cells upon STING activation is facilitated through IRF3 and relies on a feedback loop dependent on the type I IFN receptor IFNAR for full-scale activation.

Having established that STING is operational in human T cells, we set out to explore whether cGAS binding to double-stranded DNA can activate STING in human T cells and if this results in downstream type I IFN production. While transfecting dsDNA readily induced STING phosphorylation in peripheral blood mononuclear cells (PBMCs), it failed to do so in purified primary human T cells (Fig EV3D). To account for the possibility that exogenous dsDNA was not active due to insufficient delivery, we investigated if cGAS could get activated by endogenous DNA. To this end, previous work has established that DNA released in the context of mitochondrial outer membrane permeabilization (MOMP) can engage the cGAS-STING axis, if concomitant induction of intrinsic apoptosis is prevented (Rongvaux *et al*, 2014; White *et al*, 2014). To test this scenario, we treated T cells with the Bcl2-inhibiting drug ABT737, which results in the release of mtDNA into the cytosol. To prevent the cells from undergoing apoptosis that is known to otherwise interfere with cGAS activation (Ning *et al*, 2019), cells were additionally treated with the pan-caspase inhibitor zVAD. Treating human T cells with the combination of these tool compounds led to phosphorylated STING and IRF3; similar to cells treated with cGAMP (Fig 2E). Again, αCD3/CD28 co-treatment amplified STING

signaling, however, not to the same extent as cGAMP activity was amplified by αCD3/CD28. To genetically validate that the induction of type I IFNs through this treatment is a result of cGAS activation, we employed polyclonal CRISPR/Cas9 gene editing and generated CD4 T cells deficient for either cGAS or STING. Treating these cells with ABT737 and zVAD led to IFNβ release that was completely dependent on cGAS and STING, while IFNγ levels were unchanged between genotypes (Figs 2F and EV3E). In conclusion, these data support that not only STING but also the PRR cGAS is functional and can be activated by MOMP-derived mtDNA in human T cells.

TCR engagement boosts IFNβ production via at least two independent mechanisms

Based on the observation that TCR stimulation is a prerequisite for IFNβ release from human T cells, we set out to explore what signaling events downstream of TCR signaling are required for the production of IFNβ. To do so, we employed a series of small molecule inhibitory compounds acting downstream of the TCR (Fig 3A). As expected, inhibition of apical signal transduction downstream of TCR stimulation by targeting Lck with the tyrosine kinase inhibitor Dasatinib completely abrogated the IFNβ response (Fig 3B). On the other hand, the calcineurin-inhibitor Tacrolimus failed to substantially block IFNβ release at concentrations well above those needed to block NFAT activity (Dufva *et al*, 2020), excluding a role for this transcription factor in IFNβ production. However, employing TPCA-1 to block IKKβ, the critical kinase of the NF-kB activating IKK complex, potently blunted IFNβ release. Since recent findings suggested that type I IFN production is regulated by mTORC1 (Imanishi *et al*, 2019) we also employed the mTOR inhibitor Torin1. Indeed, the inhibition of mTOR reduced IFNβ release from CD4 T cells, although to a lesser extent than TPCA1. Both TPCA-1 and Torin1 inhibited the antiviral response at the level of mRNA expression, excluding a role for post-transcriptional regulation (Fig EV3F). In line with a critical role for NF-kB activation in the IFNβ response of T cells, stimuli converging on NF-κB activation, such as phorbol myristate acetate (PMA) and to a lesser extent Phytohaemagglutinin (PHA) could also substitute the anti-CD3/CD28 signal to induce IFNβ secretion in conjunction with cGAMP (Fig 3C). Conversely, the Ca^{2+} ionophore Ionomycin together with cGAMP was not able to trigger IFNβ production. Altogether, these results suggested that TCR-dependent NF-κB activation might be a critical signal required to facilitate IFNβ expression, which is well in line with the notion that the IFNβ promoter harbors NF-κB binding sites that need to be engaged to drive its expression (Iwanaszko & Kimmel, 2015). Immunoblotting confirmed impaired NF-κB signaling through TPCA-1 as evidenced by decreased levels of IκBα phosphorylation (Fig 3D). Moreover, in line with the inhibition of IFNβ production, TPCA-1 treatment abrogated paracrine and autocrine type I IFN activity as evidenced by a reduced STAT1 phosphorylation. Interestingly, TPCA-1 treatment had no impact on the phosphorylation levels of TBK1, STING, and IRF3, which suggested that TCR signaling generates at least one additional signal that boosts cGAMP-dependent antiviral activity. We noted that the Ca^{2+} ionophore Ionomycin, which failed to synergize with cGAMP to induce IFNβ production (Fig 3C), was able to trigger potent STING and IRF3 phosphorylation when added together with cGAMP (Fig 3E). These results suggested that Ca^{2+} flux could provide the signal required for synergistic STING activation. Along these lines, the treatment of cells with Thapsigargin, which increases cytosolic Ca^{2+} levels but decreases ER-Ca^{2+} levels by inhibiting ER-Ca^{2+}-ATPases, also acted synergistically with cGAMP in inducing strong STING phosphorylation (Fig 3F). In summary, these results suggest that T cell receptor engagement facilitates STING signaling at least two independent steps: On the one hand, TCR-dependent NF-kB activation is critically required to drive IFNβ expression, presumably directly at the level of the *IFNB* promoter. On the other hand, TCR-dependent Ca^{2+} flux appears to boost STING activation as early as at the level of STING phosphorylation.

STING activation induces IRF3-dependent apoptosis in primary human T cells

Unexpectedly, treating CD4 T cells with increasing concentrations of cGAMP did not translate into an increase in IFNβ production but rather a drastic decrease (Fig EV4A). Monitoring cell viability revealed that the decrease in IFNβ production was accompanied by a lower number of viable cells at high cGAMP concentrations (Fig EV4B). In light of these results and previous reports in that regard (Gulen *et al*, 2017; Larkin *et al*, 2017; Wu *et al*, 2019a), which suggested a pro-apoptotic function of STING, we further characterized cell death by staining for Annexin V, a marker for early apoptosis. Treating CD4 T cells with increasing concentrations of cGAMP resulted in increased cell death (Fig 4A), while this was not prevented by αCD3/CD28 co-treatment. Of note, slightly increased levels of cell death as observed in the αCD3/CD28 treated conditions can be attributed to the phenomenon of activation-induced cell death (AICD) (Green *et al*, 2003). As a control, we treated cells with a combination of the Bcl2-inhibitor ABT737 and the Mcl1-inhibitor S63845, which is known to robustly induce intrinsic apoptosis in human T cells (Linder *et al*, 2020). Studying the response of freshly isolated CD4 and CD8 T cells revealed that both T cell types undergo cell death upon cGAMP treatment (Fig 4B). CD8 T cells, however, appear to be more susceptible to AICD, resulting in a higher overall number of dead cells in the αCD3/CD28 co-treated conditions. Both cell types responded to ABT737/S63845-induced cell death as expected. To better understand the mode of cell death elicited by cGAMP treatment, we reevaluated our RNA-Seq dataset for differentially expressed genes under the GO term "Positive regulation of apoptotic process" (Fig EV4C). cGAMP treatment of CD4 T cells led to STING-dependent upregulation of several transcripts associated with apoptosis, including the anti-apoptotic *MCL1* and pro-apoptotic *PMAIP1* (coding for Noxa) genes, which have been well studied in this context. Other genes linked to apoptosis like *IFNG*, *FASLG*, and *RGCC* were associated with TCR stimulation rather than STING activation, because they were induced independently of cGAMP and STING in the presence of αCD3/CD28 treatment. In line with apoptosis being the main type of cell death triggered by STING activation in T cells, increasing concentrations of cGAMP led to caspase 3 and PARP cleavage like ABT737/S63845 treatment (Fig 4C). Employing polyclonal CRISPR/Cas9 gene editing revealed that STING- and IRF3-deficient T cells were completely protected from cGAMP-induced cell death, while cGAS and IFNAR1-deficiency had no effect (Fig 4D and E). As expected, intrinsic apoptosis by ABT737/S63845 occurred independently of these gene deficiencies. This again suggested that STING triggers an interferon-independent, cell-intrinsic

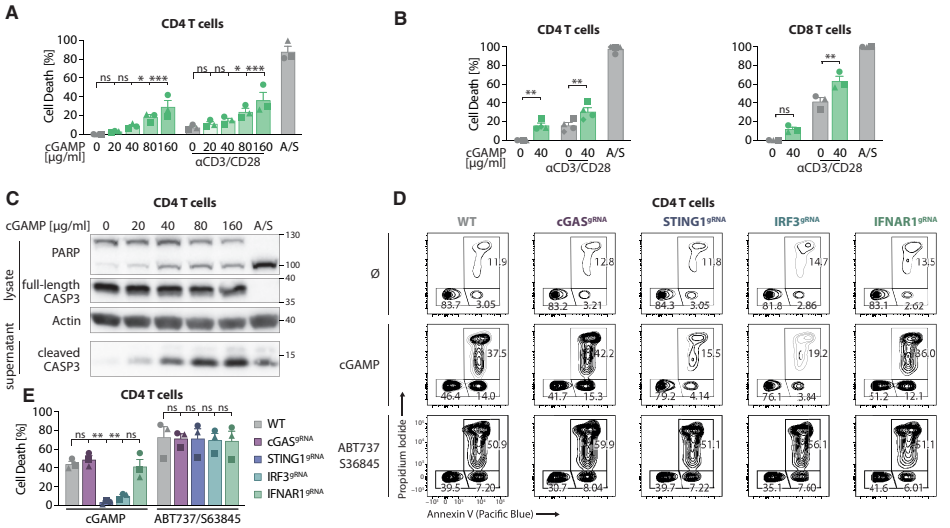

Figure 4. STING activation induces cell death in primary human T cells.

A Freshly isolated CD4 T cells were treated with cGAMP, αCD3/CD28 beads, and ABT737/S63845 (A/S) for 48 h and analyzed by flow cytometry. Treatment-induced cell death was assessed by Annexin V and propidium iodide staining. Data are depicted as mean + SEM of three independent donors. Statistics indicate significance by two-way ANOVA with Dunnett correction for multiple testing: ***$P < 0.001$; *$P < 0.05$; ns, not significant.

B Freshly isolated CD4 (left) and CD8 (right) T cells were treated as indicated for 48 h and analyzed by flow cytometry. Treatment-induced cell death was assessed by Annexin V and propidium iodide staining. Data are depicted as mean + SEM of 4 (CD4) or 3 (CD8) independent donors. Statistics indicate significance by two-way ANOVA with Šidák correction for multiple testing: **$P < 0.01$; ns, not significant.

C CD4 T cells were treated with indicated concentrations of cGAMP for 18 h, and ABT737/S63845 for 2 h. Lysates and supernatant precipitations were analyzed by immunoblotting. One representative donor out of two is shown.

D CRISPR/Cas9 targeted CD4 T cells for indicated genes were treated with the indicated stimuli for 48 h and analyzed by flow cytometry. Each panel shows propidium iodide and Annexin V intensity for one representative donor out of three. Digits indicate the percentage of the parental population (single events without subcellular debris).

E Summary from (D), whereas data are depicted as mean + SEM of three independent donors. Statistics indicate significance by two-way ANOVA with Dunnett correction for multiple testing: **$P < 0.01$; ns, not significant.

Source data are available online for this figure.

mechanism, where IRF3 most likely mediates transcriptional changes leading to apoptosis. In summary, these results suggested that STING activation in T cells induces apoptotic cell death in human T cells fully dependent on IRF3.

STING activation impairs proliferation in primary human T cells independent of IRF3 and autocrine type I IFN

Studies employing T cells ectopically overexpressing a patient-derived gain-of-function STING mutant suggested an antiproliferative effect of STING on TCR-stimulated T cells (Cerboni *et al*, 2017). To evaluate whether STING activation via cGAMP influences the proliferation of TCR-stimulated human T cells, CellTrace Violet (CTV) dilution was determined by flow cytometry (Fig 5A). When CD4 and CD8 T cells were kept resting, cells did not divide, indicated by a single brightly stained peak (light gray profile). When activated with αCD3/CD28, T cells proliferated readily resulting in a profile with several peaks representing cell division events (black profile). However, when additionally adding cGAMP to the cells on day 0 and day 2, T cell proliferation was markedly reduced (green profile). Quantification by proliferation modeling to compare results across several different donors showed that cGAMP has a substantial negative effect on T cell proliferation after activation of both CD4 and CD8 T cells (Fig 5B). Analyzing the proliferation of CD4 T cells deficient for *CGAS*, *STING1*, *IRF3*, and *IFNAR1* generated by CRISPR/Cas9 gene editing revealed that wildtype and *CGAS*-deficient T cells proliferated less when treated with cGAMP, while cGAMP-treated *STING1*-deficient T cells behaved like the αCD3/CD28 treated control condition (Fig 5C). Interestingly, *IRF3*- and *IFNAR1*-deficient cells were not protected from impaired proliferation, suggesting an IRF3-independent, cell-intrinsic mechanism rather than an effect of para/autocrine type I IFNs or IRF3-dependent transcription itself (Fig 5D). Upon TCR-mediated activation, T cells engage both

mitochondrial oxidative phosphorylation (OXPHOS) and glycolysis to meet the energy demands required for proliferation and effector functions. To investigate cGAMP-mediated alterations in the basal and maximal metabolic capacity of T cells during αCD3/CD28 activation, we next performed metabolic stress tests. Following CD3/CD28 engagement, T cells strongly increased both their respiratory capacity and their glycolytic rate. Increased mitochondrial respiration mediated by αCD3/CD28 activation was substantially reduced when T cells were additionally treated with cGAMP while resting T cells only displayed marginal changes in respiratory capacity (Fig 5E). cGAMP treatment reduced basal respiration in activated T cells, suggesting less energetic demand in baseline conditions. Moreover, maximal respiration after mimicking maximal energetic demands and the reserve capacity was substantially reduced, impacting the cells' ability to respond to metabolic challenges adequately. In addition, high basal glycolysis after glucose injection upon CD3/CD28 activation was substantially reduced when T cells were activated in the presence of cGAMP (Fig 5F). Similar to oxidative phosphorylation, basal glycolysis, maximal glycolytic capacity, and the glycolytic reserve were impaired by cGAMP treatment, indicating reduced glycolysis in baseline and anaerobic conditions, as well as a reduced capacity to respond to energetic demands. Overall, these data suggested that STING activation impairs activation-induced proliferation in human T cells in a process for which IRF3 and type I IFNs are dispensable. Moreover, STING activation compromises metabolic functions necessary for T cell proliferation.

Discussion

While extensively studied in cells of the innate immune system, fibroblasts and epithelial cells, more recent data suggest that the cGAS-STING pathway is also operational in T cells. As these data with few exceptions rely on the study of murine T cells, we here provide a detailed characterization of the cGAS-STING pathway in primary human CD4 and CD8 T cells. Employing the physiological STING ligand 2′-3′-cGAMP revealed that human T cells do not only express high levels of STING but retain functional signaling evidenced by phosphorylation of STING, IRF3, as well as secretion of considerable amounts of IFNβ and the interferon-stimulated chemokine IP10. Interestingly, and similar to the mouse system (Imanishi

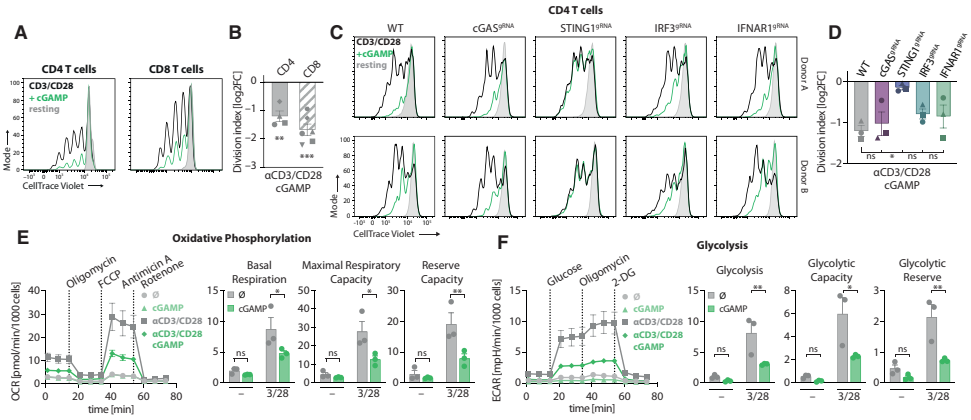

Figure 5. STING activation impairs proliferation in primary human T cells.

A CellTrace Violet (CTV) stained, freshly isolated CD4 and CD8 T cells were activated with αCD3/CD28 beads, stimulated with cGAMP for 96 h, and analyzed by flow cytometry. Each panel shows profiles from activated (black), cGAMP-treated (green), and resting (light gray) single and live cells from one representative donor.

B Summary from (A) across four (CD4) or six (CD8) independent donors. Division indices for each condition were calculated using proliferation modeling. Plot shows log2-transformed fold changes (log2FC) of division indices of treated samples compared to those of activated samples without any additional treatment. Individual data points ± SEM are shown. Statistics indicate significance by one-sample *t*-test: ***$P < 0.001$; **$P < 0.01$.

C CRISPR/Cas9 targeted CD4 T cells for indicated genes were treated with cGAMP for 96 h, analyzed by flow cytometry, and subjected to the same analysis as in (A). Two representative donors out of three are shown.

D Summary of (C) across three independent donors, analyzed as in (B). Data are depicted as mean ± SEM of three independent donors. Statistics indicate significance by one-way ANOVA with Dunnett correction for multiple testing: *$P < 0.05$; ns, not significant.

E Freshly isolated CD4 T cells were treated with cGAMP (40 μg/ml) and αCD3/CD28 (3/28) for 48 h and analyzed by Seahorse XF Mito Stress Test. Data are depicted as mean ± SEM of three independent donors. Statistics indicate significance by two-way ANOVA with Šidák correction for multiple testing: **$P < 0.01$; *$P < 0.05$; ns, not significant.

F Cells treated as in (E) were subjected to the Seahorse XF glycolysis stress test. Data are depicted as mean ± SEM of three independent donors. Statistics indicate significance by two-way ANOVA with Šidák correction for multiple testing: **$P < 0.01$; *$P < 0.05$; ns, not significant.

Source data are available online for this figure.

et al, 2019), simultaneous TCR activation was required for a potent antiviral response in T cells. TCR engagement provides at least two independent signals to boost STING signaling. On the one hand, TCR-dependent IKK activation provides the critical NF-κB activity that is necessary for efficient *IFNB1* expression together with STING-dependent IRF3 phosphorylation. On the other hand, TCR signaling is also required for efficient activation of the STING axis in the first place, as evidenced by phosphorylation of TBK1, STING, and IRF3. Here, it appears that signals that deplete ER Ca^{2+} stores potently boost STING activation, presumably by facilitating its exit from the ER. By genetically disrupting the expression of cGAS, STING, IRF3, and IFNAR1 in primary human T cells we confirm that STING signaling relies on IRF3 for cytokine production. In addition, an autocrine feedback loop reinforces type I IFN production and facilitates the induction of ISGs. While we failed to induce cGAS-dependent STING-activation through cytoplasmic delivery of exogenous immunostimulatory DNA, we readily could detect STING-activation upon MOMP-induction when caspases are inhibited pharmacologically in parallel (Rongvaux *et al*, 2014; White *et al*, 2014). Genetically, this relied on cGAS, proving that also cGAS is functional in human T cells. In addition to cytokine secretion, T cell-intrinsic STING activation induces cell death that displays features of apoptosis and in human cells genetically depends on IRF3 but is unlike cytokine secretion independent of concomitant TCR activation and autocrine IFNAR1-signaling. Upon exposure to cGAMP, T cell proliferation is heavily impaired, similar to what has been observed when *gain-of-function* STING variants were overexpressed in human T cells (Cerboni *et al*, 2017). Unlike cell death and cytokine production, the brake that STING activation puts on proliferation is independent of IRF3. Finally, we observe that also the metabolic changes associated with TCR engagement are corrupted in the presence of a STING agonist, supporting that various T cell functions are impaired when STING is activated in this cell type.

Requirement for TCR activation for STING-dependent type I IFN production

While resting CD4 and CD8 T cells were capable of canonical STING pathway activation, subsequent type I IFN production required simultaneous TCR stimulation. Based on our results, we propose at least two independent pathways to be operational:

First, using the IKKβ inhibitor TPCA-1, we found that blocking NF-κB signaling effectively abrogated type I IFN production but had no effect on STING or IRF3 phosphorylation, suggesting that TCR stimulation provides NF-κB signaling required for type I IFN production. This is in line with the notion that NF-κB acts as a critical transcription factor for *IFNB1* gene expression (Honda *et al*, 2006). Yet, unlike in other cell types, NF-κB activation downstream of STING activation appears to be insufficient for the induction of type I IFN in T cells. Our findings also confirm that TCR-dependent mTORC1 activation is required for IFNβ production, which was recently suggested for murine T cells (Imanishi *et al*, 2019). mTORC1 is a protein complex being assembled after T cell activation and linked to metabolic reprogramming and increased protein translation during T cell proliferation. As mTORC1 is also involved in NF-κB activation following TCR engagement, it remains unclear from these data if mTORC1 enhances IFNβ production through NF-κB or through a different mechanism. In fact, Imanishi *et al* (2019) show that mTORC1 inhibition reduces protein levels of IRF7, another transcription factor involved in type I IFN signaling.

Second, only the combination of CD3/CD28 stimulation and cGAMP treatment resulted in strong phosphorylation of TBK1, STING, and IRF3, which occurred independently of IKK activation. Our data suggest that TCR-dependent Ca^{2+} signaling is required for this activity. To this end, either Ionomycin, which acts as a Ca^{2+} ionophore at the plasma and ER membranes, or Thapsigargin, which depletes ER Ca^{2+} levels by inhibiting the ER Ca^{2+}-ATPase, were able to potently boost STING and IRF3 phosphorylation together with cGAMP. We hypothesize that these compounds facilitate STING activation via engaging the ER-Ca^{2+} sensor STIM1. When Ca^{2+} levels drop in the ER, STIM1 oligomerizes and subsequently translocates to the plasma membrane to activate Ca^{2+}-selective Orai channels (Soboloff *et al*, 2012). However, recent work has shown that ER-resident STIM1 also exerts a negative regulatory function on STING by restraining it in the ER. As such, the deletion of STIM1 results in the spontaneous, ligand-independent translocation of STING from the ER, resulting in its activation (Srikanth *et al*, 2019). We speculate that the lowering of ER Ca^{2+} stores, as it physiologically occurs upon TCR engagement, and as it is synthetically triggered by Ionomycin and Thapsigargin, facilitates the STIM1-dependent exit of STING from the ER to gain its signaling competent state. However, additional mechanistic studies are required to corroborate this assumption.

Mechanisms of STING-mediated effects beyond IFN production

Stimulator of interferon genes activation led to apoptosis in human T cells. We identified IRF3 as the key mediator of this cell death program, as the deletion of IRF3 completely abrogated STING-induced cell death. In fact, previous research in murine T cells reported IRF3-dependent upregulation of the pro-apoptotic BH3-only protein Noxa (*PMAIP1*) resulting in apoptotic cell death (Gulen *et al*, 2017). However, in the same study, STING activation was also found to trigger—via a yet to be defined mechanism—a p53-dependent signaling pathway that cooperates with IRF3 in the induction of pro-apoptotic genes. Specifically, the BH3-only protein Puma was shown to be highly induced in murine T cells by a p53-dependent but IRF3-independent mechanism following STING activation. Consistent with a dual requirement of IRF3- and p53-dependent mechanisms downstream of STING, murine T cells were only partially rescued from STING-dependent cell death when either transcription factor was absent. However, the fact that human IRF3-deficient T cells become fully resistant to cell death upon STING activation does not support the existence of a p53-dependent pathway in human T cells. Indeed, while we detected upregulation of the well-known ISG Noxa (*PMAIP1*) through RNA-Seq, we failed to observe cGAMP-mediated upregulation of Puma. Aside from promoting pro-apoptotic gene expression, IRF3 was also shown to directly interact with Bax, a protein of the pro-apoptotic Bcl2 family, through a BH3 domain initiating the mitochondrial apoptotic pathway (Chattopadhyay *et al*, 2010). Strikingly, the function of IRF3 as a transcriptional regulator is not necessary for the interaction with Bax, suggesting multiple death-inducing functions for activated IRF3. Noteworthy, our findings also imply that IRF3-independent modes of cell death via ER stress after STING activation as previously reported in murine T cells expressing SAVI-mutant STING (Wu *et al*, 2019a) only play a

negligible role in human T cells. However, as our model involves acute activation using the physiological agonist cGAMP these findings might not apply to T cells that chronically activate STING through a gain-of-function mutation. Worth mentioning, if GOF mutations also display synergistic activation following TCR stimulation, T cell activation during infection could exacerbate symptoms in patients carrying such mutations.

Besides cell death, we also observed impaired proliferation following STING activation in T cells. Although type I IFN facilitates impaired proliferation in T cells in certain conditions (Dickow *et al*, 2019), proliferation impairment following T cell-intrinsic STING activation occurs independently of auto- and paracrine type I interferon signaling. Surprisingly, IRF3 was also dispensable for the antiproliferative effect of STING. Previous studies identified a distinct STING domain within its C-terminal tail (termed "miniCTT") that mediates inhibition of T cell proliferation independent of TBK1 or IRF3 binding (Cerboni *et al*, 2017). In human monocytes, STING-TBK1 has been shown to promote autophosphorylation of ATM, which led to G1 cell cycle arrest through the CHK2-p53-p21 pathway independent of IRF3 (Banerjee *et al*, 2021). It is conceivable that this pathway is also involved in the impairment of cell proliferation in human T cells.

During differentiation following TCR stimulation, T cells undergo metabolic reprogramming to meet bioenergetic demands required for rapid proliferation and differentiation into effector cells, which includes increased uptake of glucose and increased glycolysis. After activation, metabolic reprogramming of T cells is orchestrated by multiple signaling pathways downstream of TCR stimulation, with a prominent role in the PI3K-AKT-mTOR pathway (van der Windt & Pearce, 2012; Le Bourgeois *et al*, 2018). In line with impaired proliferation after TCR stimulation, we also observed a drastic decrease in the ability of T cells to perform glycolysis upon STING activation. Consistent with this observation, STING activation in murine T cells inhibited the assembly of mTORC1, a protein complex that is part of the PI3K-AKT-mTOR pathway involved with metabolic reprogramming (Imanishi *et al*, 2019). Interestingly, STING activation also impaired mitochondrial respiration, which besides the initial phase after activation is characteristic mainly to quiescent T cells (i.e., naïve and memory T cells), which rely on oxidative phosphorylation, glutaminolysis, and fatty acid oxidation (Pearce, 2010). While our model more closely represents TCR-induced proliferation and differentiation into effector cells, decreased mitochondrial respiration upon STING activation further suggests impaired metabolism also in naïve and memory T cells.

Physiological function of STING in T cells

The fact that T cell-intrinsic STING signaling widely impacts T cell functionality raises the question what physiological purpose STING activation in T cells serves. We show that human T cells are capable of canonical STING pathway activation resulting in potent antiviral cytokine release and ISG induction, which opens up the possibility of STING directly sensing infections with T cell tropic viruses. Double-stranded DNA viruses HHV6A, HHV6B, and HHV7 of the betaherpesviridae family predominantly infect CD4 T cells leading to roseola fever initially and often lifelong latency afterwards. It is conceivable that during viral replication in T cells, antiviral factors initiated by cGAS sensing viral DNA are contributing to an antiviral immune response. However, HHV6/7 infection does not induce a type I interferon response (Wang & Pellett, 2007), possibly by viral proteins inhibiting IRF3 (Jaworska *et al*, 2007) as a countermeasure for the detection through a PRR system such as the cGAS-STING pathway.

Considering the substantial effect on T cell function through induction of apoptosis, as well as impaired proliferation and metabolism, cGAS-STING signaling in T cells may also serve as a "safeguard" mechanism following activation and prolonged proliferation as these processes pose a risk for malignancy through the accumulation of DNA damage. cGAS-STING signaling might then be particularly relevant for T cells given their vast proliferative capacity once activated. There is increasing evidence that cGAS-STING senses cytosolic genomic DNA that forms during prolonged TCR stimulation (Li *et al*, 2020; Concepcion *et al*, 2022). As such, cGAS-STING may sense extranuclear DNA, which forms following DNA damage during clonal expansion. Moreover, mitochondrial stress and subsequent mtDNA release were shown to activate cGAS-STING signaling, which we extend to human T cells in this study (Rongvaux *et al*, 2014; White *et al*, 2014; West *et al*, 2015; Wu *et al*, 2019b).

To capitalize on the enhanced immune response against tumor cells after intratumoral STING activation as a therapeutic concept, the application of synthetic, exogenous STING agonists is currently being investigated. While preclinical studies have provided promising results (Corrales *et al*, 2015), subsequent clinical trials have seen mixed results in terms of efficacy (Le Naour *et al*, 2020). This may be due, in part, to reduced functionality of tumor-infiltrating effector T cells following T cell-intrinsic STING activation. In studies with murine tumor models, high dosing regimens of a STING agonist indeed compromised durable tumor control by adaptive immune cells (Sivick *et al*, 2018). Adoptive transfer of STING-deficient T cells in combination with STING agonist treatment could potentially overcome this hurdle and represents a promising new concept for exploiting intratumoral STING activation.

In summary, our study highlights that T cells can indeed contribute to immediate antiviral defenses by producing large amounts of type I interferons in response to cGAS-STING activation. The flip side of the coin is a significant inhibition of T cell function. These distinct roles of STING in human T cells should be considered when this signaling pathway is targeted for immunotherapy.

Materials and Methods

Isolation and culture of human T cells

Peripheral blood mononuclear cells (PBMCs) were isolated from leukocyte reduction system chambers leftover from thrombocyte donation by healthy donors. Approval by the responsible ethics committee and informed consent from all donors according to the declaration of Helsinki were obtained (Project number: 19-238, ethics committee of the Medical Faculty at Ludwig-Maximilians-Universität in Munich). Due to privacy constraints, no information on age, sex, gender, or ethnicity is available for the study participants. Following 1:8 dilution in saline solution, the blood-saline mixture was separated through density gradient centrifugation (Biocoll, Merck #L6115) at 800 *g* for 15 min. PBMCs at the interphase

were collected, diluted 1:2 with PBS and centrifugated (450 *g*, 7 min) for removal of Biocoll. Residual erythrocytes in PBMC pellet were lysed (RBC erythrocyte lysis buffer, Biolegend, #420301) for 5 min on ice. PBMCs were then resuspended in MACS buffer for subsequent negative selection magnetic bead isolation following the manufacturer's instructions (CD4, naïve CD4 and CD8 T cell isolation kit, human; all Miltenyi; #130-096-533, #130-094-131 and #130-096-495, respectively). Sufficient purity following isolation (> 90%) was confirmed by flow cytometry (Fig EV4D).

Cells were then cultured in RPMI 1640 (Thermo Fisher Scientific, #21875-034) supplemented with 10% (v/v) FCS (Gibco, #10270106), 1 mM sodium pyruvate (Gibco, #11360070), 10 mM HEPES (Sigma-Aldrich, #H0887-100ML) and 100 IU/ml penicillin–streptomycin (Thermo Fisher Scientific, #15140163). Additionally, the medium contained 5 ng/ml human recombinant IL7 and IL15 (both Peprotech, #200-07-50ug and #200-15-50ug, respectively).

If not otherwise indicated, 2×10^6 cells were transferred to a 24-well plate coated with 10 µg/ml CD3 (BioLegend, #300438) and 5 µg/ml CD28 (BioLegend, #302902) (incubated in 200 µl PBS at 37°C for 1–2 h, then washed thrice with PBS). Cells were transferred to a new well after 2 days and resupplied once with medium with 50 IU/ml IL2 (R&D Systems, #202-IL-500). Every 2–3 days, cells were resupplied with fresh medium containing IL7 and IL15 keeping a concentration of $0.5–1 \times 10^6$ cells/ml.

CRISPR/Cas9 knockout in primary human T cells

Polyclonal and clonal CRISPR/Cas9 T cell knockouts were generated as described previously (Linder *et al*, 2020). Briefly, RNPs were produced by mixing synthesized, chemically stabilized tracr- and crRNA (both IDT; 100 pmol each), annealing them at 95°C for 5 min, then letting them cool at room temperature for 30 min. tcr:crRNA pairs were then incubated with 40 pmol of recombinant S.p. NLS-Cas9 (MPI of Biochemistry, Martinsried) for 15 min at room temperature. For the double and triple targeting approach, amounts of tcrRNA and Cas9 were scaled up 2 or 3×. In the case of IRF3, a single gRNA consisting of a fused tcrRNA and crRNA was used, so the annealing step was omitted. $1–2 \times 10^6$ cells were washed once in PBS, then resuspended in 20 µl P3 buffer (Lonza, #V4XP-3012), mixed with RNPs, and transferred to a 16-well nucleofection plate (Lonza). Cells were then electroporated using the X-unit of a 4D nucleofector (Lonza, program EH100; Seki & Rutz, 2018). After electroporation, cells were transferred to a 24-well plate coated with 10 µg/ml CD3 and 5 µg/ml CD28 in 250 µl RPMI 1640 medium without supplements. After 30–60 min, 250 µl of 2× RPMI 1640 medium with double the supplements and cytokines were added. Cells were then expanded as described above. After 14 days T cells were analyzed for KO efficiency by immunoblotting or Sanger sequencing before being subjected to analysis.

For the generation of single-cell clones with all-allelic knockout for the gene of interest, T cells were subjected to minimal dilution cloning on day 2 of activation in round-bottom 96-well plates. For these experiments, MACS-purified naïve CD4 T cells were cultivated in RPMI supplemented with 2.5% human serum (AB, Sigma-Aldrich, #H5667) containing 50 IU/ml IL2. Monoclones were restimulated on day 8 by the addition of 2,000 αCD3/CD28 beads/well. When colonies became visible after approximately 3 weeks, clones were collected and subjected to MiSeq analysis as described before (Schmid-Burgk *et al*, 2014). In order to obtain sufficient cellular material, all clones generated that were all-allelic knockouts for a certain gene or wildtype were pooled. Wildtype clones from the same donor were pooled from different genome-targeting approaches. For the generation of knockout clones only individual gRNAs were used for STING (gRNA1) and IFNAR1 (gRNA1).

The following gRNAs were used in this study: cGAS gRNA1: CAAAACCGCCCGGAGCTTCG; cGAS gRNA2: CGCATCCCTCCGTACGAGAA; STING gRNA1: GCTGGGACTGCTGTTAAACG; STING gRNA2: GACACGGGATGGATGGATGC; IRF3 sgRNA: GAGGTGACAGCCTTCTACCG; IFNAR1 gRNA1: GCGGCTGCGGACAACACCCA; IFNAR1 gRNA2: GACCCTAGTGCTCGTCGCCG; IFNAR1 gRNA3: GGACAACACCCATGGCGCCA.

Stimulation

Cells were plated at 3×10^6 cells/ml in a 24-well plate (500 µl) for western blotting and at 1.33×10^6 cells/ml in a 96-well plate (150 µl) for ELISA and flow cytometry. Stimuli were used at the following concentrations, if not indicated otherwise: 20 µg/ml 2′-3′-cGAMP (synthesized in-house, detailed synthesis instructions available upon request) for ELISA and WB, and 40 µg/ml 2′-3′-cGAMP for flow cytometry; 5:1 cells:beads αCD3/CD28 (Gibco, #11132D), 1 µM ABT737 (Selleck Chemicals, #S1002), 1 µM S63845 (Selleck Chemicals, #S8383), 6,000 IU/ml IFNα2a (Miltenyi Biotec, #130-093-874), 20 µM zVAD (R&D Systems, #FMK001), 2 µg/ml PHA (Sigma-Aldrich, #61764), 50 ng/ml PMA (Enzo Life Sciences, #BML-PE160-0005), 1 IU/ml ionomycin (Alomone Labs, #I-700), 10 ng/ml IFNγ (PeproTech, #300-02), 10 ng/ml TNFα (PeproTech, #300-01A), 50 IU/ml IL2 (R&D Systems, #202-IL-010), TPCA-1 (R&D Systems, #2559/10), Dasatinib (Selleck Chemicals, #S1021), Tacrolimus (Astellas Pharma, #06896463), Torin1 (InvivoGen, #inh-tor1), and 2 µM Thapsigargin (Sigma-Aldrich, #T9033-.5MG). For HT-DNA delivery, 200 ng of HT-DNA (Sigma-Aldrich, #D6898-1G) per condition was complexed with 0.5 µl of Lipofectamine 2000 (Thermo Fisher Scientific, #11668019) per condition in Opti-MeM (Gibco, #10149832) for 5 min at RT.

Immunoblotting

After 4 h (if not indicated otherwise) of stimulation, cells were collected from wells, washed once in cold PBS, and lysed in 30 µl DISC buffer containing protease inhibitor (Roche, #11697498001). Samples were spun clear at 18,000 *g* for 10 min. To adjust the protein amount between lanes, protein concentration was measured using a BCA assay (Thermo Fisher Scientific, #23227). Protein was denatured by adding 6× Laemmli buffer and incubating at 78°C for 10 min before freezing samples at −20°C. Supernatants were precipitated with methanol/chloroform in a ratio of 1:1:0.25, resuspended in 1× Laemmli sample buffer, and denatured at 95°C for 10 min (Jakobs *et al*, 2013). Twenty microgram of protein for each sample was separated based on molecular weight through SDS–polyacrylamide gel electrophoresis (Thermo Fisher Scientific, #XP00125BOX) at 120 V for 75 min, then blotted on 0.45 µm nitrocellulose membranes (Amersham Protran, #10600002) at 360 A for 60 min. Membranes were blocked in TBS-T with 3% BSA (Sigma-Aldrich, #A7906-100G) for 15 min, incubated with the indicated primary antibody overnight at 4°C, washed thrice in TBS-T, incubated with

corresponding HRP-linked secondary antibody for 2 h at RT, and washed again. Chemiluminescence was recorded on a Fusion Fx (Vilber) with a CCD camera directly after adding HRP substrate (Millipore, #WBLUF0500). Contrast was enhanced in a linear fashion. The following antibodies were used at 1:1,000 dilution in 3% BSA or 3% milk (for HRP-coupled antibodies): Anti-mouse IgG, HRP-linked (Cell Signaling Technology, #7076P2); Anti-rabbit IgG, HRP-linked (Cell Signaling Technology, #7074S); Human b-Actin-Ab., monoclonal, HRP-conjugated (Santa Cruz, #sc-47778); STING (D2P2F) Rabbit mAb (Cell Signaling Technology, #13647); Phospho-STING (Ser366) (D7C3S) Rabbit mAb (Cell Signaling Technology, #19781); IRF3 (D83B9) Rabbit mAb (Cell Signaling Technology, #4302S); Phospho-IRF-3 (Ser396) (4D4G) Rabbit mAb (Cell Signaling Technology, #4947); Stat1 (9H2) Mouse mAb (Cell Signaling Technology, #9176S); pSTAT1 (Y701) Antibody (Cell Signaling Technology, #7649S), cGAS (D1D3G) Rabbit mAb (Cell Signaling Technology, #15102S), PARP (46D11) Rabbit mAb (Cell Signaling Technology, #9532S), TBK1 (Cell Signaling Technology #3013S), Phospho-TBK1/NAK (Ser172) (D52C2) XP® Rabbit mAb (Cell Signaling Technology, #5483S), Phospho-NF-κB p65 (Ser536) (93H1) Rabbit mAb (Cell Signaling Technology, #3033S), Phospho-IκBα (Ser32) (14D4) Rabbit mAb (Cell Signaling Technology, #2859S), Caspase-3 Antibody (Cell Signaling Technology, #9662S).

Enzyme-linked immunosorbent assay (ELISA) and CellTiter-Glo assay

Supernatant was collected after 48 h of stimulation and frozen at −20°C until analysis. Human IFNβ ELISA, IFNγ ELISA, IFNα ELISA (all R&D Systems, #DY814-05, #DY285B, and #DFNAS0, respectively), and IP10 ELISA (BD Bioscience, #550926) was performed according to the manufacturer's instructions. CellTiter-Glo 2.0 Assay (Promega, #G9243) was performed with residual cells after supernatant removal according to the manufacturer's instructions.

Cell death assay

After 48 h of stimulation, cells were collected, washed once in PBS, and stained with Annexin V (1:40; BioLegend, #640918) in Annexin binding buffer for 15 min at RT. Cells were washed twice in Annexin binding buffer, resuspended in 100 µl buffer containing propidium iodide (1:40; eBioscience, #00-6990-50), and analyzed on a BDFortessa cytometer. Analysis was done in FlowJo. Contour plots (5% levels without outliers) show single events without subcellular debris (see Fig EV4E for gating strategy). Treatment-induced cell death was calculated as (%Annexin V^+PI^+ cells with treatment − %Annexin V^+PI^+ cells without treatment)/(100 − % Annexin V^+PI^+ cells without treatment).

Proliferation assay

Cultured T cells were counted, spun down, and resuspended in CellTrace Violet staining solution (1:1,000 in PBS, Invitrogen, #C34571) in 1 ml per 10^6 cells. Staining solution was incubated at 37°C for 20 min, then quenched with prewarmed cell-culture medium (5× volume of staining solution). Cells were then spun down and plated. Four days later, cells were collected, washed once in PBS, and stained with LIVE/DEAD™ Fixable Near-IR (1:1,000 in PBS; Thermo Fisher Scientific, #L10119) in 50 µl for 20 min at RT in the dark. Cells were washed again in FACS buffer (2% FCS (v/v) PBS + 2 mM EDTA), then stained with anti-CD25 antibody (1:40 in FACS buffer; BioLegend, #356106) in 50 µl for 30 min on ice in the dark. Before analysis on a BDFortessa cytometer (see Fig EV4F for gating strategy), cells were washed twice with FACS buffer. For quantification, individual generations for each peak were calculated using a computer-generated model fitted to the CTV profile by FlowJo. Then, the estimated total number of divisions was divided by the estimated total number of cells, resulting in the division index. Division indices of treated samples were normalized to the nontreated controls by calculating the log2-transformed fold change (log2FC).

Low-input RNA-Seq library preparation and analysis

Following stimulation, 5×10^4 cells per sample were washed lysed with RLT lysis buffer containing 0.04 M DTT and 1% Triton ×100 before storing at −80°C for at least 1 day. Samples were digested with 20 mg/ml Proteinase K for 10 min at 50°C, followed by heat inactivation at 80°C for 10 min. Subsequent RNA/DNA extraction was done by automatic pipetting (Biomek i7, Beckman-Coulter) using RNAdvance Viral Reagent Kit (Beckman-Coulter, #C63510), following the manufacturer's instructions. DNA was digested by incubation with DNAse I for 10 min at 37°C, before adding EDTA (5 mM final concentration) and heat inactivation at 70°C for 10 min. For reverse transcription, RNA barcoding, and library preparation, a modified SCRB-seq protocol (preprint: Soumillon *et al*, 2014) was followed. Samples were sequenced at NGS Core Facility (MPI of Biochemistry, Martinsried) using a NextSeq 500 (Illumina). FASTQC (Andrews, 2010) was used for initial quality control. FASTQ demultiplexing, QC, mapping, and gene counting were done with zUMIs (Parekh *et al*, 2018), and human genome GRCh38 (Howe *et al*, 2020) was used as the reference. All the postmapping analysis and visualization were conducted in R unless specifically stated otherwise. Normalization, exploratory analysis, and differential expression analysis were performed using DESeq2 (Love *et al*, 2014). ggplot2 and ComplexHeatmap were used to visualize the results. Scripts are available upon request. Normalized, filtered read counts and log2-transformed, normalized read counts are available as Datasets EV1 and EV2, respectively.

Glycolysis and mito stress assay

Freshly isolated T cells were activated with αCD3/28 beads for 48 h in the presence or absence of 40 µg/ml cGAMP. Meanwhile, a 96-well Seahorse utility plate (Agilent, #102416-100) was coated 1 day prior to analysis with 18 µl poly-D-lysine at RT for 45 min, washed twice with ddH2O, and dried. A Seahorse sensor cartridge (Agilent, #102416-100) was filled with 200 µl ddH2O and kept overnight in a CO_2-free incubator at 37°C. After 48 h of incubation, cells were depleted of magnetic beads, counted and 2×10^5 viable cells/well were seeded in the previously coated Seahorse 96-well plate and centrifuged at 300 *g* for 3 min at RT. Cells were then incubated for 45 min at 37°C without CO_2 in respective medium: (i) Mitochondria stress assay medium: XF RPMI medium (Agilent, #103576-100) containing 2 mM glutamine (Agilent, #103579-100), 1 mM sodium pyruvate (Agilent, #103578-100) and 10 mM glucose (Agilent,

103577-100), (ii) Glycolysis stress assay medium: XF RPMI medium (Agilent, #103576-100) containing 2 mM glutamine (Agilent, #103579-100). The components of the Seahorse XF Glycolysis and Cell Mito Stress Test Kits (both Agilent, #103020-100 and #103015-100) were reconstituted at the desired stock concentrations and the final dilutions were prepared: (i) Mitochondria stress test: 1 μM Oligomycin, 1 μM FCCP and 1 μM rotenone/antimycin A, (ii) glycolysis stress test: 10 mM Glucose, 1 μM Oligomycin and 50 mM 2-DG. The ddH2O in the sensor cartridge was exchanged with 200 μl calibrant solution and the assay solutions were loaded into the appropriate ports of the hydrated sensor cartridge. Hoechst dye was loaded to the last port, in order to normalize the results to absolute cell numbers. The Seahorse analyzer (Agilent) was calibrated and the cartridge containing the calibrant was exchanged with the cell-containing plate. Metabolic rate data were normalized to viable cell counts based on Hoechst staining using a Citation 1 (BioTek Instruments).

qPCR

RNA was isolated from 2×10^6 expanded CD4 T cells 4 h after stimulation using the Total RNA Purification Mini Spin Column Kit (Genaxxon Bioscience GmbH, #S5304.0250) according to the manufacturer's protocol. The remaining DNA in the extracted RNA was digested using DNaseI (Thermo Scientific, #EN0521). cDNA synthesis were performed with RevertAid Reverse Transcriptase (Thermo Scientific, #EP0442) with Oligo(dT)18 primers. The synthesized cDNA was cleaned up using solid-phase reversible immobilization magnetic beads (GE Healthcare, #GE45152105050250). For the qPCR reaction, TakyonTM No Rox SYBR® MasterMix dTTP Blue (Eurogentec, #UF-NSMT-B0705) was used with the respective primer pairs. The following qPCR primers were used in this study: *TBP1* (fwd: 5′-CCCGAAACGCCGAATATAATCC-3′, rev: 5′-AATCAG TGCCGTGGTTCGTG-3′), *IFNB1* (fwd: 5′-GGCACAACAGGTAGTAG GCG-3′, rev: 5′-GTGGAGAAGCACAACAGGAGA-3′), *OASL* (fwd: 5′-AGGGTACAGATGGGACATCG-3′, rev: 5′-AAGGGTTCACGATGAGG TTG-3′).

Experimental study design

No sample size calculation was made; the sample size was chosen based on past experience and common practice in the field. Blinding was not required for this study because no subjective analyses were performed that would have been biased by knowledge about the samples studied. Rarely, individual data points were excluded from further analysis when technical errors occurred in the measurement process. Also rarely, datasets were intentionally excluded when the positive control did not show a response.

Statistical methods

Normal distribution of the data has been tested on representative data (e.g., cytokine or LDH measurements) using the Shapiro–Wilk test. Statistical significance was calculated as outlined in the respective figure legends with corrections for multiple testing, if relevant. If multiple comparisons are depicted with one comparison bar, the major tick of the comparison bar indicates the reference data to which the statements regarding the level of significance are made. Data plotting and statistical analysis was performed with GraphPad Prism 9.

Data availability

This study includes no data deposited in external repositories. Critical reagents are available upon reasonable request.

Expanded View for this article is available online.

Acknowledgements
We kindly thank the BioSysM FACS core facility for assistance with flow cytometry, the BioSysM Automation Unit for liquid handling, and Claudia Ludwig (Gene Center, LMU) for great technical support. This study was supported by funding from the Deutsche Forschungsgemeinschaft (DFG, German Research Foundation) SFB TRR 338 (project ID 452881907) to VH, MS, and ST and SFB 1054 (project ID 210592381) to VH. AL is supported by a fellowship of the Else Kröner-Forschungskolleg: Cancer Immunotherapy and the FöFoLe program of the LMU. Open Access funding enabled and organized by Projekt DEAL.

Author contributions
Niklas Kuhl: Conceptualization; investigation; writing – original draft; writing – review and editing. **Andreas Linder:** Conceptualization; investigation; writing – original draft; writing – review and editing. **Nora Philipp:** Investigation. **Daniel Nixdorf:** Investigation. **Hannah Fischer:** Investigation. **Simon Veth:** Investigation. **Gunnar Kuut:** Investigation. **Teng Teng Xu:** Investigation. **Sebastian Theurich:** Resources; supervision; funding acquisition. **Thomas Carell:** Resources; supervision; funding acquisition. **Marion Subklewe:** Resources; supervision; funding acquisition. **Veit Hornung:** Conceptualization; resources; data curation; supervision; funding acquisition; writing – original draft; writing – review and editing.

Disclosure and competing interests statement
The authors declare that they have no conflict of interest.

References

Abe T, Barber GN (2014) Cytosolic-DNA-mediated, STING-dependent proinflammatory gene induction necessitates canonical NF-κB activation through TBK1. *J Virol* 88: 5328 – 5341

Ablasser A, Goldeck M, Cavlar T, Deimling T, Witte G, Röhl I, Hopfner K-P, Ludwig J, Hornung V (2013) cGAS produces a 2′-5′-linked cyclic dinucleotide second messenger that activates STING. *Nature* 498: 380 – 384

Andrews S (2010) FastQC: a quality control tool for high throughput sequence data. https://www.bioinformatics.babraham.ac.uk/projects/fastqc/

Au WC, Moore PA, Lowther W, Juang YT, Pitha PM (1995) Identification of a member of the interferon regulatory factor family that binds to the interferon-stimulated response element and activates expression of interferon-induced genes. *Proc Natl Acad Sci USA* 92: 11657 – 11661

Banerjee D, Langberg K, Abbas S, Odermatt E, Yerramothu P, Volaric M, Reidenbach MA, Krentz KJ, Rubinstein CD, Brautigan DL *et al* (2021) A non-canonical, interferon-independent signaling activity of cGAMP triggers DNA damage response signaling. *Nat Commun* 12: 6207

Benoit-Lizon I, Jacquin E, Rivera Vargas T, Richard C, Roussey A, Dal Zuffo L, Martin T, Melis A, Vinokurova D, Shahoei SH *et al* (2022) CD4 T cell-intrinsic STING signaling controls the differentiation and effector functions of T_H1 and T_H9 cells. *J Immunother Cancer* 10: e003459

Bouis D, Kirstetter P, Arbogast F, Lamon D, Delgado V, Jung S, Ebel C, Jacobs H, Knapp A-M, Jeremiah N *et al* (2019) Severe combined immunodeficiency in stimulator of interferon genes (STING) V154M/wild-type mice. *J Allergy Clin Immunol* 143: 712–725

Burdette DL, Monroe KM, Sotelo-Troha K, Iwig JS, Eckert B, Hyodo M, Hayakawa Y, Vance RE (2011) STING is a direct innate immune sensor of cyclic di-GMP. *Nature* 478: 515–518

Cerboni S, Jeremiah N, Gentili M, Gehrmann U, Conrad C, Stolzenberg M-C, Picard C, Neven B, Fischer A, Amigorena S *et al* (2017) Intrinsic antiproliferative activity of the innate sensor STING in T lymphocytes. *J Exp Med* 214: 1769–1785

Chattopadhyay S, Marques JT, Yamashita M, Peters KL, Smith K, Desai A, Williams BRG, Sen GC (2010) Viral apoptosis is induced by IRF-3-mediated activation of Bax. *EMBO J* 29: 1762–1773

Concepcion AR, Wagner LE, Zhu J, Tao AY, Yang J, Khodadadi-Jamayran A, Wang Y-H, Liu M, Rose RE, Jones DR *et al* (2022) The volume-regulated anion channel LRRC8C suppresses T cell function by regulating cyclic dinucleotide transport and STING–p53 signaling. *Nat Immunol* 23: 287–302

Corrales L, Glickman LH, McWhirter SM, Kanne DB, Sivick KE, Katibah GE, Woo S-R, Lemmens E, Banda T, Leong JJ *et al* (2015) Direct activation of STING in the tumor microenvironment leads to potent and systemic tumor regression and immunity. *Cell Rep* 11: 1018–1030

de Oliveira Mann CC, Orzalli MH, King DS, Kagan JC, Lee ASY, Kranzusch PJ (2019) Modular architecture of the STING C-terminal tail allows interferon and NF-κB signaling adaptation. *Cell Rep* 27: 1165–1175

Dickow J, Francois S, Kaiserling R-L, Malyshkina A, Drexler I, Westendorf AM, Lang KS, Santiago ML, Dittmer U, Sutter K (2019) Diverse immunomodulatory effects of individual IFNα subtypes on virus-specific $CD8^+$ T cell responses. *Front Immunol* 10: 2255

Diner EJ, Burdette DL, Wilson SC, Monroe KM, Kellenberger CA, Hyodo M, Hayakawa Y, Hammond MC, Vance RE (2013) The innate immune DNA sensor cGAS produces a noncanonical cyclic dinucleotide that activates human STING. *Cell Rep* 3: 1355–1361

Dou Z, Ghosh K, Vizioli MG, Zhu J, Sen P, Wangensteen KJ, Simithy J, Lan Y, Lin Y, Zhou Z *et al* (2017) Cytoplasmic chromatin triggers inflammation in senescence and cancer. *Nature* 550: 402–406

Dufva O, Koski J, Maliniemi P, Ianevski A, Klievink J, Leitner J, Pölönen P, Hohtari H, Saeed K, Hannunen T *et al* (2020) Integrated drug profiling and CRISPR screening identify essential pathways for CAR T-cell cytotoxicity. *Blood* 135: 597–609

Fang R, Wang C, Jiang Q, Lv M, Gao P, Yu X, Mu P, Zhang R, Bi S, Feng J-M *et al* (2017) NEMO–IKKβ are essential for IRF3 and NF-κB activation in the cGAS–STING pathway. *J Immunol* 199: 3222–3233

Gao P, Ascano M, Wu Y, Barchet W, Gaffney Barbara L, Zillinger T, Serganov Artem A, Liu Y, Jones Roger A, Hartmann G *et al* (2013) Cyclic [G(2′,5′)pA(3′,5′)p] is the metazoan second messenger produced by DNA-activated cyclic GMP-AMP synthase. *Cell* 153: 1094–1107

Glück S, Guey B, Gulen MF, Wolter K, Kang T-W, Schmacke Niklas A, Bridgeman A, Rehwinkel J, Zender L, Ablasser A (2017) Innate immune sensing of cytosolic chromatin fragments through cGAS promotes senescence. *Nat Cell Biol* 19: 1061–1070

Green DR, Droin N, Pinkoski M (2003) Activation-induced cell death in T cells. *Immunol Rev* 193: 70–81

Gulen MF, Koch U, Haag SM, Schuler F, Apetoh L, Villunger A, Radtke F, Ablasser A (2017) Signalling strength determines proapoptotic functions of STING. *Nat Commun* 8: 427

Harding SM, Benci JL, Irianto J, Discher DE, Minn AJ, Greenberg RA (2017) Mitotic progression following DNA damage enables pattern recognition within micronuclei. *Nature* 548: 466–470

Honda K, Takaoka A, Taniguchi T (2006) Type I inteferon gene induction by the interferon regulatory factor family of transcription factors. *Immunity* 25: 349–360

Howe KL, Contreras-Moreira B, De Silva N, Maslen G, Akanni W, Allen J, Alvarez-Jarreta J, Barba M, Bolser DM, Cambell L *et al* (2020) Ensembl Genomes 2020-enabling non-vertebrate genomic research. *Nucleic Acids Res* 48: D689–D695

Imanishi T, Unno M, Kobayashi W, Yoneda N, Matsuda S, Ikeda K, Hoshii T, Hirao A, Miyake K, Barber GN *et al* (2019) Reciprocal regulation of STING and TCR signaling by mTORC1 for T-cell activation and function. *Life Sci Alliance* 2: e201800282

Ishikawa H, Barber GN (2008) STING is an endoplasmic reticulum adaptor that facilitates innate immune signalling. *Nature* 455: 674–678

Iwanaszko M, Kimmel M (2015) NF-κB and IRF pathways: cross-regulation on target genes promoter level. *BMC Genomics* 16: 307

Jakobs C, Bartok E, Kubarenko A, Bauernfeind F, Hornung V (2013) Immunoblotting for active caspase-1. *Methods Mol Biol* 1040: 103–115

Jaworska J, Gravel A, Fink K, Grandvaux N, Flamand L (2007) Inhibition of transcription of the beta interferon gene by the human herpesvirus 6 immediate-early 1 protein. *J Virol* 81: 5737–5748

Larkin B, Ilyukha V, Sorokin M, Buzdin A, Vannier E, Poltorak A (2017) Cutting edge: activation of STING in T cells induces type I IFN responses and cell death. *J Immunol* 199: 397–402

Le Bourgeois T, Strauss L, Aksoylar H-I, Daneshmandi S, Seth P, Patsoukis N, Boussiotis VA (2018) Targeting T cell metabolism for improvement of cancer immunotherapy. *Front Oncol* 8: 237

Le Naour J, Zitvogel L, Galluzzi L, Vacchelli E, Kroemer G (2020) Trial watch: STING agonists in cancer therapy. *Oncoimmunology* 9: 1777624

Li T, Chen ZJ (2018) The cGAS–cGAMP–STING pathway connects DNA damage to inflammation, senescence, and cancer. *J Exp Med* 215: 1287–1299

Li W, Lu L, Lu J, Wang X, Yang C, Jin J, Wu L, Hong X, Li F, Cao D *et al* (2020) cGAS-STING–mediated DNA sensing maintains $CD8^+$ T cell stemness and promotes antitumor T cell therapy. *Sci Transl Med* 12: eaay9013

Lin R, Heylbroeck C, Pitha PM, Hiscott J (1998) Virus-dependent phosphorylation of the IRF-3 transcription factor regulates nuclear translocation, transactivation potential, and proteasome-mediated degradation. *Mol Cell Biol* 18: 2986–2996

Linder A, Bauernfried S, Cheng Y, Albanese M, Jung C, Keppler OT, Hornung V (2020) CARD8 inflammasome activation triggers pyroptosis in human T cells. *EMBO J* 39: e105071

Love MI, Huber W, Anders S (2014) Moderated estimation of fold change and dispersion for RNA-seq data with DESeq2. *Genome Biol* 15: 550

Mackenzie KJ, Carroll P, Martin C-A, Murina O, Fluteau A, Simpson DJ, Olova N, Sutcliffe H, Rainger JK, Leitch A *et al* (2017) cGAS surveillance of micronuclei links genome instability to innate immunity. *Nature* 548: 461–465

Ning X, Wang Y, Jing M, Sha M, Lv M, Gao P, Zhang R, Huang X, Feng J-M, Jiang Z (2019) Apoptotic caspases suppress type I interferon production via the cleavage of cGAS, MAVS, and IRF3. *Mol Cell* 74: 19–31

Parekh S, Ziegenhain C, Vieth B, Enard W, Hellmann I (2018) zUMIs - a fast and flexible pipeline to process RNA sequencing data with UMIs. *Gigascience* 7: giy059

Pearce EL (2010) Metabolism in T cell activation and differentiation. *Curr Opin Immunol* 22: 314 – 320

Rongvaux A, Jackson R, Harman Christian CD, Li T, West AP, de Zoete Marcel R, Wu Y, Yordy B, Lakhani Saquib A, Kuan C-Y *et al* (2014) Apoptotic caspases prevent the induction of type I interferons by mitochondrial DNA. *Cell* 159: 1563 – 1577

Samarajiwa SA, Forster S, Auchettl K, Hertzog PJ (2009) INTERFEROME: the database of interferon regulated genes. *Nucleic Acids Res* 37: D852 – D857

Schmid-Burgk JL, Schmidt T, Gaidt MM, Pelka K, Latz E, Ebert TS, Hornung V (2014) OutKnocker: a web tool for rapid and simple genotyping of designer nuclease edited cell lines. *Genome Res* 24: 1719 – 1723

Seki A, Rutz S (2018) Optimized RNP transfection for highly efficient CRISPR/Cas9-mediated gene knockout in primary T cells. *J Exp Med* 215: 985 – 997

Sivick KE, Desbien AL, Glickman LH, Reiner GL, Corrales L, Surh NH, Hudson TE, Vu UT, Francica BJ, Banda T *et al* (2018) Magnitude of therapeutic STING activation determines $CD8^+$ T cell-mediated anti-tumor immunity. *Cell Rep* 25: 3074 – 3085

Soboloff J, Rothberg BS, Madesh M, Gill DL (2012) STIM proteins: dynamic calcium signal transducers. *Nat Rev Mol Cell Biol* 13: 549 – 565

Soumillon M, Cacchiarelli D, Semrau S, Oudenaarden AV, Mikkelsen TS (2014) Characterization of directed differentiation by high-throughput single-cell RNA-Seq. *bioRxiv* https://doi.org/10.1101/003236 [PREPRINT]

Srikanth S, Woo JS, Wu B, El-Sherbiny YM, Leung J, Chupradit K, Rice L, Seo GJ, Calmettes G, Ramakrishna C *et al* (2019) The Ca^{2+} sensor STIM1 regulates the type I interferon response by retaining the signaling adaptor STING at the endoplasmic reticulum. *Nat Immunol* 20: 152 – 162

Sun L, Wu J, Du F, Chen X, Chen ZJ (2013) Cyclic GMP-AMP synthase is a cytosolic DNA sensor that activates the type I interferon pathway. *Science* 339: 786 – 791

van der Windt GJW, Pearce EL (2012) Metabolic switching and fuel choice during T-cell differentiation and memory development. *Immunol Rev* 249: 27 – 42

Wang F-Z, Pellett PE (2007) HHV-6A, 6B, and 7: immunobiology and host response. In *Human Herpesviruses: Biology, Therapy, and Immunoprophylaxis*, Arvin A, Campadelli-Fiume G, Mocarski E, Moore PS, Roizman B, Whitley R, Yamanishi K (eds). Cambridge: Cambridge University Press

Warner JD, Irizarry-Caro RA, Bennion BG, Ai TL, Smith AM, Miner CA, Sakai T, Gonugunta VK, Wu J, Platt DJ *et al* (2017) STING-associated vasculopathy develops independently of IRF3 in mice. *J Exp Med* 214: 3279 – 3292

West AP, Khoury-Hanold W, Staron M, Tal MC, Pineda CM, Lang SM, Bestwick M, Duguay BA, Raimundo N, MacDuff DA *et al* (2015) Mitochondrial DNA stress primes the antiviral innate immune response. *Nature* 520: 553 – 557

White MJ, McArthur K, Metcalf D, Lane RM, Cambier JC, Herold MJ, van Delft MF, Bedoui S, Lessene G, Ritchie ME *et al* (2014) Apoptotic caspases suppress mtDNA-induced STING-mediated type I IFN production. *Cell* 159: 1549 – 1562

Wu J, Chen Y-J, Dobbs N, Sakai T, Liou J, Miner JJ, Yan N (2019a) STING-mediated disruption of calcium homeostasis chronically activates ER stress and primes T cell death. *J Exp Med* 216: 867 – 883

Wu Z, Oeck S, West AP, Mangalhara KC, Sainz AG, Newman LE, Zhang X-O, Wu L, Yan Q, Bosenberg M *et al* (2019b) Mitochondrial DNA stress signalling protects the nuclear genome. *Nat Metab* 1: 1209 – 1218

Wu J, Dobbs N, Yang K, Yan N (2020) Interferon-independent activities of mammalian STING mediate antiviral response and tumor immune evasion. *Immunity* 53: 115 – 126

Yang H, Wang H, Ren J, Chen Q, Chen ZJ (2017) cGAS is essential for cellular senescence. *Proc Natl Acad Sci USA* 114: E4612 – E4620

Zhang X, Shi H, Wu J, Zhang X, Sun L, Chen C, Chen ZJ (2013) Cyclic GMP-AMP containing mixed phosphodiester linkages is an endogenous high-affinity ligand for STING. *Mol Cell* 51: 226 – 235

6. References

1. Thomas, E.D., et al., Intravenous infusion of bone marrow in patients receiving radiation and chemotherapy. N Engl J Med, 1957. 257(11): p. 491-6.
2. Daver, N., et al., T-cell-based immunotherapy of acute myeloid leukemia: current concepts and future developments. Leukemia, 2021. 35(7): p. 1843-1863.
3. Sharpe, A.H. and K.E. Pauken, The diverse functions of the PD1 inhibitory pathway. Nat Rev Immunol, 2018. 18(3): p. 153-167.
4. Li, R., et al., The CAR T-Cell Mechanoimmunology at a Glance. Adv Sci (Weinh), 2020. 7(24): p. 2002628.
5. Kantarjian, H., et al., Blinatumomab versus Chemotherapy for Advanced Acute Lymphoblastic Leukemia. N Engl J Med, 2017. 376(9): p. 836-847.
6. Topp, M.S., et al., Safety and activity of blinatumomab for adult patients with relapsed or refractory B-precursor acute lymphoblastic leukaemia: a multicentre, single-arm, phase 2 study. Lancet Oncol, 2015. 16(1): p. 57-66.
7. Locke, F.L., et al., Primary Analysis of ZUMA-7: A Phase 3 Randomized Trial of Axicabtagene Ciloleucel (Axi-Cel) Versus Standard-of-Care Therapy in Patients with Relapsed/Refractory Large B-Cell Lymphoma. Blood, 2021. 138(Supplement 1): p. 2-2.
8. Budde, L.E., et al., Safety and efficacy of mosunetuzumab, a bispecific antibody, in patients with relapsed or refractory follicular lymphoma: a single-arm, multicentre, phase 2 study. Lancet Oncol, 2022. 23(8): p. 1055-1065.
9. Moreau, P., et al., Teclistamab in Relapsed or Refractory Multiple Myeloma. N Engl J Med, 2022. 387(6): p. 495-505.
10. Bargou, R., et al., Tumor regression in cancer patients by very low doses of a T cell-engaging antibody. Science, 2008. 321(5891): p. 974-7.
11. Hoffman, L.M. and L. Gore, Blinatumomab, a Bi-Specific Anti-CD19/CD3 BiTE((R)) Antibody for the Treatment of Acute Lymphoblastic Leukemia: Perspectives and Current Pediatric Applications. Front Oncol, 2014. 4: p. 63.
12. Dufner, V., et al., Long-term outcome of patients with relapsed/refractory B-cell non-Hodgkin lymphoma treated with blinatumomab. Blood Adv, 2019. 3(16): p. 2491-2498.
13. Nagorsen, D. and P.A. Baeuerle, Immunomodulatory therapy of cancer with T cell-engaging BiTE antibody blinatumomab. Exp Cell Res, 2011. 317(9): p. 1255-60.
14. Gokbuget, N., et al., Blinatumomab for minimal residual disease in adults with B-cell precursor acute lymphoblastic leukemia. Blood, 2018. 131(14): p. 1522-1531.
15. Del Bano, J., et al., Taking up Cancer Immunotherapy Challenges: Bispecific Antibodies, the Path Forward? Antibodies (Basel), 2015. 5(1).
16. Voynov, V., et al., Discovery Strategies to Maximize the Clinical Potential of T-Cell Engaging Antibodies for the Treatment of Solid Tumors. Antibodies (Basel), 2020. 9(4).
17. You, G., et al., Bispecific Antibodies: A Smart Arsenal for Cancer Immunotherapies. Vaccines (Basel), 2021. 9(7).
18. Wang, S., et al., The state of the art of bispecific antibodies for treating human malignancies. EMBO Mol Med, 2021. 13(9): p. e14291.

19. Fourcade, J., et al., CD8(+) T cells specific for tumor antigens can be rendered dysfunctional by the tumor microenvironment through upregulation of the inhibitory receptors BTLA and PD-1. Cancer Res, 2012. 72(4): p. 887-96.

20. Chen, Y.A., et al., Extrachromosomal telomere repeat DNA is linked to ALT development via cGAS-STING DNA sensing pathway. Nat Struct Mol Biol, 2017. 24(12): p. 1124-1131.

21. Hopfner, K.P. and V. Hornung, Molecular mechanisms and cellular functions of cGAS-STING signalling. Nat Rev Mol Cell Biol, 2020. 21(9): p. 501-521.

22. Zajac, A.J., et al., Viral immune evasion due to persistence of activated T cells without effector function. J Exp Med, 1998. 188(12): p. 2205-13.

23. Wherry, E.J., T cell exhaustion. Nat Immunol, 2011. 12(6): p. 492-9.

24. Schietinger, A. and P.D. Greenberg, Tolerance and exhaustion: defining mechanisms of T cell dysfunction. Trends Immunol, 2014. 35(2): p. 51-60.

25. Weber, E.W., et al., Transient rest restores functionality in exhausted CAR-T cells through epigenetic remodeling. Science, 2021. 372(6537).

26. Philipp, N., et al., T-cell exhaustion induced by continuous bispecific molecule exposure is ameliorated by treatment-free intervals. Blood, 2022. 140(10): p. 1104-1118.

27. Sun, L., et al., Cyclic GMP-AMP synthase is a cytosolic DNA sensor that activates the type I interferon pathway. Science, 2013. 339(6121): p. 786-91.

28. Ablasser, A., et al., cGAS produces a 2'-5'-linked cyclic dinucleotide second messenger that activates STING. Nature, 2013. 498(7454): p. 380-4.

29. Burdette, D.L., et al., STING is a direct innate immune sensor of cyclic di-GMP. Nature, 2011. 478(7370): p. 515-8.

30. Ishikawa, H. and G.N. Barber, STING is an endoplasmic reticulum adaptor that facilitates innate immune signalling. Nature, 2008. 455(7213): p. 674-8.

31. Lin, R., et al., Virus-dependent phosphorylation of the IRF-3 transcription factor regulates nuclear translocation, transactivation potential, and proteasome-mediated degradation. Mol Cell Biol, 1998. 18(5): p. 2986-96.

32. Montoya, M., et al., Type I interferons produced by dendritic cells promote their phenotypic and functional activation. Blood, 2002. 99(9): p. 3263-71.

33. Kuhl, N., et al., STING agonism turns human T cells into interferon-producing cells but impedes their functionality. EMBO Rep, 2023. 24(3): p. e55536.

34. Paludan, S.R., L.S. Reinert, and V. Hornung, DNA-stimulated cell death: implications for host defence, inflammatory diseases and cancer. Nat Rev Immunol, 2019. 19(3): p. 141-153.

35. Gaidt, M.M., et al., The DNA Inflammasome in Human Myeloid Cells Is Initiated by a STING-Cell Death Program Upstream of NLRP3. Cell, 2017. 171(5): p. 1110-1124 e18.

36. Abe, T. and G.N. Barber, Cytosolic-DNA-mediated, STING-dependent proinflammatory gene induction necessitates canonical NF-kappaB activation through TBK1. J Virol, 2014. 88(10): p. 5328-41.

37. Harding, S.M., et al., Mitotic progression following DNA damage enables pattern recognition within micronuclei. Nature, 2017. 548(7668): p. 466-470.

38. Rongvaux, A., et al., Apoptotic caspases prevent the induction of type I interferons by mitochondrial DNA. Cell, 2014. 159(7): p. 1563-77.

39. West, A.P., et al., Mitochondrial DNA stress primes the antiviral innate immune response. Nature, 2015. 520(7548): p. 553-7.

40. Gluck, S., et al., Innate immune sensing of cytosolic chromatin fragments through cGAS promotes senescence. Nat Cell Biol, 2017. 19(9): p. 1061-1070.

41. Dou, Z., et al., Cytoplasmic chromatin triggers inflammation in senescence and cancer. Nature, 2017. 550(7676): p. 402-406.

42. Yang, H., et al., STING activation reprograms tumor vasculatures and synergizes with VEGFR2 blockade. J Clin Invest, 2019. 129(10): p. 4350-4364.

43. Campisi, M., et al., Tumor-Derived cGAMP Regulates Activation of the Vasculature. Front Immunol, 2020. 11: p. 2090.

44. Ghaffari, A., et al., STING agonist therapy in combination with PD-1 immune checkpoint blockade enhances response to carboplatin chemotherapy in high-grade serous ovarian cancer. Br J Cancer, 2018. 119(4): p. 440-449.

45. Dunphy, G., et al., Non-canonical Activation of the DNA Sensing Adaptor STING by ATM and IFI16 Mediates NF-kappaB Signaling after Nuclear DNA Damage. Mol Cell, 2018. 71(5): p. 745-760 e5.

46. Motwani, M., S. Pesiridis, and K.A. Fitzgerald, DNA sensing by the cGAS-STING pathway in health and disease. Nat Rev Genet, 2019. 20(11): p. 657-674.

47. Sivick, K.E., et al., Magnitude of Therapeutic STING Activation Determines CD8(+) T Cell-Mediated Anti-tumor Immunity. Cell Rep, 2018. 25(11): p. 3074-3085 e5.

48. Le Naour, J., et al., Trial watch: STING agonists in cancer therapy. Oncoimmunology, 2020. 9(1): p. 1777624.

49. Larkin, B., et al., Cutting Edge: Activation of STING in T Cells Induces Type I IFN Responses and Cell Death. J Immunol, 2017. 199(2): p. 397-402.

50. Cerboni, S., et al., Intrinsic antiproliferative activity of the innate sensor STING in T lymphocytes. J Exp Med, 2017. 214(6): p. 1769-1785.

51. Imanishi, T., et al., Reciprocal regulation of STING and TCR signaling by mTORC1 for T-cell activation and function. Life Sci Alliance, 2019. 2(1).

52. Warner, J.D., et al., STING-associated vasculopathy develops independently of IRF3 in mice. J Exp Med, 2017. 214(11): p. 3279-3292.

53. Bouis, D., et al., Severe combined immunodeficiency in stimulator of interferon genes (STING) V154M/wild-type mice. J Allergy Clin Immunol, 2019. 143(2): p. 712-725 e5.

54. Gulen, M.F., et al., Signalling strength determines proapoptotic functions of STING. Nat Commun, 2017. 8(1): p. 427.

55. Wu, J., et al., STING-mediated disruption of calcium homeostasis chronically activates ER stress and primes T cell death. J Exp Med, 2019. 216(4): p. 867-883.

56. Wu, J., et al., Interferon-Independent Activities of Mammalian STING Mediate Antiviral Response and Tumor Immune Evasion. Immunity, 2020. 53(1): p. 115-126 e5.

57. Li, W., et al., cGAS-STING-mediated DNA sensing maintains CD8(+) T cell stemness and promotes antitumor T cell therapy. Sci Transl Med, 2020. 12(549).

58. McNab, F., et al., Type I interferons in infectious disease. Nat Rev Immunol, 2015. 15(2): p. 87-103.

59. Wu, T., et al., The TCF1-Bcl6 axis counteracts type I interferon to repress exhaustion and maintain T cell stemness. Sci Immunol, 2016. 1(6).

60. Kaser, A., S. Nagata, and H. Tilg, Interferon alpha augments activation-induced T cell death by upregulation of Fas (CD95/APO-1) and Fas ligand expression. Cytokine, 1999. 11(10): p. 736-43.

61. Marshall, H.D., S.L. Urban, and R.M. Welsh, Virus-induced transient immune suppression and the inhibition of T cell proliferation by type I interferon. J Virol, 2011. 85(12): p. 5929-39.

62. Papatriantafyllou, M., Regulatory T cells: distilling regulatory T cell inducers. Nat Rev Immunol, 2013. 13(8): p. 546.

63. Teijaro, J.R., et al., Persistent LCMV infection is controlled by blockade of type I interferon signaling. Science, 2013. 340(6129): p. 207-11.

64. Wilson, E.B., et al., Blockade of chronic type I interferon signaling to control persistent LCMV infection. Science, 2013. 340(6129): p. 202-7.

65. Gan, Y., et al., The cGAS/STING Pathway: A Novel Target for Cancer Therapy. Front Immunol, 2021. 12: p. 795401.

66. Ma, R., et al., The cGAS-STING pathway: The role of self-DNA sensing in inflammatory lung disease. FASEB J, 2020. 34(10): p. 13156-13170.

67. Decout, A., et al., The cGAS-STING pathway as a therapeutic target in inflammatory diseases. Nat Rev Immunol, 2021. 21(9): p. 548-569.

68. Gallimore, A., et al., Induction and exhaustion of lymphocytic choriomeningitis virus-specific cytotoxic T lymphocytes visualized using soluble tetrameric major histocompatibility complex class I-peptide complexes. J Exp Med, 1998. 187(9): p. 1383-93.

69. Zippelius, A., et al., Effector function of human tumor-specific CD8 T cells in melanoma lesions: a state of local functional tolerance. Cancer Res, 2004. 64(8): p. 2865-73.

70. Kim, P.S. and R. Ahmed, Features of responding T cells in cancer and chronic infection. Curr Opin Immunol, 2010. 22(2): p. 223-30.

71. Knaus, H.A., et al., Signatures of CD8+ T cell dysfunction in AML patients and their reversibility with response to chemotherapy. JCI Insight, 2018. 3(21).

72. Franco, F., et al., Metabolic and epigenetic regulation of T-cell exhaustion. Nat Metab, 2020. 2(10): p. 1001-1012.

73. Belk, J.A., B. Daniel, and A.T. Satpathy, Epigenetic regulation of T cell exhaustion. Nat Immunol, 2022. 23(6): p. 848-860.

74. Sen, D.R., et al., The epigenetic landscape of T cell exhaustion. Science, 2016. 354(6316): p. 1165-1169.

75. Doering, T.A., et al., Network analysis reveals centrally connected genes and pathways involved in CD8+ T cell exhaustion versus memory. Immunity, 2012. 37(6): p. 1130-44.

76. McLane, L.M., M.S. Abdel-Hakeem, and E.J. Wherry, CD8 T Cell Exhaustion During Chronic Viral Infection and Cancer. Annu Rev Immunol, 2019. 37: p. 457-495.

77. Paley, M.A., et al., Progenitor and terminal subsets of CD8+ T cells cooperate to contain chronic viral infection. Science, 2012. 338(6111): p. 1220-5.

78. Hudson, W.H., et al., Proliferating Transitory T Cells with an Effector-like Transcriptional Signature Emerge from PD-1(+) Stem-like CD8(+) T Cells during Chronic Infection. Immunity, 2019. 51(6): p. 1043-1058 e4.

79. Raju, S., et al., Identification of a T-bet(hi) Quiescent Exhausted CD8 T Cell Subpopulation That Can Differentiate into TIM3(+)CX3CR1(+) Effectors and Memory-like Cells. J Immunol, 2021. 206(12): p. 2924-2936.

80. Khan, O., et al., TOX transcriptionally and epigenetically programs CD8(+) T cell exhaustion. Nature, 2019. 571(7764): p. 211-218.

81. Seo, H., et al., TOX and TOX2 transcription factors cooperate with NR4A transcription factors to impose CD8(+) T cell exhaustion. Proc Natl Acad Sci U S A, 2019. 116(25): p. 12410-12415.

82. Scott, A.C., et al., TOX is a critical regulator of tumour-specific T cell differentiation. Nature, 2019. 571(7764): p. 270-274.

83. Sekine, T., et al., TOX is expressed by exhausted and polyfunctional human effector memory CD8(+) T cells. Sci Immunol, 2020. 5(49).

84. Chen, J., et al., NR4A transcription factors limit CAR T cell function in solid tumours. Nature, 2019. 567(7749): p. 530-534.

85. Rao, A., C. Luo, and P.G. Hogan, Transcription factors of the NFAT family: regulation and function. Annu Rev Immunol, 1997. 15: p. 707-47.

86. Macian, F., C. Garcia-Rodriguez, and A. Rao, Gene expression elicited by NFAT in the presence or absence of cooperative recruitment of Fos and Jun. EMBO J, 2000. 19(17): p. 4783-95.

87. Crabtree, G.R. and E.N. Olson, NFAT signaling: choreographing the social lives of cells. Cell, 2002. 109 Suppl: p. S67-79.

88. Wherry, E.J., et al., Molecular Signature of CD8⁺ T Cell Exhaustion during Chronic Viral Infection. Immunity, 2007. 27(4): p. 670-684.

89. Martinez, G.J., et al., The transcription factor NFAT promotes exhaustion of activated CD8(+) T cells. Immunity, 2015. 42(2): p. 265-278.

90. Oestreich, K.J., et al., NFATc1 regulates PD-1 expression upon T cell activation. J Immunol, 2008. 181(7): p. 4832-9.

91. Utzschneider, D.T., et al., T Cell Factor 1-Expressing Memory-like CD8(+) T Cells Sustain the Immune Response to Chronic Viral Infections. Immunity, 2016. 45(2): p. 415-27.

92. Johnson, J.L., et al., Lineage-Determining Transcription Factor TCF-1 Initiates the Epigenetic Identity of T Cells. Immunity, 2018. 48(2): p. 243-257 e10.

93. Chen, Z., et al., TCF-1-Centered Transcriptional Network Drives an Effector versus Exhausted CD8 T Cell-Fate Decision. Immunity, 2019. 51(5): p. 840-855 e5.

94. Beltra, J.C., et al., Developmental Relationships of Four Exhausted CD8(+) T Cell Subsets Reveals Underlying Transcriptional and Epigenetic Landscape Control Mechanisms. Immunity, 2020. 52(5): p. 825-841 e8.

95. Jadhav, R.R., et al., Epigenetic signature of PD-1+ TCF1+ CD8 T cells that act as resource cells during chronic viral infection and respond to PD-1 blockade. Proc Natl Acad Sci U S A, 2019. 116(28): p. 14113-14118.

96. Kaech, S.M., et al., Selective expression of the interleukin 7 receptor identifies effector CD8 T cells that give rise to long-lived memory cells. Nat Immunol, 2003. 4(12): p. 1191-8.

97. Im, S.J., et al., Defining CD8+ T cells that provide the proliferative burst after PD-1 therapy. Nature, 2016. 537(7620): p. 417-421.

98. Siddiqui, I., et al., Intratumoral Tcf1(+)PD-1(+)CD8(+) T Cells with Stem-like Properties Promote Tumor Control in Response to Vaccination and Checkpoint Blockade Immunotherapy. Immunity, 2019. 50(1): p. 195-211 e10.

99. Miller, B.C., et al., Subsets of exhausted CD8(+) T cells differentially mediate tumor control and respond to checkpoint blockade. Nat Immunol, 2019. 20(3): p. 326-336.

100. Riches, J.C., et al., T cells from CLL patients exhibit features of T-cell exhaustion but retain capacity for cytokine production. Blood, 2013. 121(9): p. 1612-21.

101. van Bruggen, J.A.C., et al., Chronic lymphocytic leukemia cells impair mitochondrial fitness in CD8+ T cells and impede CAR T cell efficacy. Blood, 2019.

102. Maude, S.L., et al., Tisagenlecleucel in Children and Young Adults with B-Cell Lymphoblastic Leukemia. N Engl J Med, 2018. 378(5): p. 439-448.

103. Park, J.H., et al., Long-Term Follow-up of CD19 CAR Therapy in Acute Lymphoblastic Leukemia. N Engl J Med, 2018. 378(5): p. 449-459.

104. Long, A.H., et al., 4-1BB costimulation ameliorates T cell exhaustion induced by tonic signaling of chimeric antigen receptors. Nat Med, 2015. 21(6): p. 581-90.

105. Good, C.R., et al., An NK-like CAR T cell transition in CAR T cell dysfunction. Cell, 2021. 184(25): p. 6081-6100 e26.

106. Fraietta, J.A., et al., Determinants of response and resistance to CD19 chimeric antigen receptor (CAR) T cell therapy of chronic lymphocytic leukemia. Nat Med, 2018. 24(5): p. 563-571.

107. Zugmaier, G., et al., Long-term survival and T-cell kinetics in relapsed/refractory ALL patients who achieved MRD response after blinatumomab treatment. Blood, 2015. 126(24): p. 2578-84.

108. Duell, J., et al., Frequency of regulatory T cells determines the outcome of the T-cell-engaging antibody blinatumomab in patients with B-precursor ALL. Leukemia, 2017. 31(10): p. 2181-2190.

109. Zhao, Y., et al., Tumor-intrinsic and -extrinsic determinants of response to blinatumomab in adults with B-ALL. Blood, 2021. 137(4): p. 471-484.

110. Krupka, C., et al., Blockade of the PD-1/PD-L1 axis augments lysis of AML cells by the CD33/CD3 BiTE antibody construct AMG 330: reversing a T-cell-induced immune escape mechanism. Leukemia, 2016. 30(2): p. 484-91.

111. John, L.B., et al., Anti-PD-1 antibody therapy potently enhances the eradication of established tumors by gene-modified T cells. Clin Cancer Res, 2013. 19(20): p. 5636-46.

112. Adusumilli, P.S., et al., A phase I trial of regional mesothelin-targeted CAR T-cell therapy in patients with malignant pleural disease, in combination with the anti-PD-1 agent pembrolizumab. Cancer Discov, 2021.

113. Poorebrahim, M., et al., Counteracting CAR T cell dysfunction. Oncogene, 2021. 40(2): p. 421-435.

114. Song, W. and M. Zhang, Use of CAR-T cell therapy, PD-1 blockade, and their combination for the treatment of hematological malignancies. Clin Immunol, 2020. 214: p. 108382.

115. Mestermann, K., et al., The tyrosine kinase inhibitor dasatinib acts as a pharmacologic on/off switch for CAR T cells. Sci Transl Med, 2019. 11(499).

116. Wu, B.X., et al., Development of molecular and pharmacological switches for chimeric antigen receptor T cells. Exp Hematol Oncol, 2019. 8: p. 27.

117. Foa, R., et al., Dasatinib-Blinatumomab for Ph-Positive Acute Lymphoblastic Leukemia in Adults. N Engl J Med, 2020. 383(17): p. 1613-1623.

118. Puzzolo, M.C., et al., Host immune system modulation in Ph+ acute lymphoblastic leukemia patients treated with dasatinib and blinatumomab. Blood, 2021.

7. List of publications

7.1 Original publications

T-cell exhaustion induced by continuous bispecific molecule exposure is ameliorated by treatment-free intervals

Nora Philipp, Maryam Kazerani, Alyssa Nicholls, Binje Vick, Jan Wulf, Tobias Straub, Michaela Scheurer, Amelie Muth, Gerulf Hänel, Daniel Nixdorf, Monika Sponheimer, Malte Ohlmeyer, Sonja M. Lacher, Bettina Brauchle, Anetta Marcinek, Lisa Rohrbacher, Alexandra Leutbecher, Kai Rejeski, Oliver Weigert, Michael von Bergwelt-Baildon, Sebastian Theurich, Roman Kischel, Irmela Jeremias, Veit Bücklein, Marion Subklewe

Blood. 2022 Sep 8;140(10):1104-1118. doi: 10.1182/blood.2022015956. PMID: 35878001

STING agonism turns human T cells into interferon-producing cells but impedes their functionality

Niklas Kuhl, Andreas Linder, **Nora Philipp**, Daniel Nixdorf, Hannah Fischer, Simon Veth, Gunnar Kuut, Teng Teng Xu, Sebastian Theurich, Thomas Carell, Marion Subklewe, Veit Hornung

EMBO Rep. 2023 Mar 6;24(3):e55536. doi: 10.15252/embr.202255536. Epub 2023 Jan 27. PMID: 36705069; PMCID: PMC9986811

Adapter CAR T cells to counteract T-cell exhaustion and enable flexible targeting in AML

D. Nixdorf, M. Sponheimer, D. Berghammer, F. Engert, U. Bader, **N. Philipp**, M. Kazerani, T. Straub, L. Rohrbacher, L. Wange, S. Dapa, D. Atar, C. M. Seitz, K. Brandstetter, A. Linder, M. von Bergwelt, H. Leonhardt, J. Mittelstaet, A. Kaiser, V. Bücklein, M. Subklewe

Leukemia (2023). https://doi.org/10.1038/s41375-023-01905-0

CD33 BiTE® molecule-mediated immune synapse formation and subsequent T-cell activation is determined by the expression profile of activating and inhibitory checkpoint molecules on AML cells

Anetta Marcinek, Bettina Brauchle, Lisa Rohrbacher, Gerulf Hänel, **Nora Philipp**, Florian Märkl, Thaddäus Strzalkowski, Sonja M. Lacher, Dragica Udiljak, Karsten Spiekermann, Sebastian Theurich, Sebastian Kobold, Roman Kischel, John R. James, Veit L. Bücklein, Marion Subklewe

Cancer Immunol Immunother (2023). https://doi.org/10.1007/s00262-023-03439-x

7.2 Conference contributions

Oral Presentations

Bispecific´s Best Buddies: Combinatorial Treatment Strategies to Mitigate T-cell Exhaustion

N. Philipp*, A. Muth*, V. Bücklein, M. Subklewe

*contributed equally

Oral presentation at the Keystone Symposium "Multispecific Immune Cell Engagers for Cancer Immunotherapy", Feb 2023, Banff, Canada

Treatment-free Intervals during CD19xCD3 BiTE® Construct-mediated T-cell Stimulation Induce Functional Reinvigoration and Transcriptional Reprogramming of Exhausted T cells

Invited speaker at the international workshop on acute leukemia (iwAL) in 2022

Recovering from Burnout: CD19xCD3 BiTE®-mediated T-cell Exhaustion and Rescue Strategies

Invited speaker at the international workshop on acute leukemia (iwAL) in 2021

Treatment-Free Intervals during CD19xCD3 BiTE® Construct-Mediated T-Cell Stimulation Induce Functional Reinvigoration and Transcriptional Reprogramming of Exhausted T Cells

Nora Zieger, Maryam Kazerani Pasikhani, Tobias Straub, Alyssa Nicholls, Gerulf Hänel, Jan Wulf, Michaela Scheurer, Daniel Nixdorf, Monika Sponheimer, Sonja M Lacher, Bettina Brauchle, Anetta Marcinek, Lisa Rohrbacher, Alexandra Leutbecher, Michael von Bergwelt, Karsten Spiekermann, Oliver Weigert, Sebastian Theurich, Veit L Buecklein, Roman Kischel, Marion Subklewe

ASH Oral Presentation, Blood 2021; 138 (Supplement 1): 513, Atlanta, USA

Continuous CD19xCD3-BiTE® stimulation induces T-cell exhaustion which can be ameliorated by treatment-free intervals (TFI)

N. Zieger, A. Nicholls, M. Kazerani, B. Vick, P. Rovatti, T. Straub, G. Hänel, J. Wulf, V. Bücklein, M. Scheurer, D. Nixdorf, M. Sponheimer, M. Ohlmeyer, S. Lacher, B. Brauchle, A. Marcinek, L. Rohrbacher, A. Leutbecher, K. Spiekermann, O. Weigert, M. von Bergwelt, S. Theurich, R. Kischel, L. Vago, I. Jeremias, M. Subklewe

Oral presentation at the annual meeting of the German, Austrian and Swiss Societies of Hematology and Medical Oncology (DGHO) 2021, Berlin; Germany

Poster presentations

Partners for Bispecifics: Combinatorial Approaches to Augment T-cell Function and Mitigate Exhaustion

N. Philipp, A. Muth, M. von Bergwelt-Baildon, V. Bücklein, M. Subklewe

SITC poster presentation, Journal for Immunotherapy of Cancer Nov 2022, 10 (Suppl 2) A934; DOI: 10.1136/jitc-2022-SITC2022.0897

Treatment-free Intervals Mitigate T-Cell Exhaustion Induced By Continuous CD19xCD3-BiTE® Construct Stimulation in Vitro

Nora Zieger, Alyssa Nicholls, Jan Wulf, Gerulf Hänel, Maryam Kazerani Pasikhani, Veit Bücklein, Bettina Brauchle, Anetta Marcinek, Daniel Nixdorf, Lisa Rohrbacher, Michaela Scheurer, Roman Kischel, Karsten Spiekermann, Oliver Weigert, Sebastian Theurich, Michael von Bergwelt, Marion Subklewe

ASH Conference Poster, Blood 2020; 136 (Supplement 1): pages 44-45

Conference abstracts

Lenalidomide in combination with continuous CD19xCD3-specific T-cell recruiting antibody treatment maintains T-cell functionality and delays exhaustion

A. Muth, **N. Zieger**, M. Sponheimer, O. Weigert, M. von Bergwelt, V. Bücklein, M. Subklewe

Annual meeting of the German, Austrian and Swiss Societies of Hematology and Medical Oncology (DGHO) 2022

Augmenting Efficacy of T-Cell Bispecific Antibodies in AML through a Tumor Stroma-Targeted 4-1BB Agonist

Gerulf Hänel, Anne-Sophie Neumann, Vesna Pulko, Christina Claus, Alexandra Leutbecher, Anetta Marcinek, **Nora Zieger**, Veit L Bücklein, Pablo Umaña, Christian Klein, Marion Subklewe

ASH Conference Poster, Blood 2021; 138 (Supplement 1): 1178

CD33 BiTE Construct Mediated Immunological Synapse Formation and Downstream Signaling in T Cells Is Dependent on Expression of Costimulaotry Molecules on Target Cells

Anetta Marcinek, Bettina Brauchle, Gerulf Hänel, Sonja M Lacher, **Nora Zieger**, Roman Kischel, Michael von Bergwelt, Karsten Spiekermann, Sebastian Theurich, John R James, Veit L Bücklein, Marion Subklewe

ASH Conference Poster, Blood 2021; 138 (Supplement 1): 2237

Awards and prizes

ASH Abstract Achievement Award 2021

Treatment-Free Intervals during CD19xCD3 BiTE® Construct-Mediated T-Cell Stimulation Induce Functional Reinvigoration and Transcriptional Reprogramming of Exhausted T Cells

Nora Zieger, Maryam Kazerani Pasikhani, Tobias Straub, Alyssa Nicholls, Gerulf Hänel, Jan Wulf, Michaela Scheurer, Daniel Nixdorf, Monika Sponheimer, Sonja M Lacher, Bettina Brauchle, Anetta Marcinek, Lisa Rohrbacher, Alexandra Leutbecher, Michael von Bergwelt, Karsten Spiekermann, Oliver Weigert, Sebastian Theurich, Veit L Buecklein, Roman Kischel, Marion Subklewe

Blood 2021; 138 (Supplement 1): 513

8. Acknowledgements

I would like to thank

Marion Subklewe, for her enthusiasm, encouragement and trust as well as for the numerous opportunities she gave me to engage with the scientific community. You taught me to believe in, pursue and reach any goal I had, and to be a self-confident and independent female scientist.

My colleagues Daniel Nixdorf, Lisa Rohrbacher, Anetta Marcinek, Gerulf Hänel, Veit Bücklein, Bettina Brauchle, Yingshuai Wang, Amelie Muth, Alexandra Leutbecher, Lis Winter, Monika Sponheimer, Anne-Sophie Neumann. You were – and still are - not just colleagues but dear friends during these years. Thank you for your empathy and friendship, advice, inappropriate jokes (Daniel), for solving my recurrent IT problems (Gerulf), reminders on the whereabouts of my mobile phone (Lisa), holding female power high (Anetta), celebrations with or without specific occasion and all the fun we had together.

Especially, I want to thank Daniel Nixdorf, my PhD buddy from the very first day. You taught me to think outside the box, change perspective and constantly challenge views and opinions – including my own. Most importantly, however, you made me believe that everything is possible.

My family, especially my parents for their trust, encouragement, and unconditional love. You never doubted me and supported me throughout all these years of education. This work is dedicated to you. Without you I would (literally) not be here.

Anton Philipp, my soulmate and most important person in my world. PhD life can sometimes be hard. But having you by my side has made it the most exciting time of my life. You encourage and believe in me and you always have my back. You give me courage and the confidence to reach for the stars. Thank you for your love and for being proud of me – every day.